Using new tools to study the neural mechanisms of sensation: Auditory processing in locusts and translational motion vision in flies

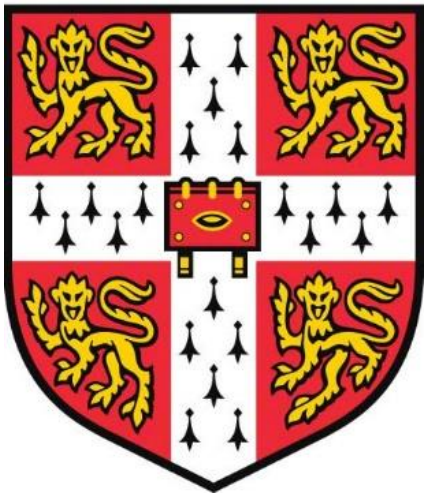

Matthew David Isaacson

St. Edmund's College

Department of Zoology

This dissertation is submitted for the degree of *Doctor of Philosophy*

26th September 2018

Summary

Using new tools to study the neural mechanisms of sensation: Auditory processing in locusts and translational motion vision in flies

Matthew David Isaacson

This thesis describes work from both the University of Cambridge in the lab of Berthold Hedwig and from the HHMI Janelia Research Campus in the lab of Michael Reiser. At the University of Cambridge, my work involved the development and demonstration of a method for electrophoretically delivering dyes and tracers for anatomical and functional imaging into animals that are not amenable to genetic labelling techniques. Using this method in locusts and crickets – model systems of particular interest for their acoustic communication – I successfully delivered polar fluorescent dyes and tracers through the sheath covering the auditory nerve, simultaneously staining both the peripheral sensory structures and the central axonal projections without destroying the nerve's function. I could label neurons which extend far from the tracer delivery site on the nerve as well as local neuron populations through the brain's surface. I used the same method to deliver calcium indicators into central neuropils for *in vivo* optical imaging of sound-evoked activity, as well as calling song-evoked activity in the brain.

The work completed at the Janelia Research Campus began with the development of a modern version of a modular LED display and virtual reality control system to enable research on the visual control of complex behaviors in head-fixed animals. The primary advantages of our newly developed LED-based display over other display technologies are its high-speed operation, brightness uniformity and control, precise synchronization with analog inputs and outputs, and its ability to be configured into a variety of display geometries. Utilizing the system's fast display refresh rates, I conducted the first accurate characterization of the upper limits of the speed sensitivity of *Drosophila* for apparent motion during flight. I also developed a flexible approach to presenting optic flow scenes for functional imaging of motion-sensitive neurons. Finally, through the on-line analysis of behavioral measures, image rendering, and display streaming with low latency to multi-color (UV/Green) LED panels, I demonstrated the ability to create more naturalistic stimuli and interactive virtual visual landscapes.

Lastly, I used this new visual display system to explore a newly discovered cell-type that had been implicated in higher-order motion processing from a large genetic screen of visually-guided behavior deficits. Using genetic silencing and activation methods, and by designing stimuli that modeled the

optic flow encountered during different types of self-motion, colleagues in the Reiser lab and I showed that this cell-type – named Lobula Plate Columnar 1 (LPC1) – is required for the stopping behavior of walking flies caused by back-to-front translation motion but is not involved in the rotational optomotor response. Using calcium imaging, I found that LPC1 was selectively excited by back-to-front motion on the eye ipsilateral to the neuron population and inhibited by front-to-back motion on the contralateral eye, demonstrating a simple mechanism for its selectivity to translation over rotation. I also examined an anatomically similar cell type – named Lobula-Lobula Plate Columnar type 1 (LLPC1) – and found that its selectivity results from a similar but opposite calculation for the detection of front-to-back translational motion. The detection of back-to-front motion had previously been hypothesized to be useful for collision avoidance, and this work provides a neural mechanism for how this detection could be accomplished, as well as providing a platform from which to explore the larger network for translation optic flow.

Preface

The work described in this dissertation was conducted at the University of Cambridge under the supervision of Berthold Hedwig (chapter 2) and at the HHMI Janelia Research Campus under the supervision of Michael Reiser (chapters 3 and 4). Most of the work described in chapter 2 has been published in the journal *Scientific Reports* (Isaacson & Hedwig, 2017). The projects completed at the Janelia Research Campus were highly collaborative in nature: The work in chapter 3 relied heavily on equipment and technology developed with numerous internal and external collaborators, which is clearly identified in the text. The work in chapter 4 also relied on collaborations with multiple Janelia departments and teams, and includes some experiments (namely, those described in section 4.4.2) conducted in collaboration with another graduate student - Jessica Eliason – as part of her doctoral degree submitted to Emory University in the fall of 2017 (Eliason, 2017). These collaborations and all work that were not entirely my own are clearly identified in the relevant text.

Declaration:

This dissertation is submitted for the degree of Doctor of Philosophy. It is the result of my own work and includes nothing which is the outcome of work done in collaboration except as declared in the preface and in the text. This dissertation is not substantially the same as any that I have submitted or is being concurrently submitted for a degree or diploma or other qualification at the University of Cambridge or any other University or similar institution except as declared in the Preface and specified in the text. I further state that no substantial part of my dissertation has already been submitted, or is being concurrently submitted for any such degree, diploma, or other qualification at the University of Cambridge or any other University or similar institution except as declared in the preface and specified in the text. This dissertation does not exceed the prescribed word limit of 60,000 words.

Acknowledgements

I am very grateful to the University of Cambridge Department of Zoology for providing the work space and shared resources during my time working in the beautiful city of Cambridge, and for the collaborative and inspiring academic environment it provided. I am also grateful to the HHMI Janelia Research Campus and the Reiser lab for the unparalleled resources provided and for their full financial and technical support over the course of my PhD.

My research at Janelia benefited greatly from the expertise of Janelia's shared resources – particularly the Connectome Annotation Team, the Janelia Experimental Technology Team, and the Scientific Computing Team – as well as our external collaborators William Dickson at IO Rodeo and Andy Chiu at Coleman Technologies. I thank Tim Bailey at Cambridge and Mai Morimoto at Janelia for sharing their technical expertise, and Ishani Ganguly for spending a summer conducting top-quality flight arena experiments. I also thank Aljoscha Nern for identifying any split-GAL4 line we could ask for, and Ed Rogers for creating and managing fly stocks, making my life in *Drosophila* research so much easier.

I appreciate the check-ins, feedback, and general support of the Janelia-Cambridge joint PhD program coordinators: Sue Jones at Cambridge and Erik Snapp at Janelia. I also appreciate the challenging and useful feedback from my advisors at Cambridge: Simon Laughlin, Matthias Landgraf, and Walter Federle. Many thanks to Kit Longden for all his creative input and insight, and to my Janelia advisor Anne Hermundstad for her feedback and for sharing her enthusiasm for all my projects. I also extend a very special thanks to Jessica Eliason for her excellent collaboration and constant hard work.

To my supervisors Berthold Hedwig and Michael Reiser, both of whom struck a great balance between supportive, hands-on mentoring and granting me freedom to explore topics on my own, I express my sincerest gratitude. I know I would not be so confident that I could manage a career as an independent scientist without the excellent training I've received these past 4 years.

Finally, I would like to thank my lovely wife Ally Isaacson for her unwavering support and cheerleading, and for giving me a happy and fulfilling life outside the lab.

List of Abbreviations

CAT: Connectome Annotation Team

CCD: charge-coupled device

CCW: counterclockwise

CNS: central nervous system

CW: clockwise

DL: Dickinson Lab

DLP: Digital Light Processing

DMA: Direct Memory Access

EM: electron microscopy

FDR: false discovery rate

FOE: focus/foci of expansion

FPGA: field-programmable gate array

G3: 3rd generation modular display system

G4: 4th generation modular display system

GUI: graphical user interface

I2C: Inter-Integrated Circuit

JET: Janelia Experimental Technology

L-R: left minus right

L+R: left plus right

LCD: liquid crystal display

LED: light-emitting diode

LLPC1: Lobula-Lobula Plate Columnar type 1

LMS: local motion sensitivity

LP: Lobula Plate

LPC1: Lobula Plate Columnar type 1

LPTC: Lobula Plate tangential cell

LPD: local preferred direction

MCBL: multicell bolus loading

MCU: microcontroller unit

MGI: medial giant interneuron

MW: molecular weight

PC: personal computer

PCB: printed circuit board

PCIe: Peripheral Component Interconnect Express

PEEK: polyether ether ketone

PLP: posterior lateral protocerebrum

RAM: random-access memory

ROI: region of interest

SEM: standard error of measurement

SPI: Serial Peripheral Interface

SPL: sound pressure level

TCP/IP: Transmission Control Protocol/Internet Protocol

TF: temporal frequency

UV: ultraviolet

VHDCI: very-high-density cable interconnect

VPN: visual projection neuron

WbF: wingbeat frequency

Table of Contents

Summary 2
Preface 4
Acknowledgements 5
List of Abbreviations 6
Table of Contents 7
Chapter 1: General Introduction 10
1.1 Contents of this thesis 10
1.2 The neuroscience of sensation and behavior in insects 10
1.3 Acoustic communication in locusts and crickets 12
1.3.1 Calling song phonotaxis 12
1.3.2 Anatomical and functional study of neurons 13
1.3.3 The auditory system of crickets and locusts 14
1.4 Motion vision in flies 15
1.4.1 The insect optomotor response 15
1.4.2 Visual stimuli and quantitative behavior 16
1.4.3 Genetic tools for *Drosophila* neuroscience 17
1.4.4 The *Drosophila* motion vision system 17
Chapter 2: Electrophoresis of fluorescent tracers for anatomical and functional imaging of insect auditory circuits 20
2.1 Abstract 20
2.2 Introduction 20
2.2.1 Current labelling methods for non-model systems 20
2.2.2 Electroporation, electrophoresis, and iontophoresis 21
2.2.3 Aims of this chapter 22
2.3 Methods 23
2.3.1 Animals and dissection 23
2.3.2 Dye solutions and suction electrode procedures 23
2.3.3 Auditory stimulation 24
2.3.4 Whole-nerve recordings and current injection 24
2.3.5 *In vivo* preparation for imaging 25
2.3.6 Data analysis 26
2.4 Results 26
2.4.1 Anatomical staining of whole nerves with electrophoresis 26
2.4.2 Neurobiotin staining for large neurons 28

2.4.3 Functional imaging of auditory neuropils 29
2.4.4 Targeting brain neurons through the sheath 32
2.5 Discussion 35
Chapter 3: Next generation LED display system for animal models of vision 38
3.1 Abstract 38
3.2 Introduction 38
3.2.1 History of visual displays for animal research 38
3.2.2 Modern display capabilities 39
3.2.3 Aims of this chapter 40
3.3 Methods 40
3.3.1 Hardware and software 40
3.3.2 Flies 41
3.3.3 *In vivo* preparation for tethered flying 41
3.3.4 *In vivo* preparation for calcium imaging 41
3.3.5 Visual stimuli 42
3.3.6 Tethered flight equipment and analysis 42
3.3.7 2-photon imaging and analysis 43
***3.3.8* Statistics** 44
3.4 Results 45
3.4.1 Technical overview of the display system hardware and software 45
3.4.2 Creating optic flow patterns 48
3.4.3 High-speed operation to probe upper limits of motion vision 52
3.4.4 Motorized pitching arena for optic flow mapping 57
3.4.5 Multicolor displays and virtual reality 64
3.5 Discussion 67
Chapter 4: Classes of small visual projection neurons detect translational motion vision in flies 70
4.1 Abstract 70
4.2 Introduction 71
4.2.1 Visual projection neurons 71
4.2.2 Genetic screen for motion deficits 71
4.2.3 Identification of LPC1 72
4.2.4 Aims of this chapter 73
4.3 Methods 74
4.3.1 Flies 74
4.3.2 *In vivo* preparation for tethered walking 75
4.3.3 Optogenetics 75

4.3.4 Visual stimuli 75
4.3.5 Tethered walking equipment and analysis 76
4.3.6 2-photon imaging and analysis 77
4.3.7 Statistics 77
4.4 Results 78
4.4.1 Calcium imaging of LPC1 shows selectivity for back-to-front translation 78
4.4.2 LPC1 modulates forward walking by back-to-front translation 80
4.4.3 Selectivity to back-to-front translation depends on contralateral motion 82
4.4.4 High-speed tuning dependent on non-T4/T5 input 85
4.4.5 LLPC1 and the detection of front-to-back motion 87
4.5 Discussion 91
Chapter 5: Final discussion and future directions 97
5.1 Electrophoretic dye delivery and cricket calling-song selectivity 97
5.2 Visual stimuli for tethered animal research 99
5.3 Neural circuits for translation selectivity in flies 100
5.4 Concluding remarks 102
References 103

Chapter 1: General Introduction

1.1 Contents of this thesis

This thesis describes work from both the University of Cambridge in the lab of Berthold Hedwig and from the HHMI Janelia Research Campus in the lab of Michael Reiser, during which I focused on separate projects but that are related under the common themes of tool-building and studying the neural mechanisms of sensation. At the University of Cambridge, my work involved the development and demonstration of a relatively non-invasive method for electrophoretically delivering both anatomical dyes/tracers and functional indicators into neurons, focusing on the locust and cricket auditory systems. This new method was developed to aid neuroscience research in animal models by developing an improved tool for anatomical and functional labelling in animals that are not amenable to genetic labelling techniques. At the HHMI Janelia Research Campus, I started with a similar goal of improving the tools available for neuroscience research in animal models, but specifically to build new tools for vision researchers. My work involved the development and demonstration of an advanced LED display and virtual reality control system that addresses an important set of technical challenges to support research on the visual control of complex behaviors in head-fixed animals. I was able to utilize the advances of this system to collect new information about the *Drosophila* visual system, such as the behavioral responses to high-speed optic flow in flying flies as well as new information regarding cell-types which are involved in the detection of translational optic flow and the behavioral functions they may be serving.

In order to provide the appropriate context for the work contained in this thesis, in the following section, I will briefly introduce the history of neuroscience research in animal models with a particular focus on the benefits of insect research. I will then provide a brief background on both the cricket/locust auditory systems as well as the fly motion vision system, including background on the tools that have historically been useful in enabling research in these systems. This background is intended to provide the context to demonstrate why the new tools I have developed and biological findings I have uncovered represent significant advances in their respective fields.

1.2 The neuroscience of sensation and behavior in insects

Ethologists (those who study animal behavior) often seek to understand and build explanatory models of behavior in terms of their function or usefulness, the mechanisms through which the behaviors operate, and how the behaviors arise from the perspectives of evolution and development (Tinbergen, 1963). Information about sensation and behavior has been gathered this way from a

wide variety of species on a number of topics, such as courtship in waterfowl (Schulze-Hagen & Birkhead, 2015), learning and memory in honeybees (Hammer & Menzel, 1995), and navigation in ants (Wehner, 2003). The advent of modern neuroscience brought a new biological framework with which to build mechanistic explanations of sensation and behavior, describing the processing of information from sensory organs and control of motor outputs by the neural processes in between (Ewert, 1980; Hoyle, 1984). Many ethologists and neuroethologists sought to deepen the investigation of the neural mechanisms of sensation and behavior by conducting experiments with animals in laboratory settings where external stimuli can be precisely controlled and behaviors can be quantified. This can be accomplished by studying freely moving animals in a somewhat restricted and controlled environment (such as mice learning to traverse a maze [Barnes, 1979] or blowflies chasing a target [Boeddeker, Kern, & Egelhaaf, 2003]) or by fixing animals still and simulating environmental stimuli in place (such as a displaying visual stimuli to a tethered, swimming zebrafish [Bianco & Engert, 2015] or by mechanically stimulating the antenna of a tethered cockroach [Okada & Toh, 2004]). The latter strategy has the advantage of allowing for the direct observation of the nervous system of these animals as sensations and behaviors are monitored (Dombeck, Khabbaz, Collman, Adelman, & Tank, 2007; Seelig et al., 2010; Sobel & Tank, 1994).

Researchers interested in studying a particular sensory modality or behavior can choose between a wide variety of animals to use as a model for that system; for instance, researchers studying the neural processing of visual stimuli have utilized cats (Hubel & Wiesel, 1962), macaques (Ringach, Shapley, & Hawken, 2002), mice (Scholl, Tan, Corey, & Priebe, 2013), and flies (Fisher, Silies, & Clandinin, 2015). The choice of a particular model system typically involves the weighing of numerous pros and cons. For example, some animal species are given a higher ethical value or moral status than others for reasons such as the degree of sentience, cognitive capacity, or the capacity to suffer or flourish (Nuffield, 2005). While this is a heavily debated subject, insects and other invertebrates are less likely to cause ethical concern (Harvey-Clark, 2011; Nuffield, 2005), making research using these species less problematic. The relatively small size and short reproduction cycle of insects makes housing and manipulating them easier (Scully & Bidochka, 2006), and their relatively small brain size is tractable for comprehensive mapping of neural circuits with modern imaging techniques (Zheng et al., 2018). Even with their relatively small nervous systems, insects are still observed to have incredibly diverse and sophisticated sensory abilities and behavioral strategies, making them highly attractive model systems in neuroscience (Borst, Haag, & Reiff, 2010a; Hammer & Menzel, 1995; Huber, 1990).

When many researchers converge on a model system, efforts can be pooled to create better tools and resources to aid further research, and standards can be created by which different labs can

directly relate and compare their findings (Jenett et al., 2012; Rodríguez, Didiano, & Desplan, 2012). However, having a variety of model systems being studied simultaneously allows for rich comparative neuroscience, which can help track the evolutionary lineage of neural processing strategies and identify between species-specific neural strategies and general principles of neural processing that is common across the animal kingdom (Keifer & Summers, 2016; Yartsev, 2017). Over the course of my PhD at the University of Cambridge and the HHMI Janelia Research Campus, I have been fortunate enough to experience the benefits of both categories of model systems. In the following section (1.3) and in chapter 2, I will describe a model system for acoustic communication in locusts (*Schistocerca gregaria*) and crickets (*Gryllus bimaculatus*), a model without the latest and greatest experimental tools but that is incredibly well-suited for the study of auditory processing and the sensory control of behavior. In the section immediately after (1.4) and in chapters 3 and 4, I will describe the use of fruit flies (*Drosophila melanogaster*) as a model system for motion-vision, a model that is both well-suited to the topic and that has one of the largest suites of experimental tools of any animal model system.

1.3 Acoustic communication in locusts and crickets

1.3.1 Calling song phonotaxis

Crickets and locusts (closely related orthopteran species) have drawn the attention of ethologists for centuries (Roesel von Rosenhof, 1749) (Figure 1.1). Even among non-scientists, the chirping and calling song of crickets is a nearly universal and unmistakable sound. The calling song is produced by male crickets by sharply and repeatedly scraping the edges of their forewings (one side with a toothed edge) together – this stridulation causes vibrations in the wings which are carried far through the surrounding air. A small number of these sound pulses produced close together constitute a “chirp”, while more sustained stridulation produce “trills” (Alexander, 1957). Distinct patterns of sound pulses comprise the calling song, which female crickets can detect among the many other sounds in their environment and locate its source by navigating towards it. This attraction towards specific sounds is referred to as “phonotaxis” (Thorson, Weber, & Huber, 1982). It has been observed that female crickets can distinguish the calling song of members of its own species (conspecifics) over the calling songs of other cricket species and may even prefer features of the song that are tied to the increased reproductive health of the individual male cricket producing the song (Thorson et al., 1982; Wagner & Reiser, 2000). This sophisticated ability to detect specific auditory frequencies and patterns have made crickets an attractive model system for studying the neural mechanisms of acoustic communication (Huber, 1990).

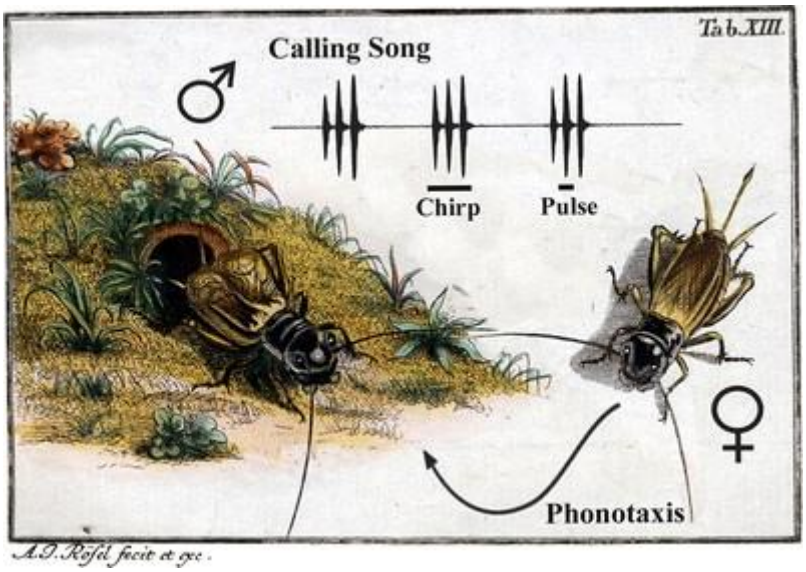

Figure 1.1: **Calling song production and phonotaxis**.

Early description of a calling song produced by a male cricket (*Gryllus campestris*) and phonotaxis by a female. The calling song is composed of sound chirps, each consisting of a number of sound pulses produced by tegmina (forewing) stridulation. The female cricket identifies the calling song and navigates to its source. Image modified from Roesel von Rosenhof (1749), reprinted and described in Hedwig (2006).

1.3.2 Anatomical and functional study of neurons

The conceptualization of the nervous system as being composed of discrete cells that transmit information across a network can largely be attributed to the Golgi stain, which led to the first visualization of neurons in their entirety (Pannese, 1999). The Golgi stain and other staining methods have been used to visualize and describe neurons and substructures within animal brains (Fischbach & Dittrich, 1989; Strausfield & Blest, 1970). Techniques for the targeted delivery of various visualizing molecules into specific subsets or types of neurons allowed for the visualization of the cell's geometry and to track the full path of its projections (Stretton & Kravitz, 1968). Neuronal labelling has led to efforts to infer the potential function of these cells and structures in the context of the processing of sensory information and control of behavior; however, the extent to which function can be inferred from anatomy alone is limited.

Since the discovery of the electrical properties of neurons and the subsequent conceptualization of action potentials as a component of interneuron communication (Hodgkin, Huxley, & Katz, 1952), the use of electrophysiology has become a dominant method to directly study the function of a neuron by identifying the stimuli that result in the neuron's excitation (i.e. the "stimulus encoding" of the neuron). Electrophysiology is often combined with anatomical labelling to gain rich

information about the structure and function of cell-types (Buchanan, 1993; Gilbert, Penisten, & DeVoe, 1991). *In vivo* imaging of functional indicators, which undergo a fluorescence change based on the transient intracellular changes that are associated with an action potential, has more recently become another popular method for studying the anatomy and function of neurons, albeit with significantly slower temporal resolution than electrophysiology (Eilers, Augustine, & Konnerth, 1995; Stosiek, Garaschuk, Holthoff, & Konnerth, 2003). These techniques grant the ability to track signal transformations as they progress through the nervous system of a healthy, behaving (tethered) animal, to see how meaningful information is extracted from basic sensory signals and how this information determines behavior.

1.3.3 The auditory system of crickets and locusts

Experiments involving anatomical imaging and electrophysiology have led to significant insights in how crickets and locusts detect and process auditory stimuli. In locusts, sound is first transduced into action potentials by Müller's organ: a structure composed of groups of mechanoreceptors that is attached to the locust tympanic membrane (Jacobs, Otte, & Lakes-Harlan, 1999). Incident sound waves generate vibrations on the tympanic membrane which, due to the thickness and tension of the membrane, focus the vibrational energy into the mechanoreceptors in a frequency-dependent manner based on the spatial location of the cells with respect to the tympanic membrane (Malkin, McDonagh, Mhatre, Scott, & Robert, 2014). This set of sound frequency information from the left and right auditory organs is carried through the auditory nerves into a central ganglion (Figure 1.2), where this information propagates into many other cells, including those that travel into the brain (Rehbein, Kalmring, & Römer, 1974).

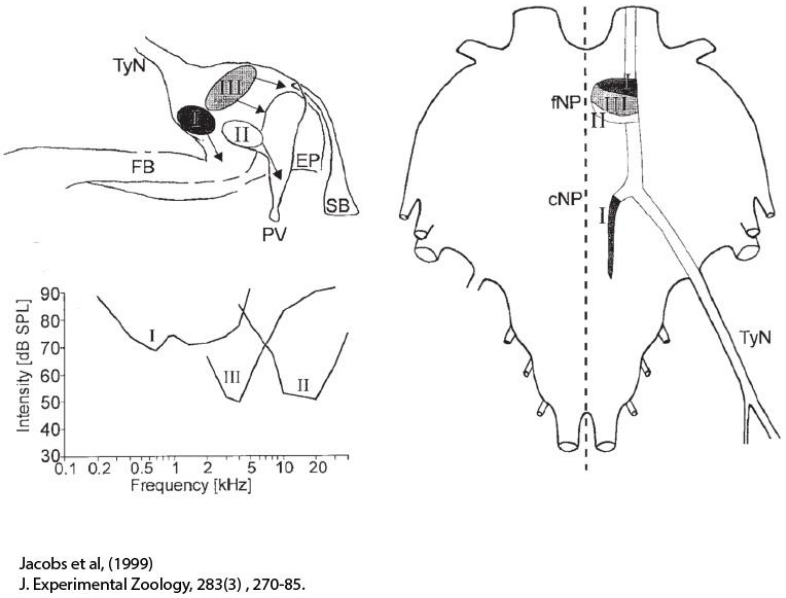

Jacobs et al, (1999)
J. Experimental Zoology, 283(3) , 270-85.

Figure 1.2: **The peripheral auditory system of the locust.**

(top-left) Müller's organ of the locust composed of 3 distinct groupings of mechanosensory cells, with group I cell dendrites attached to the folded body (FB), group II cells attached to the pyriform vesicle (PV), and group III cells attached to either the elevated process (EP) or styliform body (SB). (right) Axons from Müller's organ project into the locust metathoracic ganglion from the tympanal (or "auditory") nerve (TyN), branching primarily in the frontal and caudal auditory neuropils (fNP and cNP, respectively). (bottom-left) Frequency-intensity response curves based on electrophysiological recordings of Müller's organ cells show distinct groupings of frequency-selective neurons. Figure modified from Jacobs et al. (1999).

While the peripheral mechanisms behind the detection of specific sound frequencies have been uncovered, the central neural processes behind sound pattern and calling song detection is still not well understood, due in part to the limited methods for identifying and studying specific neuron populations in the locust and cricket brain. In chapter 2, I describe a new method of labelling both peripheral and central neuron populations and demonstrate the usefulness of this method for anatomical and functional labelling in the cricket and locust auditory circuits.

1.4 Motion vision in flies

1.4.1 The insect optomotor response

There is a rich history of neuroscience using vision in insects, and much of this research was made possible by the discovery of the optomotor response (or optokinetic reflex), where apparent motion causes a behavioral reaction in the animal which is dependent on the direction of motion (Gotz,

1968) (Figure 1.3). The ability to reproducibly observe a robust, well-defined behavioral reaction to a simple visual stimulus enabled countless studies on how insects perceive and process motion information. One of the earliest models of motion detection, the Hassenstein–Reichardt model, was formulated by utilizing the rotational optomotor response of beetles under the presentation of simulated rotational motion (Hassenstein & Reichardt, 1956). Even more general neural principles have been uncovered using this system; the theory of reafference, an attempt to explain how an animal can distinguish between sensations caused by its own behavioral actions and those from the external environment, was formulated from clever experiments of the optomotor response in flies (Von Holst & Mittlestaedt, 1950; reprinted and translated in Von Holst & Mittelstaedt, 2011).

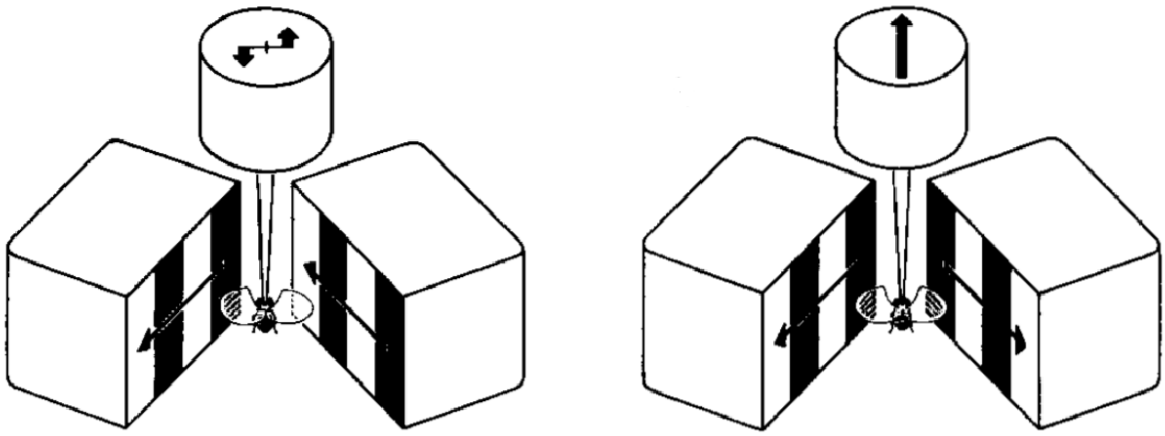

Gotz, K. G. (1968)
Kybernetics. 4(6), 199-208

Figure 1.3: **Optomotor responses of the flying fly.**

Illustration of the optomotor response in tethered flying *Drosophila*. (left) The fly is tethered to a torque meter and presented with a simulated rotational motion stimulus by continuously drifting stripes presented on translucent screens by projectors placed on either side of the fly. The arrows on the screens signify the direction of drifting gratings, and the arrows on the torque meter signify the direction of torque produced by the fly in response to the motion stimulus – a counterclockwise (CCW) rotational stimulus produces CCW torque as the fly attempts to follow the direction of moving gratings. (right) Similarly, a fly presented with a front-to-back motion stimulus will modulate its forward thrust, as measured by a thrust meter. Figure modified from Gotz (1968).

1.4.2 Visual stimuli and quantitative behavior

Two primary categories of experimental equipment are needed to conduct this sort of fly vision research in the laboratory. First, there must be a means to present well-defined visual stimuli to an

animal. This has often been accomplished with projectors or LED displays (Hubel & Wiesel, 1962; Lindemann et al., 2003), or even as simply as moving painted pictures with a motor (Gotz, 1964). Visual stimuli can consist of the presentation of unique patterns to test learning (Brembs & Heisenberg, 2000) or apparent motion in the form of gratings, moving bright/dark edges, and starfields (Strother et al., 2017; Theobald, Ringach, & Frye, 2010).

Secondly, the behavioral response of interest must be detected and recorded. Freely-moving animal behaviors are often detected and measured using optical sensors or by cameras focused on the animal and analyzed by tracking software (Lister, 1987; Robie et al., 2017). Tethered walking behaviors are typically observed by the rotation of an air-suspended ball mimicking the relative movement between a fly and the ground (Takalo et al., 2012), while tethered flying behaviors are typically measured with optical recordings of the wingbeats or mechanical measurements of flight forces (Gotz, 1964; Reiser & Dickinson, 2008).

1.4.3 Genetic tools for *Drosophila* neuroscience

Research in *Drosophila* has played an important role in the field of genetics; it was in this model system where the theory of chromosomal inheritance began to develop (Morgan, 1915). Our current extensive knowledge of and ability to manipulate the *Drosophila* genome has been an invaluable resource to many neuroscientists. Proteins have been discovered which allow researchers to visualize the morphology of neurons through fluorescence (Chalfie, Tu, Euskirchen, Ward, & Prasher, 1994), visualize neural activity through fluorescence change (Chen et al., 2013; Miyawaki et al., 1997), and grant ability to externally activate or silence neural activity (Banghart, Borges, Isacoff, Trauner, & Kramer, 2004; Kitamoto, 2001). Furthermore, the ability to target the expression of these experimental proteins to distinct subsets of neurons and neuron cell-types using expression-control systems such as the GAL4/UAS system (Brand & Perrimon, 1993) allows for an unrivaled ability to dissect neural circuits in the *Drosophila* brain, piece by piece (Luo, Callaway, & Svoboda, 2008; Sjulson, Cassataro, DasGupta, & Miesenböck, 2016).

1.4.4 The *Drosophila* motion vision system

Aided by this vast experimental toolkit, the motion vision system of the fly is one of the best examples of our ability to understand and map a complex neural computation (Borst et al., 2010a) (Figure 1.4). The fly optic lobes are characterized by a columnar structure resulting from neural superposition of the individual facets (ommatidia) of the fly's eyes (Braitenberg, 1967). The columnar structure shows persistent retinotopy throughout the optic lobe – a coordinated spatial mapping from the visual field onto the anatomy (Fischbach & Dittrich, 1989). Within each column, a

separate pathway for the detection of light increments (the ON pathway) and light decrements (the OFF pathway) is developed (Joesch, Schnell, Raghu, Reiff, & Borst, 2010). Directional selectivity emerges further "downstream" in the Lobula Plate in T4 and T5 cells (for the ON and OFF pathways, respectively) by the sequential excitation of cells with neighboring receptive fields (Strother et al., 2017) – this combination of visual stimuli offset in both space and time had long been hypothesized as a fundamental component necessary for elementary motion detection (Hassenstein & Reichardt, 1956).

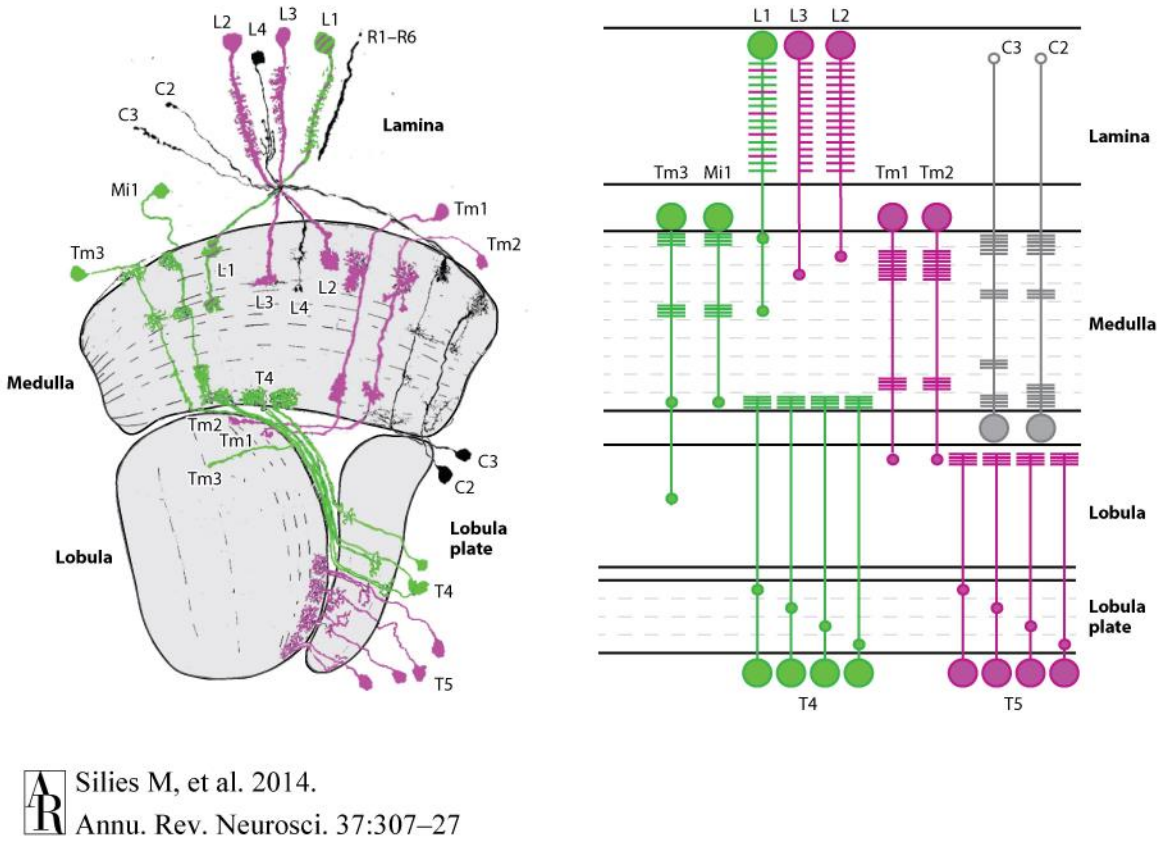

Silies M, et al. 2014.
Annu. Rev. Neurosci. 37:307–27

Figure 1.4: *Drosophila* optic lobe structures and cell types implicated in motion vision.

(left) The optic lobe of *Drosophila*, with primary structures labelled (Lamina, Medulla, Lobula, and Lobula Plate) and cell-types implicated in the motion vision pathway drawn by camera lucida of Golgi stainings. Neurons implicated in the ON motion pathway are drawn in green, and those implicated in the OFF pathway are drawn in magenta (others drawn in black). (right) A schematic representation of neurons in the motion pathways, with dendrites indicated as blocks of horizontal lines, axon terminals indicated by small circles, and somata indicated by large circles. Dashed lines indicate layers within the Medulla and Lobula Plate structures. All colored cells shown are present in all columns of the optic lobe, maintaining a consistent retinotopic map from the Lamina to the Lobula Plate. 4 subtypes of T4 and T5 cells are shown, one each for selectivity towards back-to-front, front-to-back, upward, or downward motion. Figure modified from Silies, Gohl, & Clandinin (2014).

While our ability to describe this system in such detail is impressive, there are still many gaps in our understanding of every stage of this process and new components of this system are constantly being identified and described (Takemura et al., 2017). Furthermore, relatively little is known about how elementary motion information in the optic lobe is integrated and further processed in the central brain. In chapter 3, I describe the development of a powerful and flexible new tool for delivering visual stimuli, designed to accommodate and improve a number of experiment types important for vision research. In chapter 4, I use this new visual display system to study and describe previously uncharacterized cells and circuits important for processing higher-order motion information from the optic lobe.

Chapter 2: Electrophoresis of fluorescent tracers for anatomical and functional imaging of insect auditory circuits

2.1 Abstract

The ability to deliver fluorescent dyes and tracers into populations of neurons has long proven to be an indispensable technique to visualize their anatomy and analyze their function. In some model systems, the genetically-targeted expression of fluorescent proteins is the method of choice to label neurons; however, in many organisms (such as locusts and crickets, which are of particular interest in the field of acoustic communication), these genetic tools are not available and alternative labeling methods are limited. In this chapter, I describe a new method for neuronal labelling by electrophoretic dye delivery from a suction electrode directly through the neuronal sheath of nerves and ganglia in insects. I delivered polar tracer molecules into the locust auditory nerve without destroying its function, simultaneously staining peripheral sensory structures and central axonal projections. Through the electrophoretic delivery of calcium indicators, *in vivo* optical imaging of sound-evoked activity was achieved. Furthermore, I successfully labelled local neuron populations directly through the surface of the brain, giving the ability to target more neuron subpopulations than just peripheral nerves. The method provides a new tool for studying how stimuli are processed in peripheral and central sensory pathways and is a significant advance for the study of nervous systems in non-model organisms.

2.2 Introduction

2.2.1 Current labelling methods for non-model systems

The delivery of dyes into single neurons and populations has long been used to visualize their anatomy and function. Metal ions, fluorescent dyes, and tracers delivered intracellularly into neurons can spread throughout the cytosol, allowing for the visualization of the cell's geometry and location of its projections (Stretton & Kravitz, 1968). While some methods deliver molecules to be later visualized by precipitation (Pitman, Tweedle, & Cohen, 1972) or enzymatic reaction (Huang, Zhou, & DiFiglia, 1992), the delivery of fluorescent molecules allows for more immediate observation by fluorophore activation, and when coupled with electrophysiological recordings of the stained neurons can be a particularly powerful technique (Gilbert et al., 1991). With the advent of calcium indicators, dye delivery also allows for the visualization of neuronal function in numerous areas simultaneously (Stosiek et al., 2003).

With a range of fluorescent dyes and functional indicators at many wavelengths now available, the delivery of dyes into neurons of interest remains still an important obstacle, with numerous methods being developed over the years to accomplish the task. More recently, gene-targeted expression of fluorescent proteins has offered profound improvement in ability to target both large populations as well as specific cell types and has become a dominant method (Brand & Perrimon, 1993; Duffy, 2002). However, due to the method's requirement of having a sequenced genome and a library of genetic tools, this method is not applicable for many organisms. One such system is the auditory system of orthopterans (locust/crickets), often utilized in the study of the neural basis of insect acoustic communication (Hedwig, 2006; Yager, 1999), thus motivating the use of alternative dye delivery methods.

Dyes and tracers can be delivered through diffusion into the neurons of damaged or cut nerves (Kristensson & Olsson, 1976). Anterograde or retrograde transport of a fluorescent dye – typically coupled to dextran to facilitate transport – from a nerve's cut end allows the study of morphology and central projections of nerves (Horch et al., 2011), though the destruction of the nerve precludes the possibility of simultaneously studying the activity patterns of the labelled neurons. Iontophoretic injection of polar dyes with an intracellular electrode is a popular method for staining an individual neuron to study its morphology after measuring its electrophysiological properties (Gilbert et al., 1991; Rehbein et al., 1974) and has even been coupled with delivery of calcium indicators (Sobel & Tank, 1994). Similarly, local electroporation of dyes into nearby cells by a glass microelectrode allows the extracellular labelling of individual or clusters of cells in a location of interest (Brandt & Apkarian, 1992; Spalthoff, Gerdes, & Kurtz, 2012). However, the necessarily small size of the glass microelectrode limits the number neurons that can be labelled.

Bath application or pressure-injection (multicell bolus loading, or MCBL) of cell membrane-permeant dyes allows for the simultaneous staining of much larger populations, which is particularly useful when using calcium indicators to simultaneously study the activity of a large number of neurons in an animal (Ogawa & Kajita, 2015; Stosiek et al., 2003). However, even this method is not without its limitations; only a fraction of fluorescent indicators are cell-permeant, and the amount of delivered dye is relatively low as compared to microelectrode delivery techniques, resulting in a relatively low contrast of labelled cells to background.

2.2.2 Electroporation, electrophoresis, and iontophoresis

A significant difficulty in delivering dyes into neurons comes from connective tissue, including the neural sheath or neural lamella (Carlson, Juang, Hilgers, & Garment, 2000), and glial cells which cover nervous tissue, acting as a blood-brain barrier in the insect and prevents entry of foreign

molecules. All dye delivery methods described in the previous section involve physically breaking this barrier in some way, even if only to slightly puncture using a micropipette. However, molecules have been delivered through other kinds of biological barriers without causing manual physical damage of the tissue. Iontophoresis, for example, allows the transfer of polar molecules across a variety of biological membranes, including connective tissue. In this method, an external electric field can be used to deliver drugs through the skin, e.g. for transdermal medication delivery in humans (Rawat, Vengurlekar, Rakesh, Jain, & Srikarti, 2008).

Successful transport across dense connective tissue is not enough to deliver molecules into cells; the cell membrane of individual cells acts as the final barrier to entry. Some dyes have been developed to be cell-permeable and are able to cross cell membranes to enter into neurons from the surrounding tissues (Johnson, 1998). However, electric fields can also be used to transport non-cell-permeant molecules into cells by electroporation — theorized to be caused by the electric field's stabilization of spontaneous pores which transiently form in cell membranes – allowing molecules to transfer across the cell boundary (Weaver & Chizmadzhev, 1996). Electrophoresis – the movement of charged particles through a liquid by the electrostatic force – may further promote the transfer of polar molecules across cell membranes if the polarity of the electric field is chosen to align the electrostatic force in the direction of the target cells (Dukhin & Derjaguin, 1974). It may be possible to simultaneously leverage these concepts of electrophoresis, iontophoresis, and electroporation with a single electric current/field to facilitate transport of polar molecules across a variety of membranes and barriers.

2.2.3 Aims of this chapter

The shortcomings of non-genetic labelling methods prompted us toward the development of an alternative dye delivery method that can be used in a variety of animals while maintaining the integrity of the tissue. In this work I focused on the nervous system of locusts and crickets, aiming to use an electrophoretic/iontophoretic technique to deliver tracers across the neural sheath to label populations of neurons. I aimed to validate this technique through the anatomical labelling of known circuits in the locust nervous system and explore new areas in which this technique could be useful. Finally, I aimed to apply this technique to the delivery of functional indicators to measure neural activity in the auditory system of locusts and crickets.

2.3 Methods

2.3.1 Animals and dissection

Locusts (*Schistocerca gregaria*) and crickets (*Gryllus bimaculatus*) were reared in crowded conditions (28° C, 12:12 h light:dark cycles). Animals were selected for experiment 1-4 weeks following their final molt. The locust tympanal nerve and metathoracic ganglion were accessed by pinning the insect ventral side up in a lump of Plasticine and cutting a rectangular window in the ventral cuticle of the thorax. The dorsal side of the brain in locusts (Figure 2.8) was exposed by cutting through the cuticle behind the eyes and bending the anterior portion of the head forward. The brain in female crickets (Figures 2.9 and 2.10) was accessed by removing the cuticle between the eyes. In all cases some fat tissue and trachea were removed to provide a clear view of the nervous tissue. For all experiments, insects were placed on a custom modified microscope stage that could be fitted beyond a dissecting microscope or into the fluorescence compound microscope used for imaging.

2.3.2 Dye solutions and suction electrode procedures

For anatomical studies, the dye and tracer solutions used were Cobalt Chloride (Sigma-Aldrich 232696), Lucifer Yellow (Sigma-Aldrich L0259), Alexa Fluor 568-10,000 MW dextran, Texas Red-3,000 MW dextran (ThermoFisher Scientific D-22912 and D-3329), and Neurobiotin (Vector Laboratories SP-1120), were diluted to 2% in 4% tylose in water. For functional imaging, 2% solutions of Oregon Green 488 BAPTA-1 hexapotassium salt (ThermoFisher Scientific O-6806) and Fluo-6 hexapotassium salt (Luke Lavis, Jon Grimm, unpublished results) were used.

Suction electrode pipettes were hand pulled to size from polypropylene tubing (CTPC500-1000-5; 0.5 mm ID, 1.0 mm OD, Paradigm Optics, Vancouver, WA, USA) over a heat source. Smooth ends were cut with a scalpel and inner tip diameters measured under a microscope. Pipette tips of ~50 µm ID were used for the locust auditory nerve and pipettes of ~100 µm ID were used for cricket connective stainings and for brain surface stainings. Pipettes were back-filled with a 6% tylose solution (Tylose H200 NP2, ShinEtsu, Wiesbaden, Germany) in saline, with tylose serving as a thickening agent to prevent the dye from diffusing along the pipette shaft or leaking out of the tip. Dye solutions (2% dye in 4% tylose in water) were front-loaded into the pipette tip with suction. The pipette tip was inserted into a custom-made electrode holder with an internal cavity filled with the tylose/saline solution. The cavity allowed for the formation of small air bubbles at the interface of the electrode and the current-carrying solution without them breaking the electrical connection to the pipette (Figure 2.1).

2.3.3 Auditory stimulation

Sound stimuli were generated using Cool Edit 2000 audio software (Syntrillium, Phoenix, AZ, USA, now Adobe Audition) and were presented by Sinus Live, Neo 13s speakers (Conrad Electronics, Hirschau, Germany) placed 60 cm from the animal at 45 degrees left and right of the animals' midline and calibrated to 70 dB SPL using a measuring amplifier and microphone (Brüel and Kjær models 2610 and 4939, respectively; Nærum, Denmark). Sound was not delivered in a sound-proof chamber so background noise (<50 dB) was present. For experiments studying frequency response characteristics of the target neurons, sound pulses were generated as pure tones of the following frequencies: 2, 4, 6, 8, 10, 15, and 20 kHz. For all other experiments, 5 kHz sound pulses were used. For whole nerve recordings, each sound pulse was 100 ms in duration and presented at 2 Hz, while for calcium imaging each pulse was 200 ms in duration presented every 5 s to allow the calcium fluorescence signal to return to baseline between stimuli. For presenting calling song patterns, 0.25 s chirps were created, consisting of 3, 6, or 25 5 kHz pulses (at 50% duty cycle) with each chirp spaced 0.1 s apart and lasting for 30 s. For all experiments, each sound pulse began with a 10 ms linear rise to 70 dB and ended with a 10 ms linear fall.

2.3.4 Whole-nerve recordings and current injection

After dye had been loaded into the suction electrode, the pipette tip was carefully sealed to the target tissue by gentle suction. A platinum reference electrode was placed in the hemolymph beside it. Whole-nerve activity was recorded via potential readings between the suction and reference electrode with a differential amplifier (model 1700, A-M Systems Inc. Carlsborg, WA, USA,) and sampled at 44 kHz with Spike2 (v7, Cambridge Electronic Design, Cambridge, UK). For electrophoretic dye delivery, 40 µA current pulses with the polarity chosen to match that of the dye were delivered at 1 Hz and 250 ms width with a stimulus isolation unit (stimulus isolator A360, World Precision Instruments Ltd, Hitchin, UK) (Figure 2.1). Current pulses were delivered for 15 seconds for functional labelling and either 30 seconds or 2 minutes for anatomical stainings, depending on the tracer. Following current injection, the insect was kept at 4° for 6-48 hours to allow the dye to spread in the target neurons; the dye spreading speed was approximated at 500 µm/hr. Spread time for dye delivery was typically 6 hours, but with two exceptions: for delivery in the tympanal nerve ~4 mm from the ganglion the spread time was 24 hours to allow visualization in both the metathoracic ganglion and the auditory organ (Fig. 2.2), and for delivery in the cricket abdominal A3-A4 connective the spread time was 48 hours to reveal projections in the brain and terminal ganglion (Fig. 2.4).

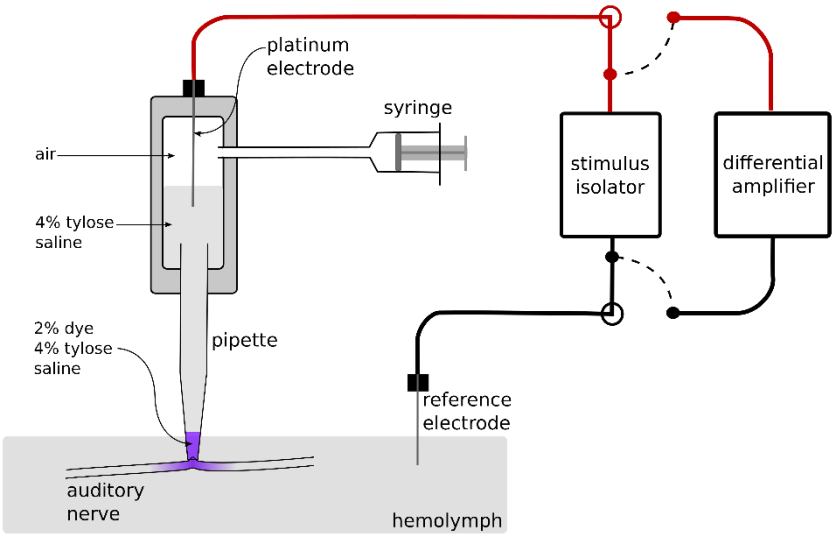

Figure 2.1: **Diagram of apparatus for dye delivery and whole-nerve recording.**

A custom designed electrode holder connects a pipette front-loaded with dye solution to a syringe for creating suction and to a platinum electrode for measuring voltage or supplying current. The target nerve of an insect is attached to the pipette tip with gentle suction. A reference electrode in the hemolymph surrounding the target nerve closes the electrical connection to the pipette electrode. The electrodes can be connected either to a differential amplifier for whole-nerve recording or to a stimulus isolator unit for applying direct current for electrophoretic dye delivery.

2.3.5 *In vivo* preparation for imaging

For anatomical imaging, after the dye had spread, ganglia and hearing organs were dissected, fixed, and cleared using standard histological methods with para-Formaldehyde, ethanol, and methyl salicylate. Cobalt stainings were first bathed in 2% ammonium sulfide for 5 minutes to produce a black cobalt-sulfide precipitate prior to fixation. Neurobiotin stainings were processed as previously described (Stefan Schöneich, Schildberger, & Stevenson, 2011). Images of stained tissue were taken with a Zeiss Axiophot microscope under bright-field or epifluorescent illumination using a Canon EOS 6D SLR camera. Confocal stacks of fluorescent stainings were obtained with a Leica SP5 with laser excitation light and filter cubes matching the excitation and emission spectra of the fluorophores. Max projections of confocal stacks were calculated in ImageJ (Abràmoff, Magalhães, & Ram, 2004).

For live imaging of delivered calcium indicators, insects tethered in plasticine were mounted under a Leica DMLFS microscope. The locust metathoracic ganglion was mechanically stabilized by cutting the ascending connectives, placed on a small silver plate and lifted away from surrounding tissues; the cricket brain was stabilized with minutien pins placed through the head cuticle. The

microscope was fitted with a monochromator (Cairn, Faversham, UK; 488 nm, 10 nm band width) for indicator excitation and a cooled CCD camera (Andor iXon DV887, Andor Technologies, Belfast, UK) for image recording. Camera image timing was controlled by an external trigger set at a rate of 20 Hz and recorded simultaneously with an acoustic stimulus using Spike2. Image time-series were motion-stabilized by template matching in ImageJ. ΔF/F fraction change in fluorescence maps were calculated by normalizing the measured fluorescence of all frames to the average of the first 50 frames pre-stimulus, selecting the frame with the peak response, and smoothing the frame with the "Mean 3D" filter in ImageJ by 2 pixels in the x, y, and t dimensions.

2.3.6 Data analysis

During electrophysiological recordings of the locust tympanal nerve, animals were presented with numerous repetitions of each sound pulse: 13-25 repetitions for each frequency in frequency responses curves and 25-50 repetitions for the 5 kHz presented alone. A rectified average recording for each animal and condition was calculated by taking the root mean square of the multiple repetitions at each data point; the signal for each repetition being aligned to the stimulus onset. The recordings displayed were down-sampled to 4.4 kHz by averaging in 10-sample bins. An overall average and standard error of measurement (SEM) signal was calculated from the rectified average recordings from 4 insects.

In calcium imaging experiments, ΔF/F traces for drawn regions of interest (ROIs) were calculated for each ROI by the per-frame average fluorescence change relative to the pre-stimulus average. An average ΔF/F trace for each staining and condition was calculated by averaging the ΔF/F traces for 5 repetitions of the presented stimulus in that staining. To calculate the average ΔF/F trace over multiple stainings, the average trace for each staining was first normalized to its own maximal response, since the absolute response varied significantly between stainings, from 5-40% maximum ΔF/F. The average/SEM was then calculated from the normalized average traces from the multiple stainings.

2.4 Results

2.4.1 Anatomical staining of whole nerves with electrophoresis

I initially focused staining efforts on the locust auditory nerve, both for its ease of access and prior characterization of its central and peripheral projections. I attached the tip of a suction electrode (filled with polar tracers) to the surface of the intact nerve halfway between the metathoracic ganglion and the hearing organ to attempt to simultaneously stain both structures

(Figure 2.2, left). The ability to detect whole-nerve field potentials and extracellular spike activity in response to acoustic stimuli served to indicate a good contact and tight seal between the electrode tip and the surface of the nerve. Pulsing current through the electrode (-40 µA, 250 ms pulse width at 1 Hz for 30 seconds) caused transfer of the dye from the pipette through the sheath into the auditory nerve. (See Figure 2.1 for a diagram of the dye delivery apparatus.) Following the procedure, the specimens were kept at 4° C and the dye allowed to spread for 24 hours. After dissection and standard histological processing, fluorescent imaging of the auditory organ and the CNS demonstrated the simultaneous anterograde and retrograde transport of the tracers. Both the peripheral cell bodies and dendrites of the scolopidial sensory neurons in the auditory organ and their central axonal projections in the auditory neuropils in the metathoracic ganglia were successfully stained. (Figure 2.2, right).

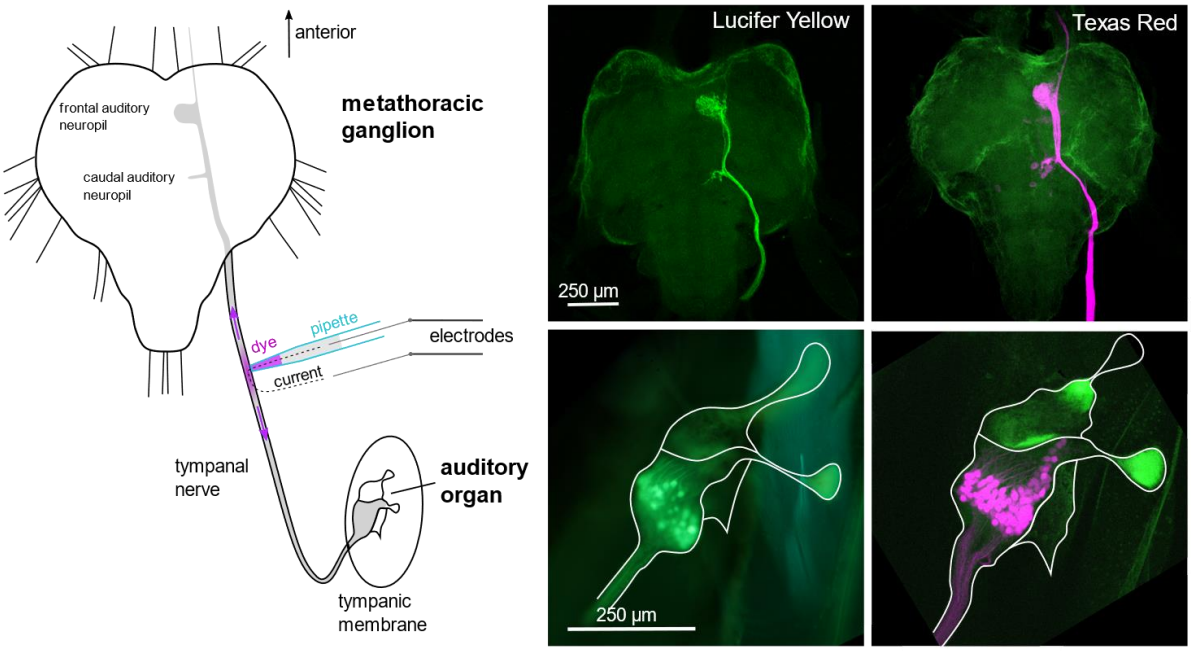

Figure 2.2: Neuroanatomical imaging of tracers delivered by electrophoresis across the nerve sheath.

(left) Diagram of electrophoresis of dye across the sheath of the locust auditory nerve using a suction electrode. The auditory pathway in the ganglion is indicated in light grey. (right) Lucifer yellow and Texas Red-3,000 MW dextran stainings of auditory afferents visualized by confocal microscopy of fixed/cleared metathoracic ganglia and auditory organ. Both the metathoracic ganglion and auditory organ were labelled in the same specimen by bidirectional spreading of the tracer. Background tissue autofluorescence and Lucifer yellow fluorescence is shown in green, and Texas Red-3,000 MW dextran fluorescence in magenta.

With an increase in the total current injection time to 2 minutes, Cobalt ions as well as Alexa-568-10,000 MW dextran were also successfully delivered (Figure 2.3). Under this protocol, dye was observed to spread to the mesothoracic ganglion 6 mm from the injection site and beyond; however, dye concentrations in fibers ascending beyond the mesothoracic ganglion became too dilute to easily visualize.

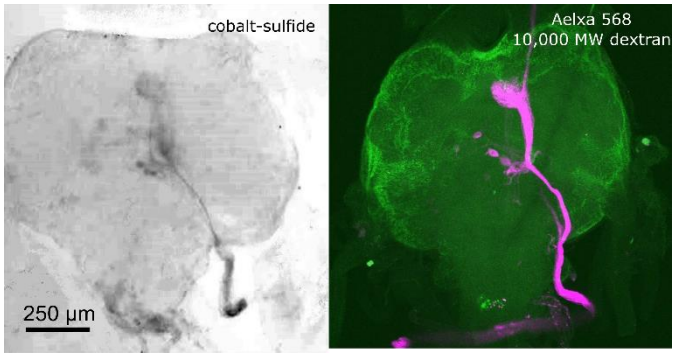

Figure 2.3: **Anatomical imaging of locust auditory neuropils using other molecular tracers.**

(left) Bright-field imaging of cobalt-sulfide precipitate in locust metathoracic auditory neuropils following electrophoretic delivery of cobalt into the auditory nerve. (right) Epifluorescence imaging of auditory fibers and neuropils following electrophoretic delivery of Alexa 568-10,000 MW dextran.

2.4.2 Neurobiotin staining for large neurons

To investigate the ability of this technique to label neurons over even greater distances, I electrophoretically delivered Neurobiotin into the abdominal connective of the cricket CNS and allowed 2 days for the tracer to spread in both directions. After conventional antibody staining against Neurobiotin which served to enhance tracer detection (tracer concentration was expected to be very dilute in long distance labelling), I observed numerous stained fibers reaching the entire length of the CNS (~20 mm), with the cell body and main dendrites of the cercal medial giant interneuron (MGI) (S Schöneich & Hedwig, 2015) clearly identifiable in the terminal ganglion as well as its putative axonal arborizations in the brain (Figure 2.4).

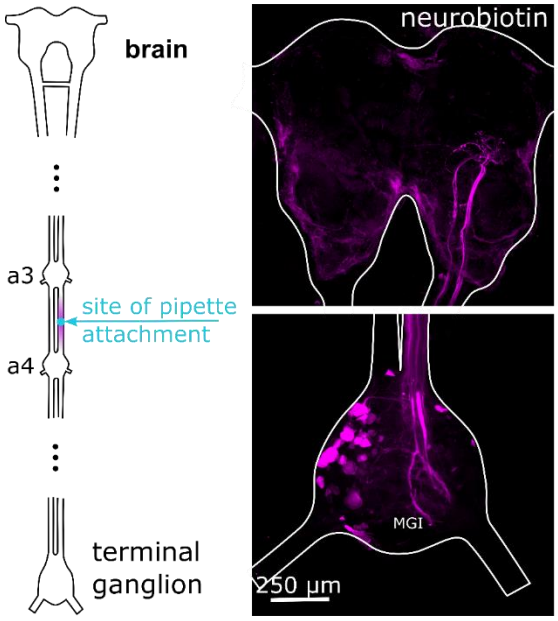

Figure 2.4: Long distance labelling with Neurobiotin.

Delivery of Neurobiotin (neurobiotin-antibody staining shown in magenta) into a cricket connective between abdominal ganglia 3 and 4 labelled neuronal projections in the brain and terminal ganglion; the dendrites of the cercal medial giant interneuron (MGI) are indicated.

2.4.3 Functional imaging of auditory neuropils

Having validated the method for delivering indicators for anatomical and imaging, I next aimed to adapt this labelling technique to allow optical imaging of neural activity through the delivery of calcium indicators. While this electrophoretic dye delivery imposed no observable physical damage to the nervous tissue, the possibility that the current and dye injection caused unseen electrical damage of the stained neurons remained. To assess potential nerve damage from the technique, I measured whole nerve field potentials of the auditory nerve, evoked by sound pulses presented to the locust, both before and after the dye injection procedure. Comparing the pre and post-dye injection neural activity for a small number of electrophoretic parameters, I observed that increasing current amplitude or duration caused both more dye to be delivered but also caused more functional disruption (Figure 2.5).

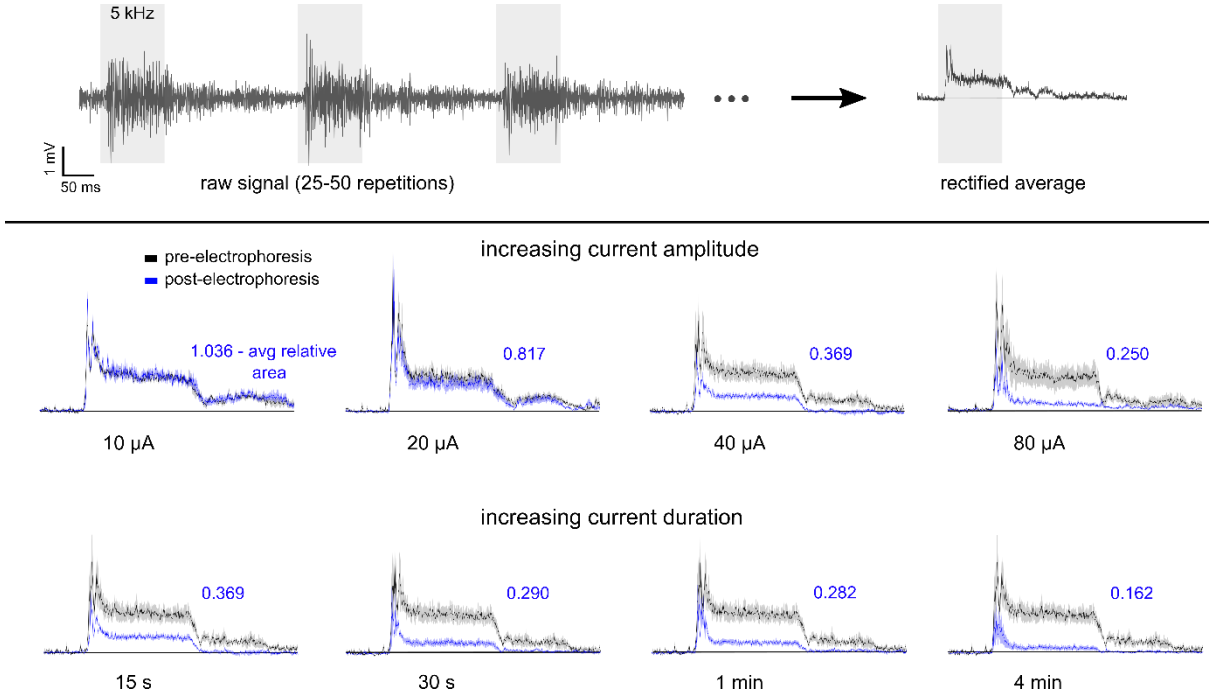

Figure 2.5: **Effects of electrophoretic parameters on sound-evoked auditory nerve potentials.**

(top) Illustration of calculating the rectified average signals from multiple repetitions of the 5 kHz stimulus-evoked whole nerve field potentials. Due to background noise being present while delivering the sound stimuli, a minimum of 25 repetitions of sound-evoked activity were averaged for each recording. (middle) Effects of increasing the electrophoresis current amplitude on sound-evoked potentials. Current pulses of 10, 20, 40, and 80 µA were delivered for 15 seconds (1 Hz pulse rate at 25% duty cycle; Fluo-6 loaded in the pipette) to the auditory nerve of different locust specimen. Pre-electrophoresis signals were recorded prior to any current injection; post-electrophoresis signals were recorded immediately after. The area under the curve of the post-electrophoresis responses relative to their corresponding pre-electrophoresis recordings are displayed for each condition. (bottom) Effects of increasing current injection duration on sound-evoked potentials. After a pre-electrophoresis recording was taken, a total of 4 minutes of 40 µA current injection was delivered, with additional recordings being taken at intervals of 15 s, 30 s, 1 min, and 4 min.

A current injection amplitude of 40 µA was chosen for the electrophoretic delivery of calcium indicators in order to deliver a significant amount of dye into the nerve so that dye concentrations would be high after spreading, while keeping the nerve functional. I targeted the intact locust auditory nerve ~1 mm to the metathoracic ganglion with the aim of labeling these sensory neurons for functional imaging in the central neuropils. Current injection times of 15 seconds were sufficient to deliver the calcium indicators Fluo-6 (Figure 2.6, left) and Oregon Green (Figure 2.7, left) into the afferents; longer injection times overloaded the neurons with dye and reduced their viability.

With this protocol the calcium indicators spread within 6 hours into the metathoracic auditory neuropils. Upon acoustic stimulation, activity of the live afferents as indicated by changes in the brightness of the fluorescence signal could be detected with a sensitive CCD camera. I presented 100 ms sound pulses in the range of 2-20 kHz at 70 dB SPL while imaging the neuronal responses. Normalizing the fluorescence signal to the pre-stimulus average, I observed a 5-40% raw ΔF/F correlated to the sound pulses in the 2-10 kHz frequency range. The optical signals accurately reflected the frequency-response characteristics of the electrical signals from the auditory nerve as determined by whole-nerve recordings taken prior to the dye-loading procedure (Figure 2.6, right), demonstrating that the method effectively labels auditory sensory neurons for functional imaging without apparently altering their encoding properties.

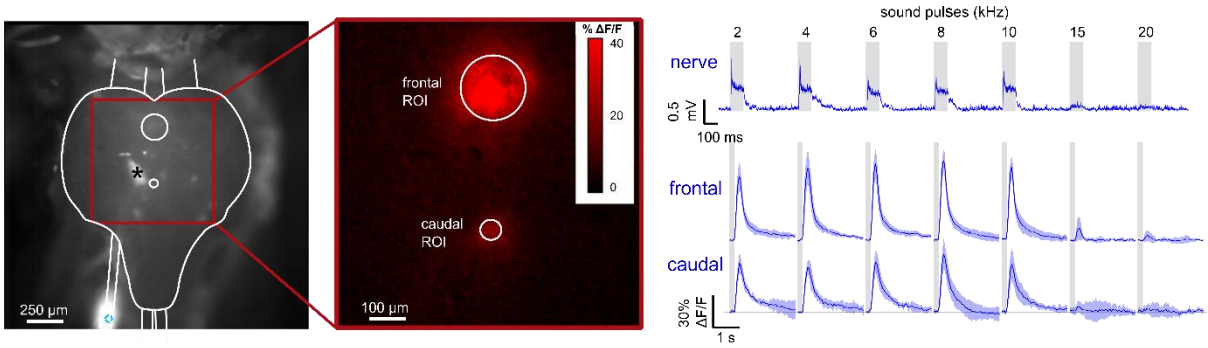

Figure 2.6: Functional imaging of locust metathoracic auditory neuropils by delivery of calcium indicators

(left) Calcium indicator Fluo-6 delivered into the locust auditory nerve and imaged in the live metathoracic ganglion by epifluorescence microscopy. The bright white patches in the center-left of the ganglion (asterisk marking largest patch) are artefacts due to reflections in the saline. (middle) Map of peak fluorescence change (ΔF/F) of the metathoracic ganglion in response to 5 kHz sound pulses; ROIs drawn for frontal and caudal neuropils. (top-right) electrophysiological recording of tympanal nerve activity to sound pulses of 2-20 kHz as measured by suction electrode prior to dye delivery; traces are rectified average signals (± SEM in light blue, n=4). (bottom-right) Normalized ΔF/F traces showing frequency-response characteristics of frontal and caudal ROIs assigned to the corresponding auditory neuropils (± SEM, N=6).

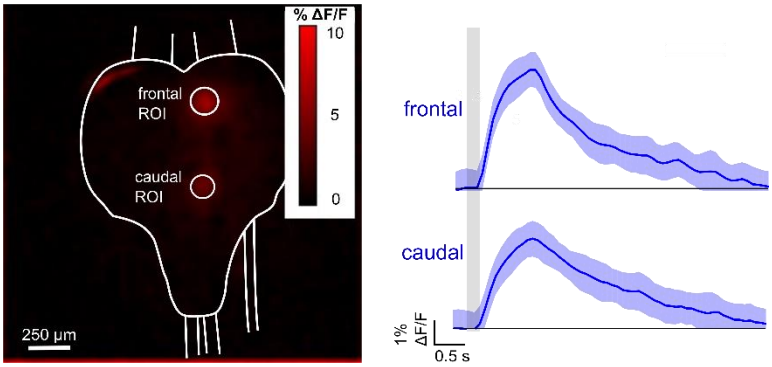

Figure 2.7: **Functional imaging in locust auditory neuropils using Oregon Green 488.**

(left) Fluorescence change map of a locust metathoracic ganglion during acoustic stimulation following electrophoretic delivery of Oregon Green 488 BAPTA-1. ROIs drawn for frontal and caudal neuropils. (right) Average fluorescence change of locust metathoracic auditory neuropils during 20 repetitions of a 5 kHz sound pulse (± SEM in light blue).

2.4.4 Targeting brain neurons through the sheath

To explore further new targets for this technique, I attached the suction electrode to the surface of the locust brain, delivering Texas Red-3,000 MW dextran through the sheath into the dorsolateral protocerebrum to which axons of the ascending auditory pathway project (Rehbein, 1976) (Figure 2.8). The neural tissue directly beneath the injection site became highly saturated with dye, though fibers of ascending or descending interneurons and cell bodies of local brain neurons were clearly labelled outside this area, demonstrating that the technique can also allow tracing and visualizing local neuron populations in ganglia and the brain.

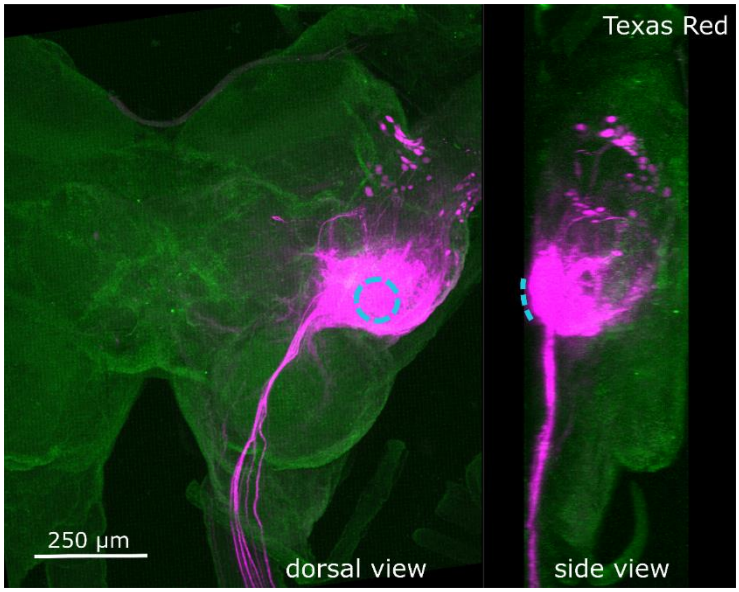

Figure 2.8: Locust brain surface staining.

Texas Red-3,000 MW dextran delivered into the locust brain through its surface without removing the sheath (teal dotted-line showing site of pipette attachment), imaged by confocal microscopy.

Finally, I applied this method to the anterior ventral neuropil of the cricket brain where studies with intracellular recordings have identified a network of local auditory neurons for song pattern recognition (Stefan Schöneich et al., 2011). Suction electrodes attached to the surface of this brain area reliably recorded auditory evoked field potentials which facilitated precise electrophoretic delivery of Fluo-6 through the sheath into the auditory neuropil, labelling numerous cell bodies and neurites (Figure 2.9, left). Presenting sound pulses at the carrier frequency of the species-specific calling song caused an increase in relative fluorescence change in small subset of all labelled neurons (Figure 2.9, right). Repeated presentation of the sound stimulus (0.1 s, 5 kHz, 70 dB SPL) revealed cell bodies of neurons close to the midline of the brain that were reliably activated by sound, with one region (ROI 1) potentially showing an accumulation of activity.

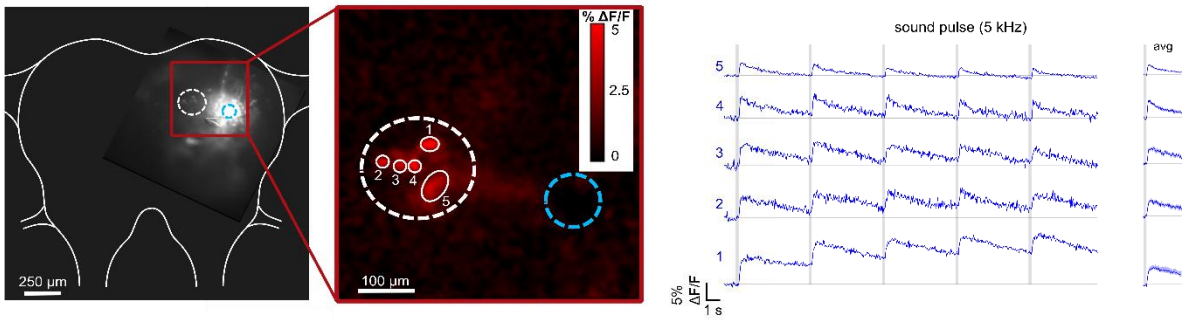

Figure 2.9: Sound-evoked activity directly visualized in the cricket brain.

(left) Fluo-6 delivered into the anterior auditory neuropil in a cricket brain; site of pipette attachment circled in light blue and region of sound-evoked activity circled in white. (middle) Fluorescence change map with ROIs drawn for active cell bodies or neuropil regions. (right) Absolute ΔF/F traces of each ROI showing activation correlated to 5 kHz sound pulses. (right), average ± SEM of these 5 activations for each ROI.

Another instance of calcium indicator delivery into this region revealed not only activity to the carrier frequency auditory stimulation, but also was most strongly activated by the carrier-specific song pattern. 5 kHz sound pulses presented at the species-specific pulse rate produced a greater excitation than those presented at higher or lower pulse rates, even though the total duration of 5 kHz sound pulses was the same in all cases. For the correct pattern only, I observed both a transient increase for each chirp as well as a sustained tonic activity over the duration of the calling song (Figure 2.10).

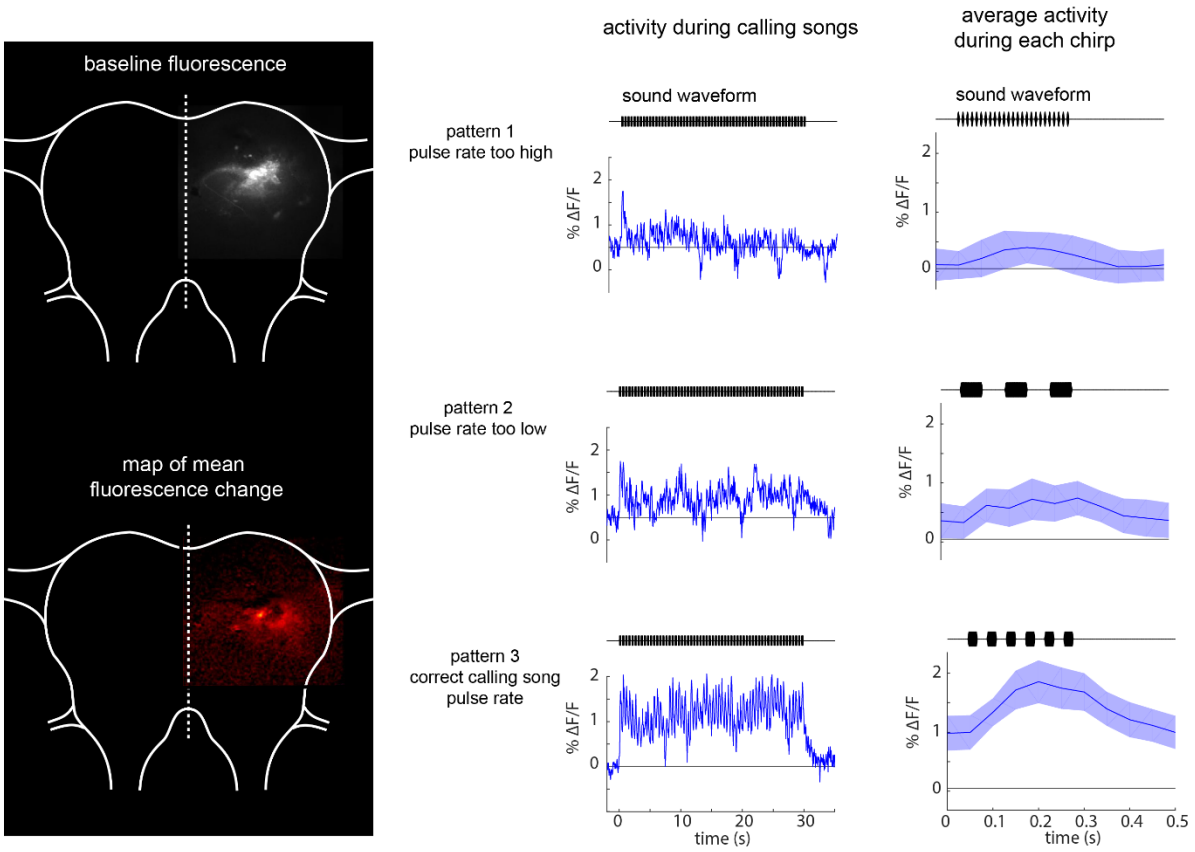

Figure 2.10 Calling song pattern specificity in the cricket brain.

(top-left) Fluo-6 delivered into the anterior auditory neuropil in a cricket brain. (bottom-left) Fluorescence change map with ROIs drawn for active cell bodies or neuropil regions. (middle) Absolute ΔF/F traces during presentation of calling song patterns (right). Incorrect calling song pulse rates (patterns 1 and 2) produced little activity, but the correct pulse rate (pattern 3) caused sustained high activity. Average ± SEM response to each chirp.

2.5 Discussion

While the conditions of electrophoresis/electroporation used in this study successfully delivered dye for both anatomical and functional imaging, the parameter space was not completely explored and may further be improved to optimize dye delivery and minimize possible adverse effects. Higher current amplitudes (20-40 µA vs 5-10 µA) and extended injection times (1-4 minutes vs 15-30 seconds) increased the amount of dye delivered, though at the expense of disrupting signal transduction in the nerve as measured by recording whole-nerve activity before and after the procedure under the various conditions. Anatomical studies may not be concerned with signal disruption and opt for conditions that deliver more dye, while functional imaging experiments or

behavioral studies that require unaffected neural function – and lower indicator concentrations to prevent oversaturating the neuron with the indicator – may use more gentle conditions.

All functional imaging presented in this study was recorded approximately 6 hours after calcium indicator delivery, as this minimum time was required to allow a proper spreading of the dye. Neuronal activity in the neuropils could also be imaged 24 hours after dye delivery in the auditory nerve though typically resulting in a lower ΔF/F, possibly due to the indicator not being retained within the neurons or due to the declining health of the animal. Functional imaging may be possible beyond one day and even greater timescale after dye delivery, if the animal can be kept in a good physiological condition.

There are many considerations when interpreting circuit function using this electrophoretic method of calcium indicator delivery. Due to the apparent degradation of function as measured by whole-nerve field potentials (Figure 2.5) some neuronal function may be lost over the course of the procedure, potentially due to disruption of electrical signaling or intracellular transport of molecules caused by the electroporation procedure or by dye precipitate, which was often observed at the site of dye injection. Furthermore, as is the case with all methods using calcium indicators, the presence of large amounts of the functional indicator may act to buffer significant amounts of intracellular calcium, effectively increasing the amount of calcium necessary to perform the same circuit functions. The relatively slow dynamics of calcium indicators as compared to electrophysiological recordings of neurons means that calcium imaging is likely to miss fast, brief electrical activity and thus may only be suited to detecting circuit functions that feature sustained neuronal activation. It is encouraging that the frequency-response characteristics of the locust auditory nerve appeared unchanged after electrophoretic delivery of a calcium indicator (Figure 2.6), though one test which could potentially provide even stronger evidence for the relative innocuousness of the method would be to test the phonotaxis behavior of the animal before and after the procedure to the species-specific calling song over non-preferred songs, as that could directly test whether any essential circuit function for this complex sensation and behavior was lost.

Only polar tracer molecules were used in this work, though uncharged tracers might also be delivered by electro-osmosis as has been reported for transdermal iontophoresis (Pikal, 2001). Since neurons could be successfully loaded with 10,000 MW polar dye molecules, DNA plasmids may also be capable of being delivered via a suction electrode, which has been demonstrated by local electroporation from a glass microelectrode (Haas, Sin, Javaherian, Li, & Cline, 2001). Plasmids encoding fluorescent proteins for cell labelling would require longer survival times but would overcome the issue of local extracellular dye buildup at the injection site, as well as advance the possibility of genetic modification in more systems.

This relatively non-invasive method delivers selectively anatomical and functional indicators into sensory pathways and neuropils of animals not amenable to genetic techniques; it thereby opens a new range of imaging studies. To the best of my knowledge, this method of dye delivery is currently the only non-genetic method that allows simultaneous anterograde and retrograde labelling of fiber populations in insect peripheral nerves and that allows the labelling of local interneuron populations in fully-intact ganglia and brains. This work also confirms that this technique of electrophoretic dye loading can be successfully used for functional labelling of populations of neurons in various locations in the insect CNS. I propose that it may also be used in other invertebrate species and that it may advance functional imaging studies in non-genetic model systems.

Chapter 3: Next generation LED display system for animal models of vision

3.1 Abstract

Simulating visual environments to head-fixed animals is a powerful method for studying the sensory control of complex behaviors in a laboratory setting. Advances in display technology have led to visual stimulus systems that produce more accurate, dynamic, and ethologically relevant simulations of natural environments. While consumer-based display technologies – such as LCDs and DLP projector systems – have been widely adopted for animal displays, we have established a display system based on custom-built modular LED 'panels' better suited to the needs of animal vision research. The primary advantages of our LED-based display are its high-speed operation, dynamic range and brightness, color control, brightness uniformity, ability to be configured into a variety of display geometries, and ability to be integrated and synchronized with other experimental equipment. Utilizing the faster display refresh rates of the system (up to 1 kHz), I conducted experiments that probed the upper limits of motion vision in *Drosophila melanogaster*. I also developed a flexible approach to presenting optic flow scenes for electrophysiology and functional imaging of motion-sensitive neurons. Finally, the system has been optimized for the on-line analysis of behavioral measures, image rendering, and display streaming with high frame rates and low latency, providing the ability to create fast and complex interactive virtual visual landscapes. To our knowledge, this is the first such system that addresses this full set of important technical challenges to support many vision science experiments.

3.2 Introduction

3.2.1 History of visual displays for animal research

Some of the earliest strategies for presenting visual stimuli to tethered animals were as simple as painting the inside of a drum and using a motorized unit to rotate the drum around the animal, simulating rotation within an environment (Gotz, 1964; Hassenstein & Reichardt, 1956); this method has still found use in recent studies (Liu et al., 2006). Projectors with screens placed in front of the tethered animal have long been popular to deliver a wide range of visual stimulus types (Gotz, 1968; Hausen, 1982; Hubel & Wiesel, 1962). Many other visual displays have been created to fill specific experimental needs; for example, using multiple rotating dots on a rotating stage allowed the fast mapping of the optic flow sensitivity of neurons over a large visual field area (Krapp & Hengstenberg,

1997). In recent decades, LED-based systems have also come into widespread use (Lehmann & Dickinson, 1997; Lindemann et al., 2003).

Typically, display systems have been designed to meet the demands of a specific experiment type or a small number of experiment types. One effort to build a display system using modular LED panels was undertaken to accommodate a wide range of vision research approaches (Reiser & Dickinson, 2008). This flexible system has been utilized for a wide variety of experiment types, such as visual place learning (Ofstad, Zuker, & Reiser, 2011), landmark orientation (Seelig & Jayaraman, 2015), and multi-sensory integration (Chow, Theobald, & Frye, 2011). As useful as this display system has proven to be, it remains limited in the complexity, resolution, and speed of visual stimuli it can deliver, leaving significant room for improvement.

3.2.2 Modern display capabilities

Significant progress has been made on the commercial side of LED-based display systems. Pixel density has increased, dynamic range has improved, and larger displays have been built – all while decreasing in price. Much of the technological improvements can be attributed to smaller components and faster processors. However, modern displays are not well-suited for insect visual systems for several reasons. LED-based displays are typically built from red, green, and blue (RGB) LEDs to match the responsivity spectra of photoreceptors in human cone cells (Wald, 1964), but most animals have a different set of photoreceptor responsivities (Osorio & Vorobyev, 2005). Modern displays typically have a refresh rate of 60 Hz, which satisfies human vision requirements but is below the flicker fusion frequency of many insect visual systems (Miall, 1978) and leaves little room for displaying fast apparent motion. Furthermore, commercial displays can often have significant latency between receiving and displaying frame information (due to buffering of frames in graphics cards), making them less than ideal for experiments that require precise timing and synchronization of the display to other elements of the experimental setup, such as in electrophysiology experiments. The resolution of modern displays are very impressive, but this is one aspect that may not add much benefit to insect vision research; the interommatidial angular distance in *Drosophila* is typically not below 4° (Buchner, 1971), so the bandwidth and processing power used to accommodate the significantly higher display resolution may be better spent elsewhere, such as to increase refresh rates.

Human eyes are forward-facing with a relatively limited visual field and a concentrated fovea in the center, making a flat rectangular screen sufficient to deliver a significant amount of visual information. For insects, whose side-facing eyes can receive visual input from a near-360° field of view, a flat rectangular screen is a poor representation of their typical visual experience. For

example, in *Drosophila*, the field of view encompasses almost the entire visual sphere, with a blind spot behind the fly that only spans a region of approximately 40° in azimuth (Buchner, 1971). This problem can be somewhat circumvented by arranging multiple individual displays around the animal (Straw, Lee, & Dickinson, 2010); however, flat screens often appear dimmer at greater viewing angles (which is greatest when two flat screens meet at an angle) which can make it difficult to maintain uniform brightness uniformity across the visual field.

3.2.3 Aims of this chapter

Researchers who study the visual systems of insects have benefited from custom-building display systems and should continue to benefit from the technological improvements in commercial electronics. The original modular LED display system described in Reiser & Dickinson (2008) has since received many incremental updates to improve the functionality of the system. It is currently in its 3rd generation, although it is still based on display technology that is ~15 years old. In this work, we aimed to develop and validate an entirely revamped system that includes modern technological advances and a simplified yet more integrated experimental control system. In this 4th generation (G4) LED display system, our goal was to incorporate as many of the design objectives as possible for animal vision research. We aimed to build a system with a faster refresh rate, brightness control and uniformity suitable to test luminance and contrast sensitivity, provide adequate visual field coverage, ability to choose LED colors tailored to the animal model and experimental setup, and ability to be synchronized and integrated with other experimental components. After validating the technical aspects of this system, I aimed to use these new capabilities to demonstrate the advances relative to other display technologies for addressing a variety of experimental questions.

3.3 Methods

3.3.1 Hardware and software

LED arenas were built using custom LED panels and arena printed circuit boards (PCBs), powered by 5V/10A desktop power supply – design files for arena components are available at https://bitbucket.org/iorodeo/panels_g4_hardware. The LED arena was controlled by a PC running Windows 7 with an FPGA PCIe card installed (National Instruments NI 7842R) and running a customized LabVIEW (Elliott, Vijayakumar, Zink, & Hansen, 2007) executable. MATLAB (Mathworks, Inc, Natick, Massachusetts, US) is used as the high-level control software to communicate with the LabVIEW program and control the display using custom MATLAB scripts and graphical user interfaces (GUIs); all software is available at https://github.com/misaacson01/G4_Programs.

3.3.2 Flies

Flies were reared under standard conditions (60% humidity, 16h light / 8h dark, cornmeal agar diet) at 25° C. Behavior experiments were performed on female Dickinson Lab (DL) genetic background flies, 3-5 days post-eclosion, while imaging experiments were performed on female flies 1-4 days post-eclosion expressing GCaMP6m in LPC1 cells (see Table 4.1 for full genotype information). Cell-type-specific expression was achieved using the Split-GAL4/UAS expression control system (Pfeiffer, et al., 2010).

3.3.3 *In vivo* preparation for tethered flying

Flies were prepared for flying behavior experiments as previously detailed (Reiser & Dickinson, 2008) and summarized here. Cold-anesthetized flies were glued to a tungsten rod (catalog #71600; A-M Systems) by the thorax with UV-curing glue (KOA 300-1; KEMXERT) and were given at least 30 minutes of recovery time (at room temperature and brightness) before testing, with all testing being completed within 5 hours of tethering. Tethered flies were positioned in a hovering posture (60° body angle) in the center of the LED arena for visual experiments.

3.3.4 *In vivo* preparation for calcium imaging

Flies were prepared for 2-photon imaging experiments using a method based on a previously described preparation (Seelig et al., 2010) with several modifications as summarized here. Cold-anesthetized flies were tethered to a fine tungsten wire using UV-curing glue (Loctite 3972; Henkel). The two most anterior legs (T1) were severed and sealed with glue to prevent the fly from grooming and obstructing its visual field. The tethered fly was positioned up to the opening of a custom-machined PEEK plastic conical mount to allow access to the back of the head for dissection and imaging while obstructing as little of the fly's visual field as possible (Figure 3.11). The fly was glued to the mount at the rim of the head and the upper thorax, sealing most of the mount's opening. The proboscis was glued to the stumps of the severed legs to further immobilize the head. The back surface of the fly's head was bathed in saline (Seelig et al., 2010) and a hole in the cuticle was cut to expose the posterior lateral protocerebrum (PLP) region of the brain using a fine tungsten needle and holder (Fine Science Tools #10130-05, # 26018-17). Muscles 1 and 16 (Demerec, 1965) were severed to reduce motion of the brain within the head capsule and excess fat was removed from the surface of the brain.

3.3.5 Visual stimuli

Visual stimuli were presented to tethered flies using 2 cylindrical configurations of the G4 display system as described in the main text (Figure 3.2). For imaging experiments, to further separate the LED emission spectra from GCaMP6m fluorescence, a long-pass gel filter (Deep Golden Amber gel filter, LEE Filters #L135S) was laid on top of the LEDs along with a diffusing filter (Full White Diffusion filter, LEE filters #216R) to prevent reflections from the gel filter.

All patterns that were displayed on the cylindrical displays were generated using a set of MATLAB scripts for parameterizing and visualizing moving grating patterns for this display system (described in the text, code available at https://github.com/misaacson01/Motion_Maker_G4). Displaying these patterns at multiple different speeds/temporal frequencies was accomplished by changing the rate at which the frames of the patterns are presented. These rates were defined using a set of MATLAB scripts for parameterizing and visualizing so-called "position functions", which specify the frame to be displayed for each refresh cycle (500 or 1000 Hz) of the display (code available at https://github.com/misaacson01/Function_Maker_G4). All experimental stimuli consisted of 100% contrast square-wave gratings.

For tethered flying experiments measuring behavioral reactions to optic flow gratings, a single trial of visual stimuli started with 2 seconds of closed-loop stripe fixation, followed by 2 seconds of the moving grating stimulus, followed by another 2 seconds of stripe fixation. The 4 seconds of stripe fixation segments were interspersed between all moving grating stimuli to promote good flying behavior for the duration of the experiments and to standardize their behavior at the start of each moving grating stimulus.

For calcium imaging experiments measuring the neuronal activity due to small-field motion stimuli, a single trial consisted of 2 seconds of a uniform frame (where the entire display is set at a brightness level halfway between that of the bright and dark bars of the grating patterns), followed by 1 second of moving gratings, followed by 2 seconds of the uniform frame, after which the arena was turned dark for 4 seconds to allow the arena to pitch to its new position. The increased time in between experimental visual stimuli allowed more time for the GCaMP6m fluorescence signal to return to baseline fluorescence levels. Experiments were organized using a randomized block trial structure – within a block, the complete set of visual stimuli were presented in a randomized order, and 3 blocks were presented such that each stimulus was shown 3 times.

3.3.6 Tethered flight equipment and analysis

The methods used for these behavioral experiments have been detailed previously (Lehmann & Dickinson, 1997; Reiser & Dickinson, 2008) but are summarized here. Wing motion of tethered flies

was measured using a “wingbeat analyzer” (designed and manufactured by D. Smith, JFI electronics shop, University of Chicago) that detects changes in the left and right wingbeats using an optical infrared detector of the wingbeat shadow created by an infrared (940 nm) LED placed above the fly. The relevant behavioral outputs of the wingbeat analyzer are the instantaneous measurements of the wingbeat amplitude of the fly’s left and right wings, the instantaneous difference between the left and right wingbeat amplitudes (left minus right, “L-R”), and the wingbeat frequency. These signals were acquired and logged at 1 kHz using the on-board data logging of the G4 display controller, and the L-R signal was processed separately using the fast (1 kHz refresh rate) on-board closed-loop mode of the G4 controller for stripe-fixation experiments. All flies were positioned such that the wingbeats as measured by the wingbeat analyzer and visualized through an oscilloscope were of similar shape and amplitude, and that the flies were able to fixate a stripe in fast closed-loop operation, where the L-R signal (a reliable measurement of yaw rotational torque) controlled the apparent rotation of a dark vertical stripe (30° wide) on a bright arena background.

Using the logged data of left and right wingbeat amplitudes, a time-series of “L-R” was calculated by subtracting the right wingbeat amplitudes from the left for every timepoint, and a time-series of “L+R” was calculated by adding the left and right amplitudes. The time-series of L-R, L+R, and wingbeat frequency (WbF) measurements in response to multiple repetitions of each visual stimulus were averaged together to produce a mean response for each fly, and this was computed for all visual stimuli. For the mean time-series of L-R, all data points were then normalized to the 98th percentile of the L-R measurement (a more robust procedure than normalizing to peak), which scaled the values to range from approximately -1 to +1, where -1 represents an approximately maximum yaw left (counter-clockwise) turn and +1 indicates an approximately maximum yaw right (clockwise) turn. For the mean time-series of L+R and WbF, all data points were normalized to the mean L+R and WbF measurements (respectively) during the 2 seconds prior to all experimental visual stimuli (2 seconds of stripe fixation immediately preceding the experimental stimuli), scaling the values from approximately 0 to 1, where 1 represents the baseline L+R and WbF levels prior to the start of experimental visual stimuli. For summary plots, a single value of the L-R, L+R, and WbF responses was computed from the time-series by averaging the mean time-series values during the 2 seconds of open-loop visual stimulus presentation. Both time-series and summary data are plotted as mean of all flies +/- SEM.

3.3.7 2-photon imaging and analysis

Calcium imaging in the posterior lateral protocerebrum (PLP) brain region was conducted using a two-photon microscope (Prairie Ultima) with near-infrared excitation (930nm, Coherent Chameleon

Ultra II) and a 40x objective (Nikon CFI APO 60XW). The excitation power never exceeded 25 mW at the sample. T-series of z-stacks (z-series) were taken at 128x128x5 pixel resolution (0.446 µm/pixel along x and y axes and 5 µm/pixel in z-axis, resulting in a 57x57x25 µm imaging volume) at a rate of 2.02 Hz, using galvo-galvo scanning in the x and y dimensions and piezo scanning in the z-dimension. For each experimental condition, the acquisition of 10 z-stacks were triggered to start precisely 2 seconds before the start of the visual stimulus using the on-board analog outputs of the display system: 4 z-stacks were recorded in the 2 seconds prior to the experimental stimulus, 2 recorded during the 1 second stimulus, followed by another 4 after the stimulus had ended.

The time-series of image volumes (X-Y-Z) was converted into a time-series of 2D images (X-Y) by computing a mean z-projection of all volumes. Forming a t-series by collapsing z-stacks helped compensate for motion in the z-direction. Motion in the x and y directions was corrected using "imregister" in the MATLAB image processing toolbox: each image was first gaussian filtered (alpha=3 pixels) to improve registration of noisy images, then registered using the 'multimodal' metric and 'rigid' transformation. Using this motion-stabilized t-series, an ROI was hand-drawn over the entire LPC1 glomerulus, excluding any additional axon tract that didn't overlap with the glomerulus. The mean pixel value within the entire ROI was used as the population average fluorescence for each frame. Since each experimental condition resulted in 10 values for each experimental condition (4 values before the stimulus, 2 during, and 4 after), the fluorescence change (ΔF/F) was calculated by dividing all 10 fluorescence values by the baseline fluorescence – the mean of the first 4 'pre-stimulus' values. Peak ΔF/F was computed by finding the max value of values 5-10 in each time-series; values 1-4 are ignored as they are the pre-stimulus fluorescence change values. Both ΔF/F time-series and peak ΔF/F are plotted as mean of all flies +/- SEM.

3.3.8 Statistics

To identify "non-zero" average responses to visual stimuli, p-values were calculated using a 1-sample, 2-tailed t-test ("ttest" function in MATLAB). The Benjamini-Hochberg Procedure was used to correct for the false discovery rate (FDR) associated with multiple comparisons. For behavioral experiments (Figures 3.6 to 3.9), 288 comparisons were made: 3 measurement types (L-R, L+R, and WbF), 2 directions (e.g. CW and CCW), 6 motion types (yaw, roll, pitch, lift, thrust, and slip), and 8 temporal frequencies (0.5, 1, 2, 4, 8, 16, 32, and 52.5 Hz). Statistically significant differences were noted with 1 star for $p<0.05$ and FDR=5%, and with 2 stars for $p<0.01$ and FDR=1%.

3.4 Results

3.4.1 Technical overview of the display system hardware and software

In keeping with past generations, our 4th generation (G4) display system is built from modular LED panels to allow multiple display shapes and configurations, but now with many new features and technical improvements. An overview of this system is schematized in Figure 3.1. The primary components of this display system are a desktop computer with an FPGA PCIe "controller card" installed and a visual arena consisting of a printed circuit board (PCB) with many individual LED panels installed.

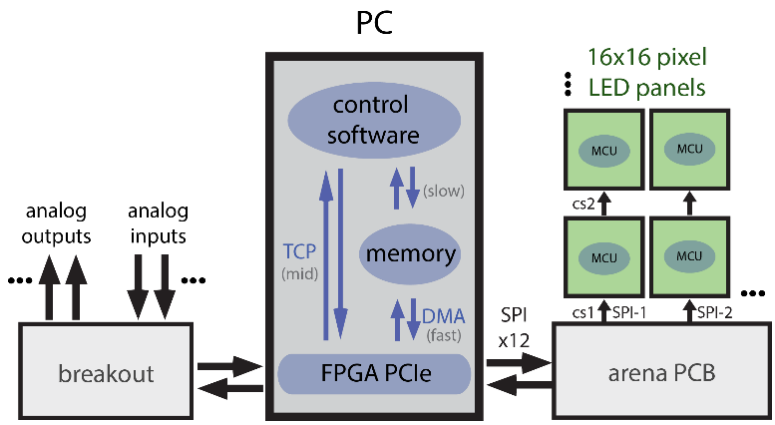

Figure 3.1: Overview of the G4 display system.

An LED arena (formed from columns of LED panels connected to an arena PCB) receives frame information through Serial Peripheral Interface (SPI) channels (with chip select [cs] lines to identify each row of panels) from an FPGA PCIe "controller card" installed in a Windows PC. The controller card receives commands from the "high-level" control software and streams frames to the arena through Direct Memory Access (DMA) of stored pattern files while simultaneously controlling analog outputs and logging analog inputs accessible through a breakout box.

Individual LED panels – the display units of the LED arena – are similar in design to the previous generation (referred to as "G3") but have significantly improved functionality. Designed in collaboration with Jim Chen in the Janelia Experimental Technology department (JET) and based on designs from William Dickson at IO Rodeo, each panel contains four times more LEDs per panel (16x16 instead of 8x8) in a package that is ~56% larger (40 mm per side versus 32 mm per side), resulting in ~2.5x increase in pixel density. LED pixels are now small-package surface mount LEDs rather than built into a custom-ordered plastic block, making it easier to choose different LED colors and to replace individual bad pixels. Each LED panel contains 5 high-speed microprocessors (MCUs),

4 of them each servicing an 8x8 quadrant of the 16x16 panel allowing for faster row/column switching and faster refresh rates, and the final one serving as the communication interface for signals from the controller (via the arena board).

Individual LED panels are connected to the arena PCB or “arena board”, also designed in collaboration with Jim Chen (JET), and can be daisy chained into columns. Previous generations of this display used I^2C as the communication interface, but this version has been improved by using SPI – a faster digital communication interface, but one that is less convenient for numerous devices. We overcome this limitation by providing multiple, parallel SPI busses (or channels). Each column of panels receives its own SPI channel, with multiple daisy-chained panels in a column operating on the same SPI channel but with separate chip select lines to allow individual access to each panel. The selection of individual panels is accomplished by wiring – the position of a panel, without additional software settings establishes the address of each panel (another improvement over previous generations). 12 SPI channels (columns of panels) are available and connect to an FPGA PCIe “controller card” (National Instruments NI 7842R) through a 68-pin VHDCI to D-sub cable. The 96-pin cable houses the 12 SPI lines as well as 8 chip select lines to accommodate the daisy-chained LED panels. (While there are enough dedicated chip select lines to accommodate 8-panel-tall columns, only columns of at most 4-panel have been validated.) The arena board can be custom-built to create different arena sizes and shapes. Two configurations (referred to as the “270°“ and “240°“ arenas) have been developed and validated so far, as shown in Figure 3.2.

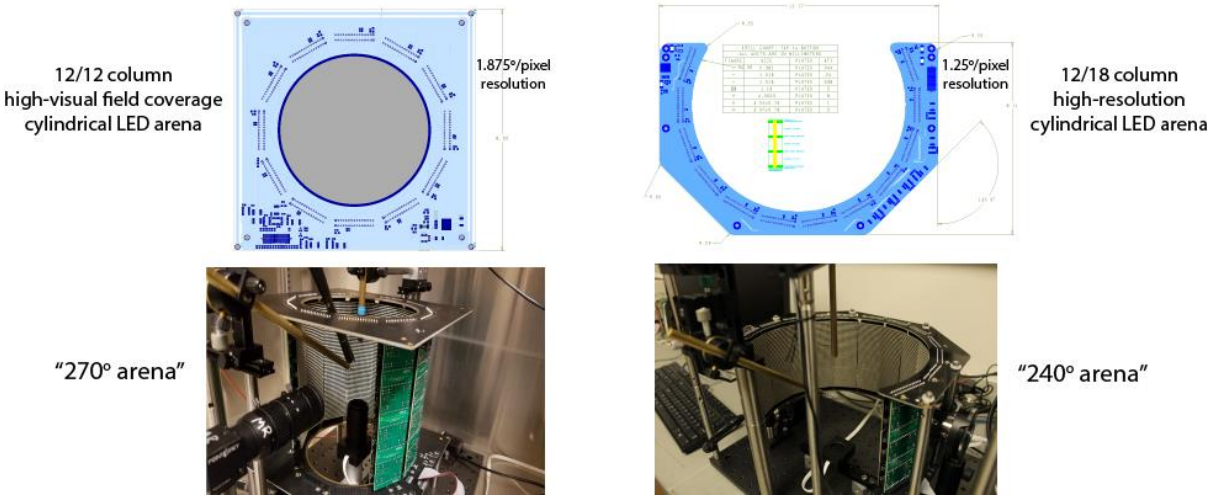

Figure 3.2: Configurations of LED arenas.

(left) Arena design that supports up to 12 columns of LED panels (forming an enclosed cylinder) up to 4 panels high. This version is used for providing large coverage of the fly's visual field in behavioral experiments in section 3.4.3. The 3 back columns of the arena are removed to accommodate other experimental equipment, resulting in a visual field coverage spanning 270° in azimuth – this configuration is referred to as the "270° arena". (right) 12-column arena for presenting higher resolution stimuli in a more limited area of the visual field (covers up to 240° across the azimuth). This configuration is used in the imaging experiments in section 3.4.4 and is referred to as the "240° arena".

The controller card runs the primary display control software, accessed by a LabVIEW executable developed by Andy Chiu at Coleman Technologies. This directly controls the 12 SPI channels and 8 chip select lines at 4 MHz (with higher speeds possible). The patterns to be displayed on the LED arena are stored in the PC's file system and accessed by the display controller using Direct Memory Access (DMA). This system allows for precise timing of the display at very fast refresh rates (1 kHz for 1-bit greyscale patterns or 500 Hz for 4-bit greyscale patterns) without the need to store the patterns on the LED arena onboard storage as was required for previous generations of this display system. Patterns can be generated and stored in memory a fraction of a second before they can be displayed on the LED arena without any other user interactions – an improvement that allows on-line stimulus generation, that among other applications can be used for characterizing individual neurons (Gruntman, Romani, & Reiser, 2018).

High-level control software (MATLAB) is used to pre-render patterns and send commands to the display controller through a TCP/IP connection (on the very same PC or across a network). In typical use-cases, the high-level control software is used to create patterns prior to the start of an

experiment and to handle the logic of the experimental structure through timed commands to the display controller (e.g. to implement a randomized block trial structure, example available at github.com/misaacson01/G4_Experiments). A breakout box can be connected to the R-series board allowing multiple analog inputs and outputs: 4 analog inputs can be logged at a high-rate and are stored incrementally as "technical data management system" (.tdms) files, which have been optimized for fast loading. Concurrently, up to 4 analog outputs can be controlled at a rate of 1 kHz (1-for-1 with displayed frames), creating the ability to log experimental data and control external equipment in a way that is precisely synchronized with the display refresh cycles.

3.4.2 Creating optic flow patterns

Upon validating the correct basic operation of the G4 display system, I aimed to develop a comprehensive method to generate patterns useful to study behavioral reactions to motion stimuli and to study motion-sensitive neurons. To that end, I set out to understand how the *Drosophila* visual system would see the arena. I first mapped the optical axes of all ommatidia of the left and right eyes (Buchner, 1971) in spherical coordinates (Figure 3.3, top). Then, based on the layout and dimensions of the 270° arena (as shown in Figure 3.2, bottom-left), I calculated the spherical coordinates of every pixel and plotted them in a Mercator projection, overlaid on top of the mapped *Drosophila* visual field (Figure 3.3, bottom). From this, I can estimate that this 270° arena covers approximately 60% of *Drosophila* ommatidia, while the 240° arena (shown in Figure 3.3, right) covers approximately 35% of ommatidia, though at a higher resolution (1.25^{o}/pixel angular apparent distance across the horizon compared to 1.875^{o}/pixel of the 270° arena). From this analysis I estimate the amount of overlap between the left and right eye visual fields of *Drosophila* to range between 10-30° in longitude over the elevation (latitude) that the arena covers.

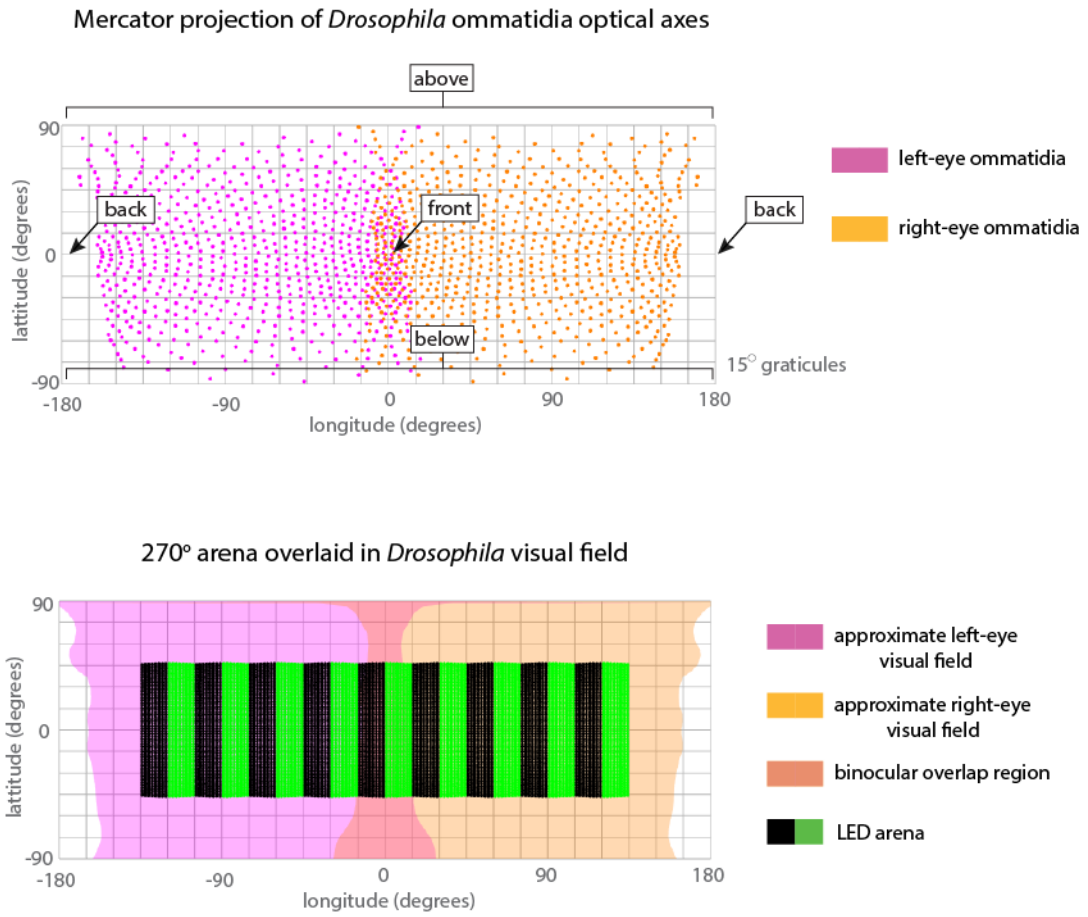

Figure 3.3: Mapping the *Drosophila* visual field and LED arena.

(top) The optical axes of the right and left eyes in *Drosophila*, mapped in a Mercator projection – data from Buchner (1971). (bottom) The regions of left and right eye coverage were roughly traced from a 5° circle centered on each ommatidia's optical axis. The pixel coordinates of the 270° arena was also mapped into this visual field.

Calculating the approximate spherical coordinates of the LED arena pixels allowed me to develop a general strategy for generating visual stimuli, inspired by rotating/translating starfield stimuli generated by Jamie Theobald (Theobald et al., 2010). In visual experiments with cylindrical displays, one of the most common types of stimuli presented is yaw rotational motion – the geometry of an upright cylindrical display makes this stimulus easy to generate, as it only consists of vertical lines that shift to the left or right in subsequent frames. Not only is this stimulus easy to generate, due to its vertical uniformity, it can be displayed at higher refresh rates than previous versions of the modular LED panel display system (Reiser & Dickinson, 2008). To maximize the utility of our new display system which is no longer limited by the complexity of the frames, I set out to create optic

flow patterns for all 6 principle types of self-motion (rotation: yaw, roll, pitch; translation: lift, thrust, slip).

To briefly summarize the general strategy for creating yaw rotational motion (around the vertical axis): the azimuth angle (i.e. longitude coordinate) of every pixel was sent through a square wave function to generate the rotational square-wave grating pattern; this leads to a grating pattern that varies across longitude positions, as shown in Figure 3.3 (bottom). This can be conceptualized as a rotation around the south pole coordinates (-90° latitude, 0° longitude). For lift translational motion (translation along the vertical axis), the vertical coordinate (height) of each pixel was similarly sent through a square wave function, resulting in a square wave that varied across the height of the arena. This can be conceptualized as a translation from the south pole coordinate to the north pole.

To generate rotation and translation about other axes, the arena coordinates were rotated so that their longitudes could always be used to generate the desired rotational gratings and the vertical-coordinate could always generate the desired translation gratings (i.e. the desired pole of rotation/translation is shifted to the south pole). For example, to simulate rotation or translation around the transverse axis (pitch or slip, respectively), the desired pole of rotation or translation is located at -90° longitude, 0° latitude. Rotating the arena coordinates by 90° in both yaw and pitch will now place the desired pole of rotation/translation on the south pole of the spherical coordinate system (0°, -90°), where a square wave function through the longitudinal coordinate or vertical coordinate will now produce a grating pattern for pitch and slip, respectively. Using this method, I created grating patterns for the 6 types of optic flow for the 270° arena, shown in Figure 3.4.

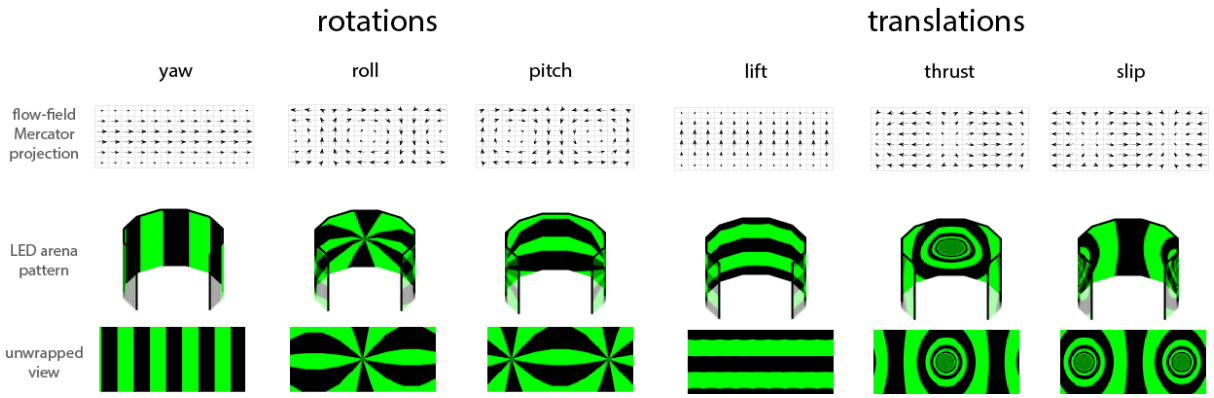

Figure 3.4: Grating stimuli for types of 6 types of optic flow.

Grating patterns for 6 principle types of self-motion were generated for the 270° arena. 6 motion types include rotation around the vertical, forward, and transverse axes (yaw, roll, and pitch, respectively) and translation across the same axes (lift, thrust, and slip, respectively). (top) Mercator projections of flow-fields of these motion types are displayed. (bottom) The grating patterns are also shown how they would be displayed on the arena along with a view of an unwrapped cylinder for easier visualization.

The full program used to generate these patterns is available online (https://github.com/misaacson01/Motion_Maker_G4), which includes options for generating different types of motion stimuli such as sine wave gratings and edges. The program allows for controlling many parameters of grating and edge stimuli, such as the bright/dark bar brightness, spatial wavelength, duty cycle, and per-frame step-size. Any axis of rotation or translation can be used, not only the 3 principle axes. Starfield stimuli can also be generated for rotation about or translation along any axis, with parameters setting the number of dots, size and brightness of dots, whether closer dots appear larger, and whether dots occlude one another, among other parameters. An associated GUI allows for these parameters to be easily modified and visualized (shown in Figure 3.5).

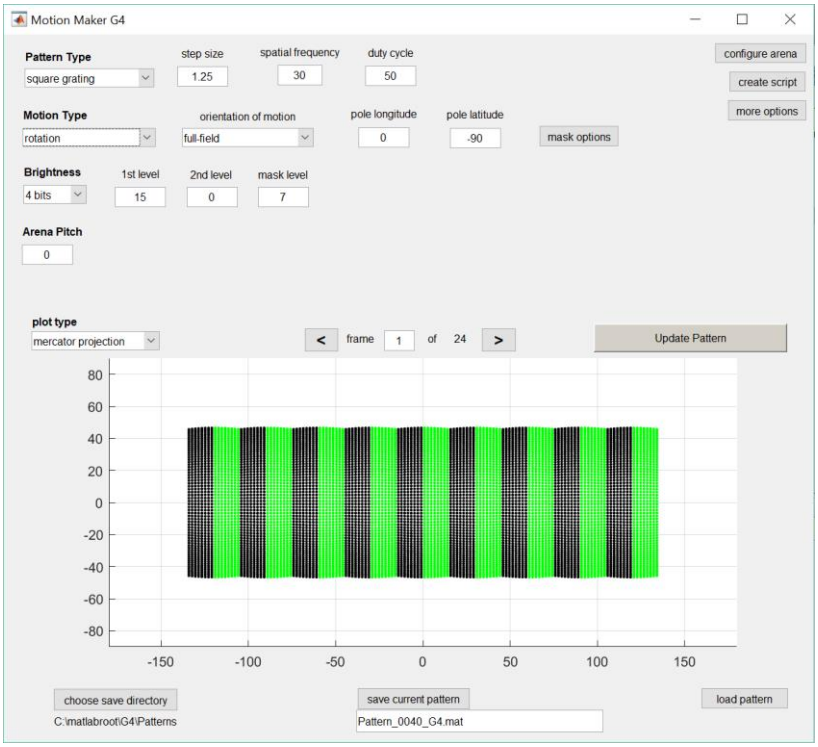

Figure 3.5: Program for creating motion stimuli.

Motion Maker GUI allows the simple generation and visualization of moving patterns. Supported pattern types include gratings, edges, and starfields, with many of their properties parameterized. The patterns are visualized on either a Mercator or grid projection of the arena, where the configuration of the arena (240°, 270°, or any other cylindrical arena) can also be defined within the GUI.

3.4.3 High-speed operation to probe upper limits of motion vision

Previous research presented the 6 principle types of rotational and translational motion (depicted in Figure 3.4) to tethered flying flies while monitoring their behavioral reactions, using starfields instead of gratings (Theobald et al., 2010). However, unlike starfields, grating stimuli can be defined by temporal frequency and spatial wavelength which provides precise quantification of the tuning properties of the motion vision system being studied. Furthermore, using previous display systems, it was not possible to present complex visual motion stimuli accurately and at sufficiently high speeds to probe the upper limits of motion detection. With our new display system that operates with higher spatial resolution and at a high refresh rate, I set out to determine how flying flies respond to the 6 types of optic flow gratings at temporal frequencies up to the *Drosophila* flicker fusion frequency.

I presented these 12 motion patterns (6 motion types each presented in the forward and backward direction) at temporal frequencies of 0.5, 1, 2, 4, 8, 16, 32 and 62.5 Hz (at a 1000 Hz refresh rate, 62.5 Hz is the fastest possible speed to display a 16-frame pattern) to flying flies while using the onboard data logging of the G4 display system to log behavioral measurements of the difference in wingbeat amplitude (L-R, a proxy of the flies turning response), the sum of wingbeat amplitudes (L+R), as well as the wingbeat frequency (WbF) of the flies. For the historically most common grating stimuli used in vision research (yaw rotation and lift translation gratings, which simply consist of drifting vertical or horizontal bars, respectively), I observed strong directional behavioral reactions that peaked at 8 Hz and were completely extinguished at the highest presented frequency (Figure 3.6), validating that the high-speed operation of the G4 display system is fast enough to fully map the upper-limits of *Drosophila* motion vision. Furthermore, the measurement of non-zero responses at 32 Hz demonstrates a clear directional response to quite fast visual motion – a result that was not well established in *Drosophila* using previous display systems.

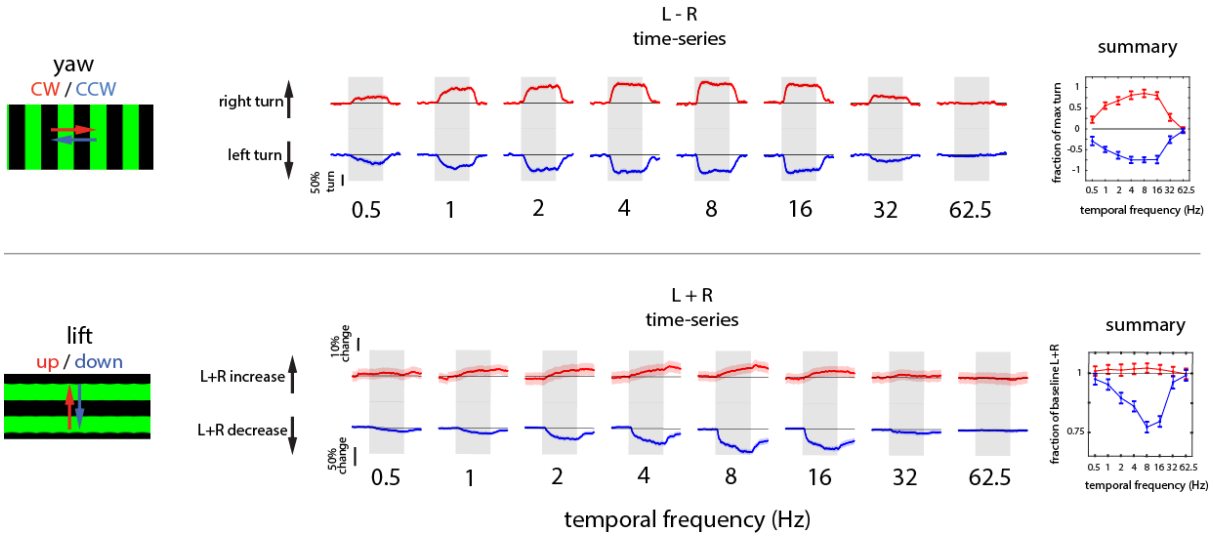

Figure 3.6: Temporal frequency tuning curves of behavioral reactions to yaw and lift stimuli.

(top) Time-series data of the L-R turning measurment (normalized to the 98th percentile turning response, used as a more robust approximate measurement of a maximal turn) is plotted in reponse to clockwise (CW, in red) and counterclockwise (CCW, in blue) yaw rotational gratings at temporal frequencies of 0.5, 1, 2, 4, 8, 16, 32, and 62.5 Hz. The solid red/blue lines represent the mean turning response of all flies (N=21), and the shaded red/blue region represents the SEM. A summary of time-series plots is created by averaging the response over the 2-second stimulus window (shaded grey region). (bottom) Similarly, time-series data of the L+R measurement (normalized to the pre-stimulus baseline) is plotted in response to up and down lift translational gratings; due to significant asymmetry in responses, time-series of responses to up motion are plotted in a different vertical scale than those to downward motion for better visibility. (N=21)

By plotting the turning measurement in response to all presented stimuli, I found that bilaterally asymmetric stimuli (yaw, roll, and slip) cause significant turning responses up to 16 or 32 Hz ($p<0.01$, FDR=1%), while the bilaterally symmetric stimuli (pitch, lift, and thrust) did not cause significant turning responses ($p>0.05$ at FDR=5%) (Figure 3.7). These stimuli also caused a noticeable change in the L+R response (Figure 3.8) and transients in the wingbeat frequency (Figure 3.9).

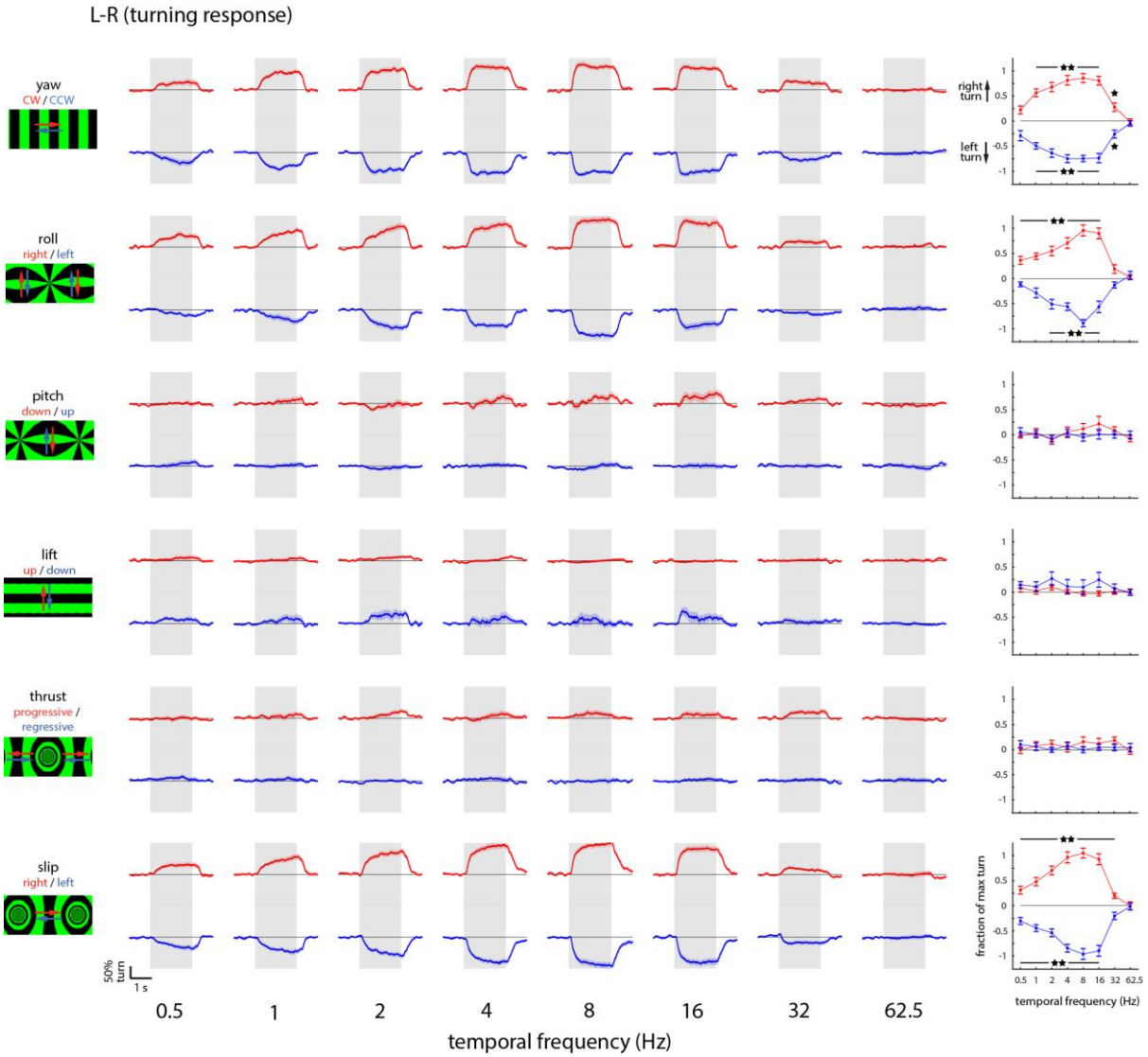

Figure 3.7: Temporal frequency tuning curves of L-R response to 6 motion types.

Time-series data of the L-R turning measurment (normalized to the 98th percentile turning response, used as a more robust approximate measurement of a maximal turn) is plotted in response to bidirectional motion of the 6 motion types, for temporal frequencies of 0.5, 1, 2, 4, 8, 16, 32, and 62.5 Hz. Responses to the 2 directions of each motion type are plotted in red and blue as shown in the patterns to the left of each set of time-series data. The solid red/blue lines represent the mean turning response of all flies (N=21), and the shaded red/blue region represents the SEM. Summary of time-series plots is created by averaging the response over the 2-second stimulus window (shaded grey region). Statistically significant non-zero values are denoted by 1 star for $p<0.05$;FDR=5% and 2 stars for $p<0.01$, FDR=1%, as determined by a 1-sample (2-tailed) t-test with FDR correction by Benjamini-Hochberg procedure.

Some bilaterally symmetric stimuli (particularly lift and pitch) caused a significant directional L+R response; these strong bilaterally symmetric reactions also appear to be visible as increased noise in the corresponding L-R signal.

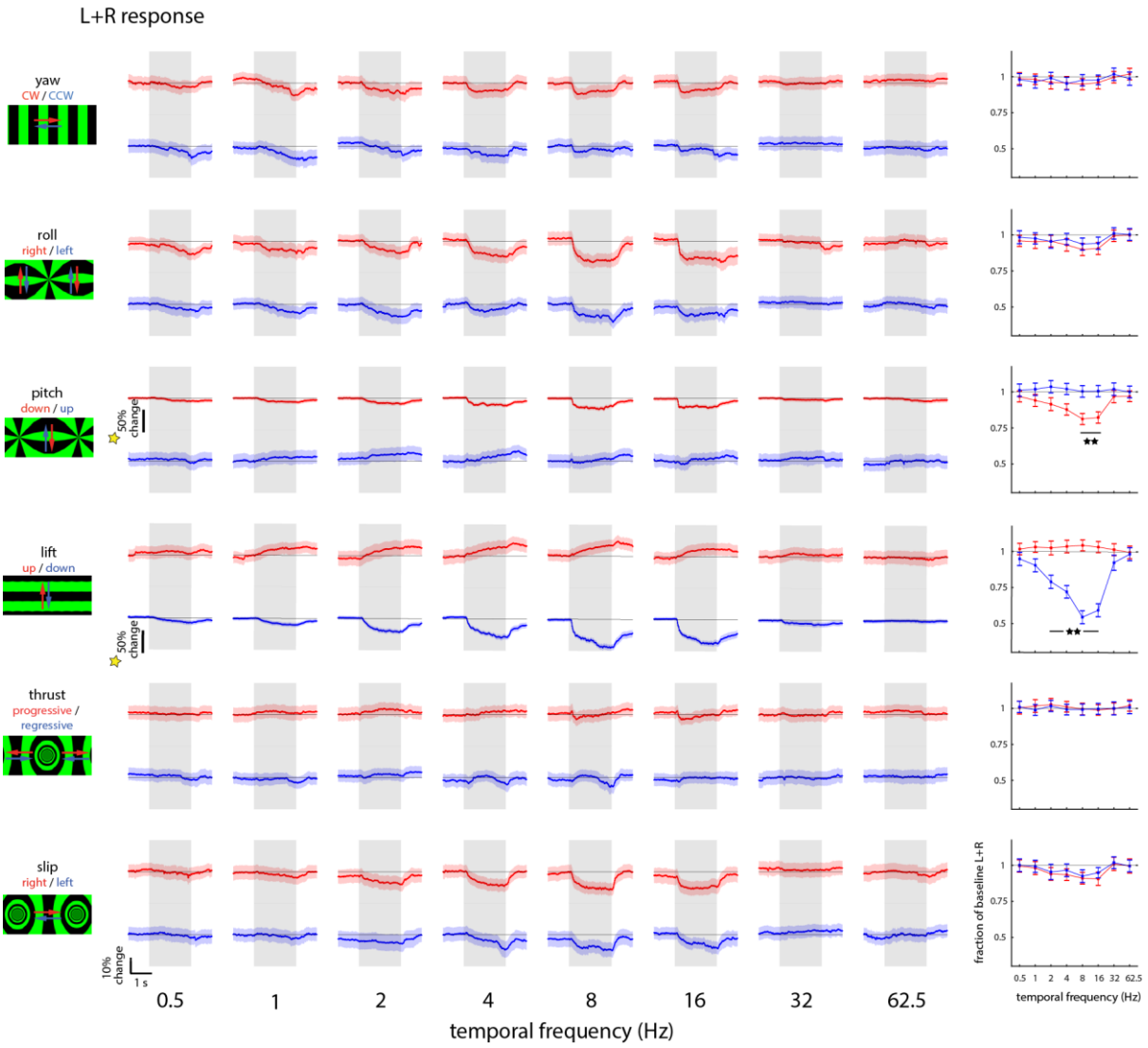

Figure 3.8: Temporal frequency tuning curves of L+R response to 6 motion types.

Time-series data of the L+R measurement (normalized to the pre-stimulus baseline L+R) is plotted in response to bidirectional motion of the 6 motion types, for temporal frequencies of 0.5, 1, 2, 4, 8, 16, 32, and 62.5 Hz. Responses to the 2 directions of each motion type are plotted in red and blue as shown in the patterns to the left of each set of time-series data. The solid red/blue lines represent the mean L+R response of all flies (N=21), and the shaded red/blue region represents the SEM. Summary of time-series plots is created by averaging the response over the 2-second stimulus window (shaded grey region). Responses to both downward pitch and downward lift were significantly larger than all others and their time-series data are plotted with a different scale factor, denoted by a gold star. All other time-series data are plotted at the scale on the bottom left.

Large directional responses in wingbeat frequency (WbF) were only observed for the lift stimulus; however, small directional changes can also be seen to the two other bilaterally symmetric stimuli: pitch and thrust.

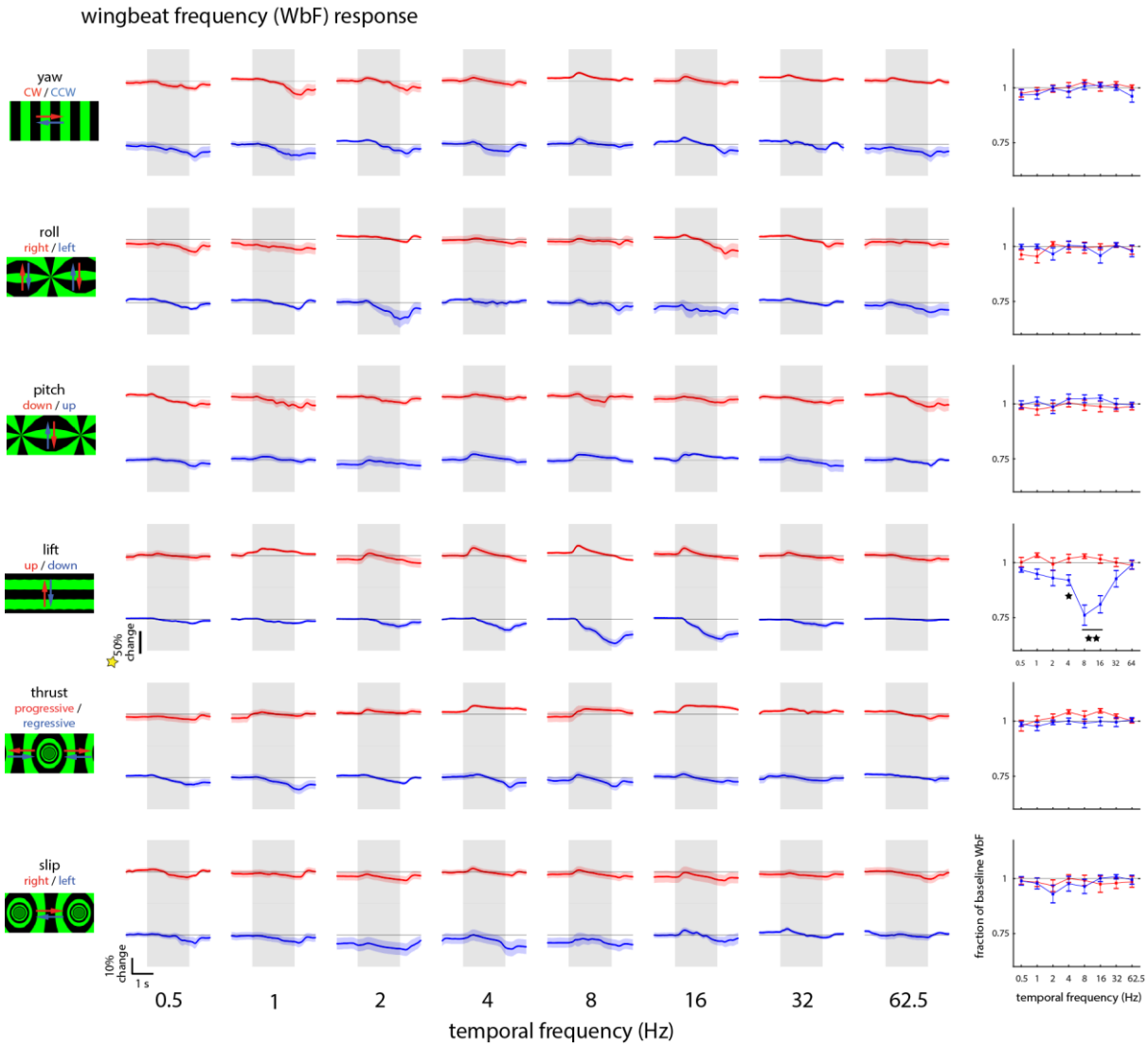

Figure 3.9: Temporal frequency tuning curves of wingbeat frequency response to 6 motion types.

Time-series data of the wingbeat frequency (WbF) measurement (normalized to the pre-stimulus baseline WbF) is plotted in response to bidirectional motion of the 6 motion types, for temporal frequencies of 0.5, 1, 2, 4, 8, 16, 32, and 62.5 Hz. Responses to the 2 directions of each motion type are plotted in red and blue as shown in the patterns to the left of each set of time-series data. The solid red/blue lines represent the mean WbF response of all flies (N=21), and the shaded red/blue region represents the SEM. Summary of time-series plots is created by averaging the response over the 2-second stimulus window (shaded grey region). Responses to downward lift were significantly larger than all others and their time-series data are plotted with a different scale factor, denoted by a gold star. All other time-series data are plotted at the scale on the bottom left.

By overlaying the summary temporal frequency tuning curves of the 5 largest directional behavioral responses (L-R response to yaw, roll, and slip, average of both directions; L+R response to downward pitch and downward lift) each normalized to their respective maximal response, we can compare the tuning curves across the different motion types. The speed tuning of these behavioral reactions to different patterns of motion are remarkably similar. All responses are maximal at 8 Hz, and all are completely extinguished by 62.5 Hz.

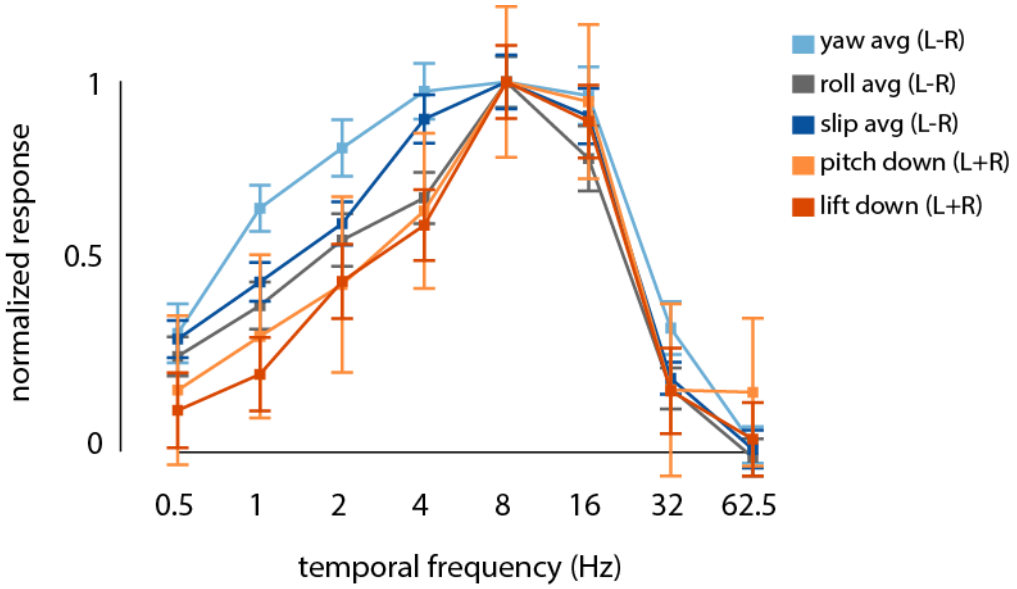

Figure 3.10: Temporal frequency tuning curves of L-R and L+R.

The summary tuning curves of yaw, roll, and pitch directional L-R responses (data from Figure 3.7, average of both directions), and pitch down and lift down L+R responses (data from Figure 3.7), are plotted with each curve normalized to their respective max response. Average +/- SEM of all flies are plotted (N=21).

3.4.4 Motorized pitching arena for optic flow mapping

In addition to understanding the behavioral responses to visual stimuli, we are also interested in dissecting the neural mechanisms behind the sensory processing of these stimuli. A well-known class of visual projection neurons (the Horizontal and Vertical System Lobula Plate Tangential Cells) have been shown to be selective to certain types of optic flow patterns by identifying the spatial location of their receptive field and their selectivity to local motion (local motion selectivity, or LMS) and direction within that location (local preferred direction, or LPD) through electrophysiological recordings (Krapp & Hengstenberg, 1996). I next sought to adapt a related optic flow mapping approach to use with the G4 display system, but for neuronal activity measurement with calcium imaging rather than electrophysiology. While the temporal dynamics of calcium indicators are much

slower than what can be measured with electrophysiology, calcium imaging can make use of cell-specific driver lines to measure many neurons at once, and is more conducive to stable, long-lasting activity measurements.

One general challenge in measuring neural activity during visual stimulation is that the dissection and placement of the fly in imaging and electrophysiology setups can results in significant portions of the fly's visual field being occluded by equipment such as microscope objectives, dissection and tethering mounts, cameras, etc. To reduce the amount of visual occlusion in these experimental setups, a custom-machined PEEK plastic mount in the shape of an inverted conical pyramid with a slope of 20° was designed with the assistance of Igor Negrashov and Bill Biddle in Janelia Experimental Technology (JET), inspired by angled mounts used by other researchers (Maimon, Straw, & Dickinson, 2010). This decreased the extent of visual field occlusion by up to 20° as compared to a previously used asymmetric metal mount (Strother, Nern, & Reiser, 2014) (Figure 3.11).

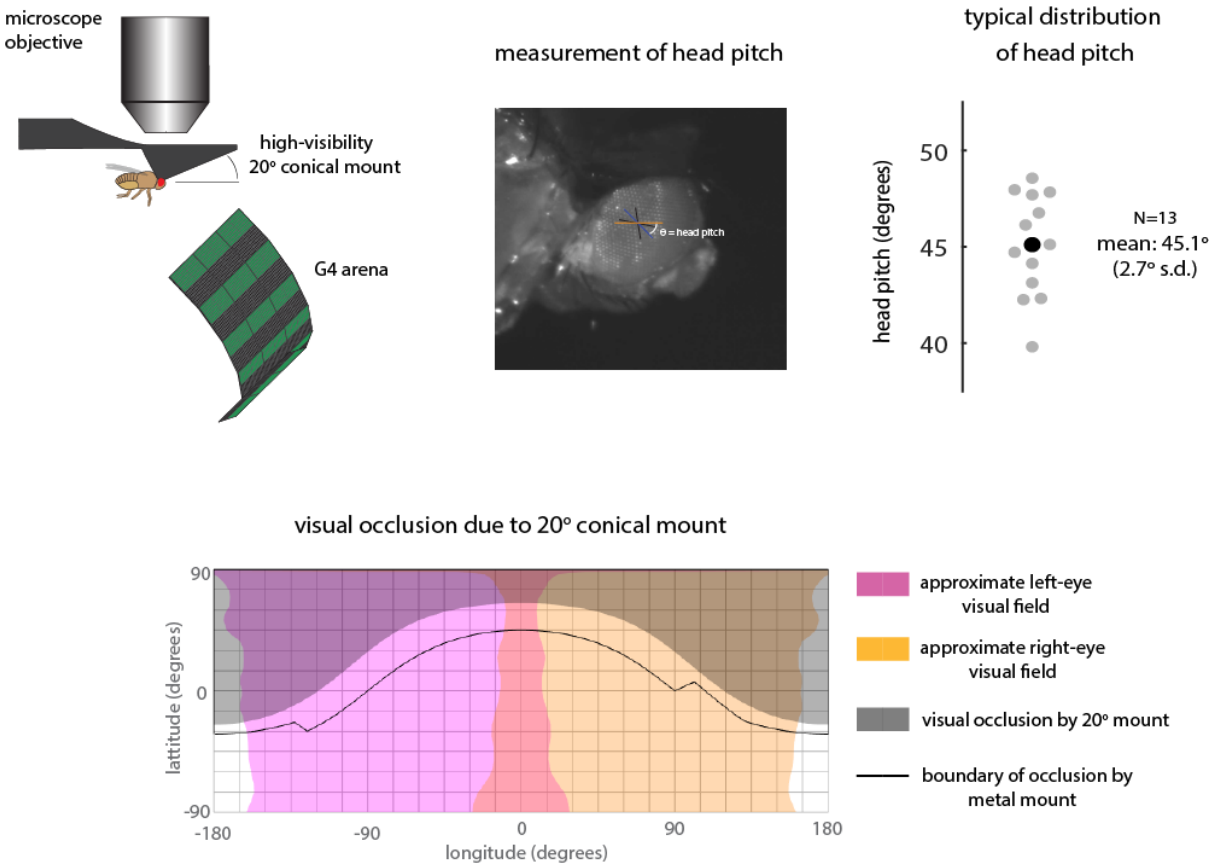

Figure 3.11: Imaging setup with high-visibility mount and high-resolution 240° arena.

(left) Overview of the functional imaging setup with a 240° G4 display. 2-photon imaging of *Drosophila* using a 20° conical mount with the fly's head tilted down to expose the dorsal side of the brain. (top-right) The amount of head pitch is measured by tracing the eye lattices to find the eye equator: typical head pitch in this setup is 45° down from the horizon (65° down from the conical mount). (bottom) Map of the visual field occlusion caused by the 20° conical mount, compared to the occlusion caused by a previously used metal mount, when the fly's head is pitched 45° down from the horizon.

To make use of this enlarged visual field under the constraints of a 2-photon microscope setup (only allowing a set vertical distance beneath the microscope objective), I attached a 240° arena to a motorized mount and stage (developed by Jon Arnold in JET), allowing control of the arena pitch to present stimuli farther above and below the equator of the eyes. Using this system, I designed a protocol to generate a course receptive field map of directional selectivity under the temporal and visual constraints of calcium imaging with a 2-photon microscope. By presenting 8 directions of local motion in 9 spatial locations across the un-occluded visual field (stimuli presented in a random order to minimize the effects of neuronal adaptation, and with a large time-delay in between each stimulus to allow transient calcium fluorescence to return to baseline), I aimed to map the local motion sensitives of visual projection neurons using calcium imaging and the G4 display system.

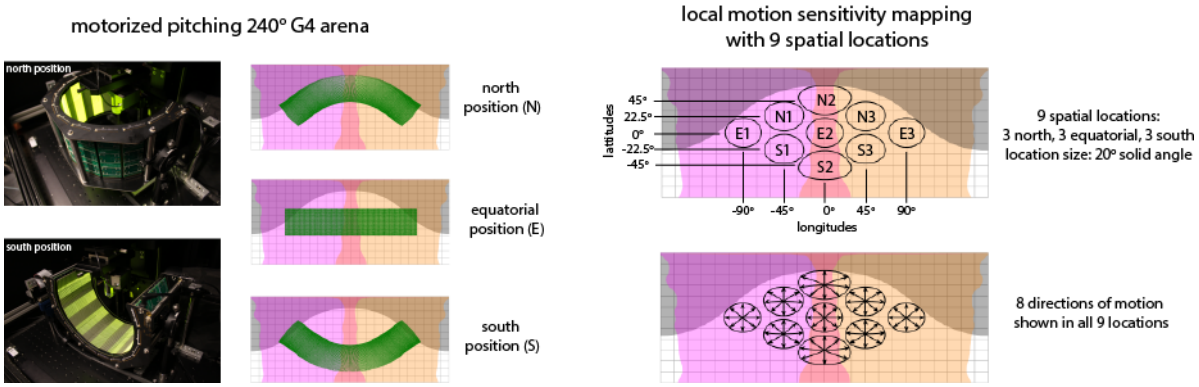

Figure 3.12: Motorized pitching arena for presenting local motion stimuli.

(left) 240° arena mounted under a 2-photon microscope by motorized pitching mounts on the left and right sides. Pitching the arena up and down allows presentation of stimuli further north and south of the eye equator in the fly's visual field. (right) Map of spatial locations for mapping local motion sensitivities of VPNs. Each spatial location size is a 20° solid angle. 9 spatial locations chosen: 3 locations north of the eye equator (north positions: N1, N2, N3), 3 along the equator (equatorial positions: E1, E2, E3), and 3 south of the equator (south positions: S1, S2, S3). The 3 left-most locations are only visible to the fly's left eye (E1, N1, S1), the 3 right-most are only visible to the right eye (E3, N3, S3), and the middle 3 are located within the binocular overlap region, being at least partially visible to both eyes. (E2, N2, S2).

Applying this technique to a recently identified class of small-field visual projection neurons (named Lobula Plate Columnar type 1 or LPC1, described in detail in Chapter 4), I was able to map the local motion sensitivities (LMS) of this cell-type, within the spatial limits of this setup (Figure 3.13). I found that the LPC1 population was highly directionally selective to back-to-front motion at all 3 locations presented to the ipsilateral eye.

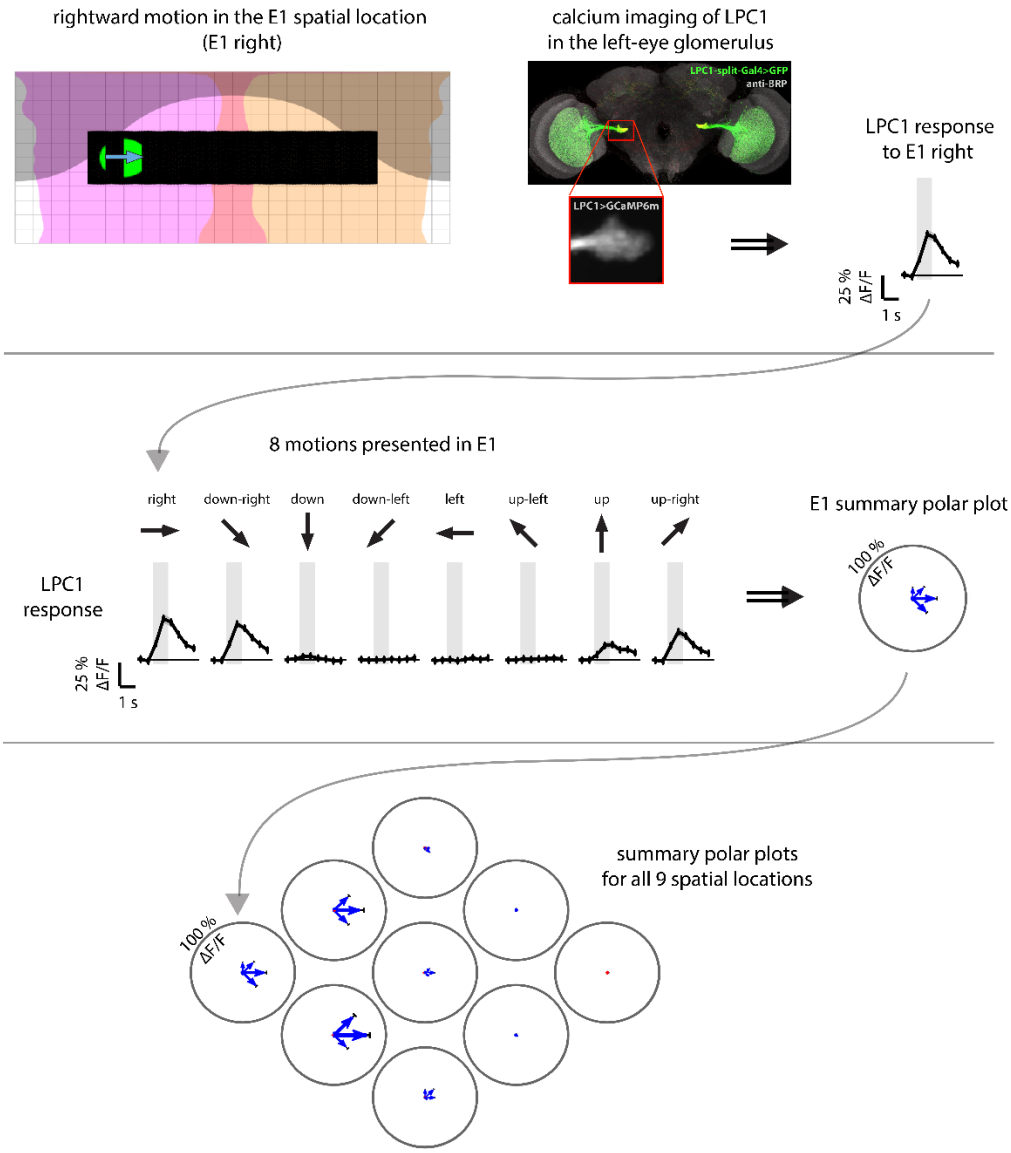

Figure 3.13: Mapping the local motion sensitivity of LPC1

(top) An example stimulus condition for mapping local motion sensitivities is described. The LPC1 population response is measured (by calcium imaging in the left-eye LPC1 glomerulus) to rightward motion (100% contrast gratings) in the E1 spatial location (located along the equator of the left eye's visual field, see Figure 3.12). Image of LPC1 anatomy from Aljoscha Nern. (middle) LPC1 responses to 8 directions of motion in E1, summarized in a polar plot. In the polar plot, the direction of the arrow signifies the direction of motion stimulus, and the size of the arrow signifies the peak LPC1 response measured to that stimulus. (bottom) Summary polar plots for the LPC1 population responses to 8 directions of motion in 9 spatial locations. Average +/- SEM of peak responses of all flies (N=8) are plotted.

One common limitation of using a calcium indicator to measure neural activity is that they are typically insensitive to hyperpolarizations. In many neurons, a calcium indicator's fluorescence level

at baseline cannot be decreased by reducing the calcium present in the cell (either because calcium levels are already very low at baseline or because of indicator limitations); this can make it difficult to measure inhibition or membrane hyperpolarization, which could lead to missing information in local motion sensitivity maps generated by calcium imaging. To overcome this limitation and to be able to map inhibitory contributions from motion stimuli rather than only excitatory effects, I created a second LMS mapping procedure where one of the spatial locations was dedicated to providing a baseline level of excitation from which the excitation caused by the simultaneous presentation of motion in a different spatial location can be compared (Figure 3.14, top).

The E1 location was chosen to provide baseline excitation, since out of the 3 spatial locations that caused LPC1 excitation (E1, N1, and S1), only the E1 location can be stimulated when the arena is in any of the 3 pitch positions. By presenting back-to-front motion on E1 and simultaneously pairing it to a motion stimulus in one of the other spatial locations, I created a map of local motion sensitivities that can detect inhibition (Figure 3.14, bottom). While the changes in LPC1 responses are smaller than the overall level of excitation (making signals noisier), I was able to detect consistent inhibition by front-to-back motion on both the ipsilateral and contralateral eyes – the implications of these findings will be explored more deeply in Chapter 4, which includes a much broader examination of this cell type. These data demonstrate a technique and preparation that is useful in mapping both the excitatory and inhibitory components of optic flow maps in visual projection neurons, using genetically targeted calcium imaging.

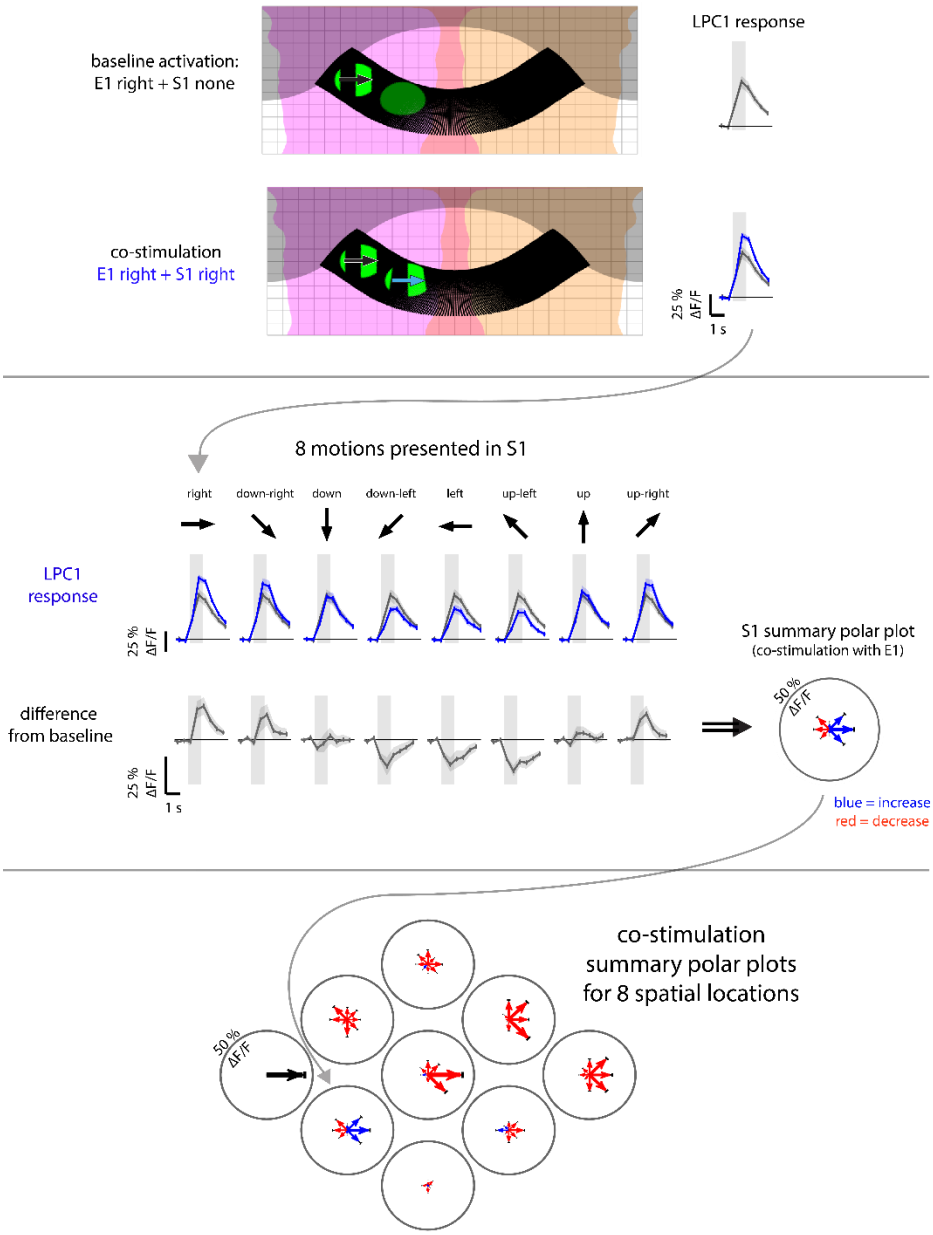

Figure 3.14: Mapping the local motion sensitivity of LPC1 during co-stimulation.

(top) An example stimulus condition for mapping local motion sensitivities during co-stimulation with E1 is described. A baseline level of LPC1 excitation is measured to rightward motion in the E1 location with no motion shown in S1; a uniform stimulus at an intermediate brightness level to the bright/dark grating stimuli is shown in S1 so that the overall brightness will be the same for (S1 right + S1 none) and (S1 right + E1 right). The LPC1 response to co-stimulation of E1 right and S1 right is measured and compared to the baseline excitation. (middle) LPC1 responses to 8 directions of motion in S1 during co-stimulation with E1 right, summarized in a polar plot. In the polar plot, the direction of the arrow signifies the direction of motion in S1 (E1 motion is always rightward), the size of the arrow signifies the peak change in LPC1 response (change from baseline), and the color of the arrow signifies whether the response is greater (blue) or smaller (red) than the baseline response. (bottom) Co-stimulation (with E1 right) summary polar plots for the LPC1 population responses to 8 directions of motion in 8 spatial locations. Average +/- SEM of peak responses of all flies (N=8) are plotted.

3.4.5 Multicolor displays and virtual reality

Significant effort is being placed into delivering more naturalistic visual stimuli to tethered animals (Dombeck & Reiser, 2012); this includes not only delivering a better representation of natural scene statistics but also incorporating behavioral feedback to influence the visual stimuli, as would happen under natural closed-loop conditions.

Since the G4 display system is composed of LED panels containing standard-manufactured surface-mount LEDs, multiple options for LED colors are available for the assembly of the LED panels. Taking advantage of this feature, we have implemented (in collaboration with Jim Chen in JET) a multi-color arena composed of LED panels with UV and green LEDs arranged in a checkerboard (Figure 3.15). Even though some spatial resolution is sacrificed by alternating the two colors, the higher resolution of the G4 arenas can accommodate this lowered spatial resolution and still present stimuli at higher resolution than the interommatidial angular distance of *Drosophila*. The ability to incorporate UV and green in visual scenes is a step toward delivering more naturalistic stimuli and establishing reliable tools for probing critical visual inputs for color-motion in major genetic model organisms (flies, zebrafish and mouse, which all have photoreceptors sensitive to UV).

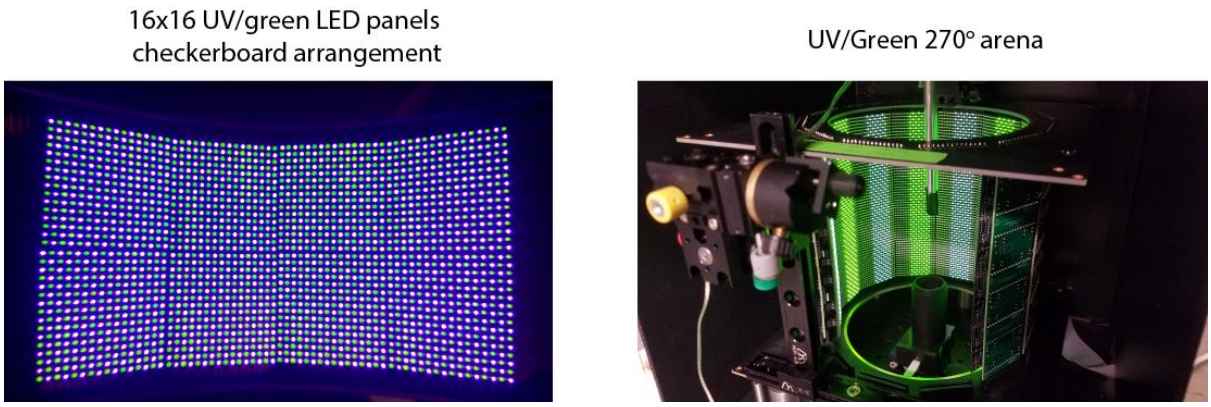

Figure 3.15: UV-green checkerboard LED panels for a multicolor arena.

(left) 16x16 UV/green LED panels composed of separate UV and green pixels arranged in a checkerboard pattern, designed in collaboration with Jim Chen in JET. (right) Arena built from 2-color panels displaying a grating pattern of alternating green and UV color. Stimuli generated from a simple conversion script to adapt patterns generated from the program describe in section 3.4.2, which maps patterns to either the green pixels or the UV pixels.

In order to support real-time, flexible control of visual stimuli, two closed-loop methods to manipulate the visual stimuli based on behavioral feedback were implemented in the G4 display system: one using a single behavioral measurement to index into pre-rendered frames, and another

using multiple behavioral measurements to calculate and render frames on-line. The first method allows for extremely fast closed-loop experiments using virtual environments simple enough so that all frames can be pre-rendered and a sequence through the frames can be controlled by a single measurement dimension. An example of this method is the closed-loop stripe fixation described previously, where the turning behavior (L-R multiplied by a gain term) determines the rotational velocity (frame increments) of a vertical stripe around the fly. This method operates at the same speeds as open-loop stimuli (500 Hz or 1 kHz refresh rate, depending on the bit-depth of the pattern).

The second method uses the TCP/IP connection between the controller card and the high-level control software to stream behavioral input channels into the high-level control software for generating and then streaming frames back to the display control software. Up to 4 channels of 16-bit analog input data can be streamed into the high-level software from the controller card at a rate of 100 Hz, allowing the high-level software to handle the calculation of the animal's position and orientation within a virtual world and rendering a new frame, after which the frame is streamed back to the controller card and out to the display. An overview of these 2 methods for closed-loop control of the G4 system is shown in Figure 3.16.

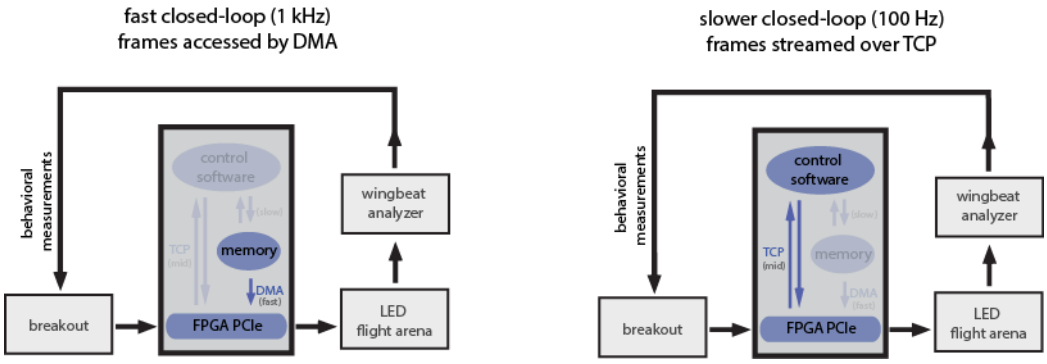

Figure 3.16: Two modes of closed-loop operation in the G4 display system.

(left) Fast closed-loop (500-1000 Hz update rate) mode is accomplished by pre-rendering all patterns and loading them in PC memory (RAM), to be accessed through DMA by the controller card (FPGA PCIe). A single 16-bit channel behavioral measurement is fed into the controller card to allow internal logic stored in the card to determine which frame index of the pre-rendered frames display next. (right) A slower closed-loop (100 Hz) mode is accomplished using TCP/IP streaming of behavioral measurements and patterns between the controller card and the high-level control software. Up to 4 16-bit behavioral measurement channels can be streamed into the control software, from which a new frame can be rendered and streamed back to the controller card.

The streaming (100 Hz) closed-loop method was tested by implementing a standard stripe-fixation experiment. A stripe that was pre-rendered and loaded into the MATLAB workspace could be streamed through TCP/IP to the G4 display at a rate of 95-100 Hz, with only a 5-10 ms latency between acquiring a sample of behavioral data and streaming the next frame to the arena (~5 ms latency for 1-bit frame streaming, ~10 ms for 4-bit frame streaming, after significant software optimization). Comparing this method to the fast 1 kHz closed-loop method shows that both are adequate to reproduce high-quality stripe fixation in tethered flies (Figure 3.17).

While this comparison suggests that a display update rate of 100 Hz is fast enough, I next set out to determine what update rate is required for realistic visual feedback in this sensorimotor closed loop tethered flight setup. By adding a set delay after each behavioral data sample, I could determine how different display update rates affect how the animal responds to the stimuli as the update rate becomes slower and the motion becomes choppier. I found that an added delay of 10 ms (for a ~50 Hz update rate) had virtually no effects on the closed loop behavior. Furthermore, an added delay of up to 20 ms had only modest effects on the behavioral responses to the stripe-fixation experiment, indicating that in this flying *Drosophila* assay, the speed of operation may accommodate significantly more complex interactive visual environments that requires up to 20 ms per-frame rendering time. It is noteworthy that a 40 ms or longer update rate produces a marked reduction in the closed loop behavioral performance – suggesting that projector-based systems (which typically feature a ~60 ms latency to update the stimulus) may underperform in closed-loop visual stimulus generation.

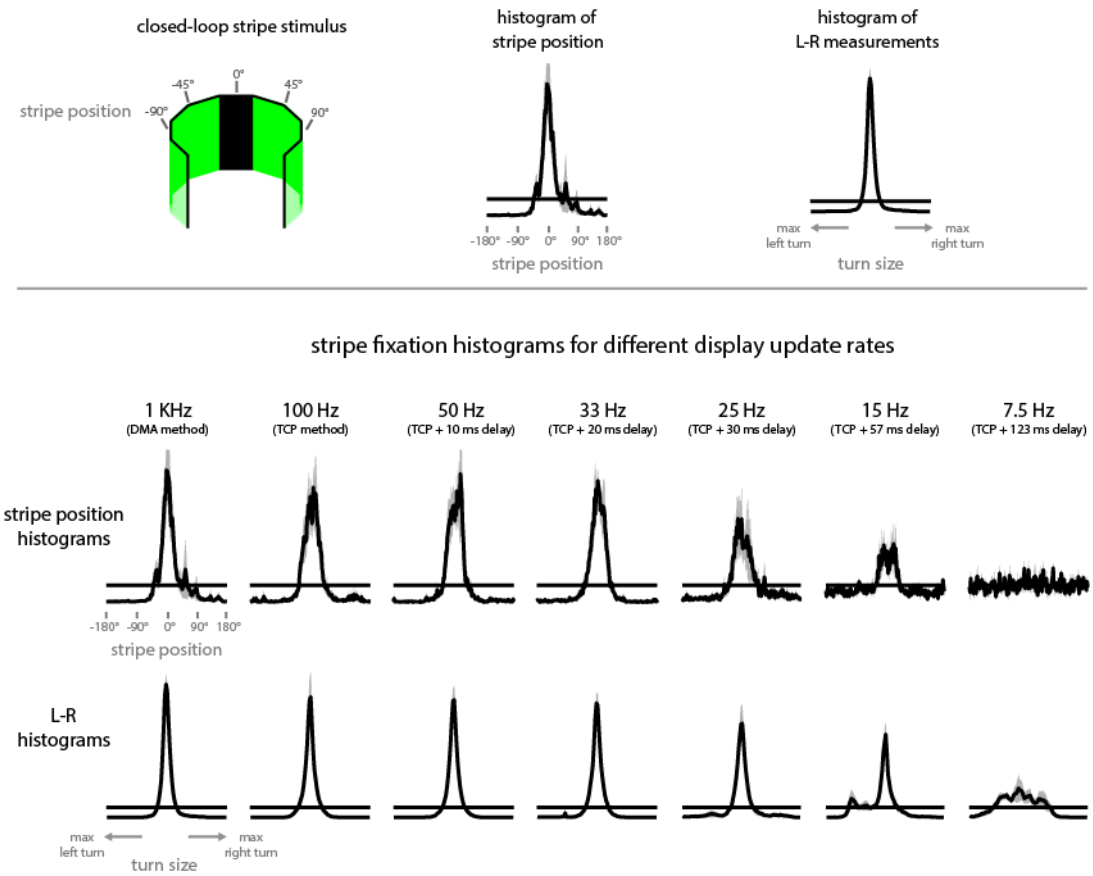

Figure 3.17: Effects of display update rate and latency on closed-loop flying behavior.

(top-left) Cartoon of a stripe pattern used for stripe-fixation assays; a single dark vertical bar is displayed on a bright background, with the bar straight in front of the fly. The L-R measurement of a flying fly controls the rotational position of the stripe, where an increase in L-R (indicative of a right turn) will rotate the stripe to the left and vice-versa. A stripe is first presented at a random position, and the fly is given 20 seconds to control their apparent orientation with respect to the stripe. (top-right) Histograms of stripe position and turning measurements during a typical stripe-fixation experiment in DL flies (N=6). A peak around 0° in the stripe fixation histogram indicates consistent stripe fixation (the stripe is most often positioned directly in front of the fly). A peak around 0 in the L-R histogram indicates primarily small turning behaviors over the course of the experiment. (bottom) Consequences of decreasing the display update rate on a fly's ability to fixate a stripe and the turning behaviors observed during stripe fixation.

3.5 Discussion

I have presented a complete approach based on a new display system to mapping the optic flow encoding properties of visual projection neurons; both excitatory and inhibitory contributions of local motion could be mapped onto specific visual locations. While the number and extent of stimulus mapping locations is limited by the constraints of a 2-photon calcium imaging experiment,

multiple locations could be targeted in the left and right eyes independently, as well as the binocular overlap region. The combination of excitatory and inhibitory optic flow tuning seen in the LPC1 population response strongly implicates selectivity to back-to-front optic flow in a way that selects again rotational motion, but discussion of LPC1 responses will be a focus of chapter 4 where this cell-type is explored in depth.

Presenting all types of rotational and translational optic flow is made easy in this display system, which quickly generated a comprehensive dataset for behavioral measurements of a flying fly in response to optic flow across a wide range of temporal frequencies. The L-R behavioral measurement is a good proxy for a fly's intention to turn clockwise or counter-clockwise, as has been measured directly in the past by torque meters in response to rotational motion (Gotz, 1964). This can be interpreted as the fly's attempt to stabilize its orientation against externally caused deviations from its intended course. The L+R behavioral measurement may be a reasonable proxy for a lift response as well as a pitch response, though the relationship between L+R and pitch is potentially more complicated; the L+R signal can change by an actual wingbeat amplitude (i.e. stroke angle) change or by a pronation/supination of wingbeat rotation angle – a wingbeat angle which is more parallel to the plane of the optical sensor will cause a greater amplitude signal. Wingbeat frequency appeared to be a better proxy for a lift or upward force response, as there were similar directional responses to both lift and pitch stimuli in the direction expected to stabilize its flying height and pitch orientation, which is in agreement with our current understanding of *Drosophila* flight control (Dickinson & Muijres, 2016).

While the experimental observations of fly flight behavior in this project are consistent with our understanding of how flies should respond to different types of stimuli representing self-motion, it is important to consider how tethered behavioral setups might influence the animal's natural behavioral characteristics. During free flight for instance, information on changes in body position due to steering behaviors can from non-visual sources such as the halteres or Johnston's organ of the antennae (Dickinson & Muijres, 2016). When a visual stimulus representing self-motion is presented to a tethered animal, we cannot assume that the animal will have the same behavioral reaction as when it also receives similar self-motion information from other sensory systems. Tethered behavioral setups which incorporate functional imaging or electrophysiology can be even more invasive and put the animal in a highly unnatural behavioral state. Preparations that include cutting windows in cuticle, fixing the head position, and cutting limbs may also have a profound effect on the behavioral state of the animal, which has been shown to have effects on circuit properties even very early in the visual system (Strother et al., 2018).

While tethered flight setups have their own set of limitations, they have still been highly useful in isolating the visual component of external stimuli which influence flight behaviors, and the improvements in visual display technology made in this project allowed for experiments that were not possible with other display systems. The ability to measure the temporal frequency tuning of these flight behaviors up to and including speeds that are fast enough to no longer produce any consistent behavioral response allowed us to more comprehensively compare temporal frequency tuning across different motion types. All 6 optic flow fields produced a similar tuning curve, with the peak behavior observed at 8 Hz. The overall similar profile of these turning responses supports the nearly consensus view of the fly motion pathway: the tuning properties of the motion pathway come from elementary motion detectors (now understood to be the T4 and T5 neurons) that feed spatial filters (such as LPTCs) generating the diverse behavioral responses (Borst, 2014). Therefore, it is not expected that different patterns of motion would reveal very different tuning.

The usefulness of the high-speed operation of the G4 display system is not limited to the presentation of high-speed motion; faster display rates also mean smoother motion stimuli at all speeds and pattern complexities. The higher pixel-density contributes to more accurate stimuli for all patterns, whether moving or static. Multi-color LED panels further add to the available options for generating visual stimuli; it is possible to test navigation by sunlight, horizon stabilization by a UV-lit sky, or to simulate UV-reflecting objects in a complex simulated natural environment. The ability to incorporate this level of color control in a system that can operate in closed-loop without needing pre-rendered frames represents a significant advance in virtual reality systems for vision research. The ability to present UV stimuli expands the spectral options for color-vision research, as well as for avoiding spectral overlap with various fluorescent indicators and optogenetic tools.

These technical improvements in the G4 display system could make this attractive for many animal research labs, including those that study model systems beyond flying flies. Even while these results are currently being prepared for publication, I have already assisted in assembling G4 display systems for other labs at the Janelia Research Campus; in the labs of Brad Hulse and Stephen Huston for use in walking and flying fly behavior setups, and in the lab of Marius Pachitariu in a multi-sensory setup for walking mice. I believe this is the only display system currently available that addresses the important set of technical challenges faced in experimental vision research described in this chapter.

Chapter 4: Classes of small visual projection neurons detect translational motion vision in flies

4.1 Abstract

The perception of visual motion is useful for animal navigation and moving object detection, and flies are a prominent model system for elucidating the neural mechanisms behind this process. In *Drosophila*, directionally selective neurons in the optic lobe (T4 and T5 cells) compute local motion and project retinotopically into direction-selective layers in the Lobula Plate. Several large visual projection neurons (VPNs) have been extensively studied that integrate Lobula Plate local motion information across a large field-of-view of the fly eye and project to the central brain. However, the *Drosophila* visual system also features small-field visual-projection neurons which have received little attention. Here I present the results of studying one such cell type, called Lobula Plate Columnar type 1 (LPC1), in tethered flies while presenting visual stimulation with an LED display capable of delivering all types of rotational and translational motion stimuli. Using 2-photon calcium imaging in LPC1 terminals in the central brain, I found that a unilateral LPC1 population is highly selective to back-to-front translation optic flow. Through tethered behavioral experiments done in collaboration with graduate student Jessica Eliason, we found that LPC1 was strongly tied to the detection of back-to-front translation and caused flies to cease or reduce forward walking, while having no effect on turning behaviors. I found through further functional imaging that unilateral LPC1 cells gain selectivity to back-to-front translation by the selective excitation in response to back-to-front motion on the ipsilateral eye and inhibition induced by front-to-back motion on the contralateral eye. This simple mechanism functions to differentiate between translation optic flow and patterns associated with self-rotation. Additionally, I found that the high temporal frequency tuning of LPC1 may be attributed to TmY3 cells in the Lobula Plate, enhancing its directional responses to faster speeds. Finally, I found that another class of small-field visual projection neurons, named Lobula-Lobula Plate Columnar type 1 (LLPC1), selects for front-to-back translation over rotation using the same mechanism of contralateral eye motion inhibition that LPC1 does. This work provides a platform from which to explore and understand the larger network surrounding small-field visual projection neurons and the detection of translational motion.

4.2 Introduction

4.2.1 Visual projection neurons

In fly vision research, significant effort has focused on identifying the cellular processes that lead to elementary motion detection (Leong, Esch, Poole, Ganguli, & Clandinin, 2016; Maisak et al., 2013; Strother et al., 2017). Directional selectivity is known to emerge in the Lobula Plate in T4 and T5 cells; however, less is known about how this elementary motion information is further processed and propagated into the central brain. Previous research has identified tangential cells which receive input spanning large regions of the Lobula Plate (Lobula Plate Tangential Cells, or LPTCs) and project this integrated motion information to the central brain (Hausen, 1984; Krapp, Hengstenberg, & Hengstenberg, 1998). Some of these visual projection neurons (VPNs) have been found to encode patterns of wide-field visual motion that correspond to self-rotation (Krapp & Hengstenberg, 1996); however, only a small number of translational motion-encoding LPTCs have been identified and characterized (Longden, Wicklein, Hardcastle, Huston, & Krapp, 2017). Furthermore, there exists many uncharacterized small-field VPNs which are more difficult to study using standard electrophysiology methods, suggesting that there are many aspects of the network of VPNs yet to be understood.

4.2.2 Genetic screen for motion deficits

To identify new cells important for visual motion information processing, a high-throughput behavioral assay (known as the Fly Vision Box, designed by Michael Reiser and engineered by Gus Lott, Tanya Tabachnick, and Magnus Karlsson) was recently developed at Janelia to screen for cell-type-specific deficits in behavioral responses to motion stimuli (Figure 4.1). Freely-walking flies were placed in corridors with a series of LEDs lining the walls, where drifting grating stimuli could be presented at various spatial wavelengths and temporal frequencies. The walking responses of these flies were monitored with cameras mounted above, and directional reactions to drifting gratings were calculated for groups of flies. Thousands of GAL4 and split-GAL4 lines driving expression of a silencing effector were screened through this assay (behavioral screen performed by William Rowell, Austin Edwards, Wyatt Korff, and Jessica Eliason; analysis by Lihi Zelnik-Manor, Kristin Branson, Allen Lee, the Fly Light team, and the Fly Core; results not yet published).

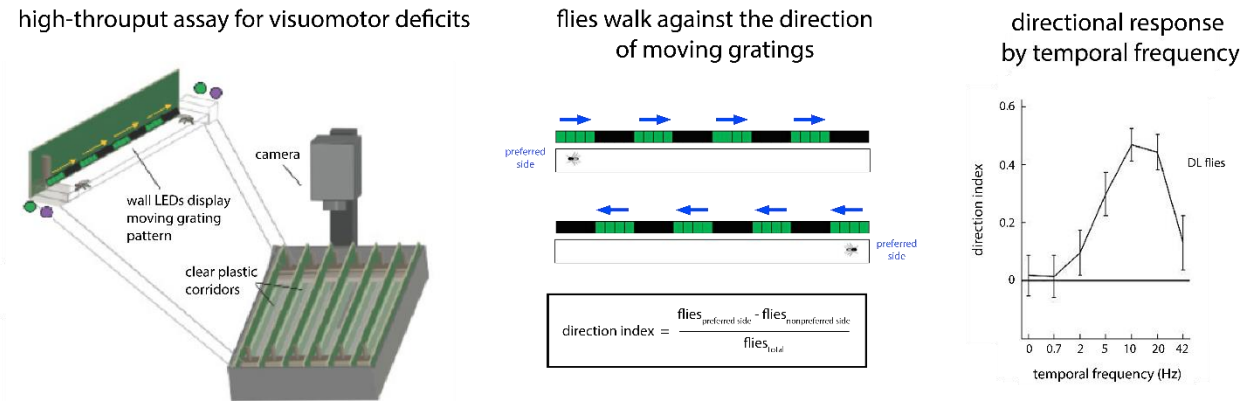

Figure 4.1: Fly Vision Box motion assay for genetic screening of visuo-motor deficits.

(left) Cartoon of a free-walking corridor assay in the Fly Vision Box. LEDs along corridor wall deliver stimuli while a camera from above tracks the movement of flies within multiple corridors. (middle) Motion-assay delivers a moving grating pattern along the wall, while flies are observed to walk in the opposite direction as the gratings; direction index quantifies the amount of directionality. (right) Directional response of Dickinson Lab (DL; a standardized genetic strain of *Drosophila melanogaster*) flies as a function of the temporal frequency of the moving gratings; peak response observed around 10 Hz. Figures from Jessica Eliason, not yet published.

4.2.3 Identification of LPC1

Many visual deficits were observed when silencing cells in the optic lobe as expected, since the early visual system provides input to all aspects of higher visual information processing. One split-GAL4 line that resulted in a significant motion vision deficit in the Fly Vision Box assay which was not entirely localized within the optic lobe targeted a population of ~100 cells with inputs in the Lobula Plate and outputs in the central brain. This cell-type (named Lobula Plate Columnar type 1, or LLPC1) had been previously identified to have a distinct glomerulus located in the optic ventrolateral neuropil (Panser et al., 2016) and is likely to be cholinergic based on a recently published resource of *Drosophila* visual system cell-type transcriptomes (Davis et al., 2018). Dendrites of these cells are columnar and small-field in the Lobula Plate, primarily targeting layer 2 (Figure 4.2, left), and based on their anatomy are estimated to have a receptive field covering a ~20° solid angle.

Due to the observed silencing phenotype of LPC1 in the Fly Vision Box assay, follow-up experiments were conducted in LPC1-silenced flies in a tethered walking assay, as described in Strother et. al (2017). In contrast to the Fly Vision Box assay in which a group of freely walking flies are tested simultaneously in a single corridor, a single-fly tethered walking assay – while significantly lower throughput – allows more precise control over what visual stimuli a fly receives and more precise measurements of their walking behaviors. Despite the large behavioral deficit with moving

gratings in the Fly Vision Box motion assay, it was observed that tethered-walking flies with LPC1 cells silenced did not have any large deficits to their turning response to clockwise (CW) or counter-clockwise (CCW) rotational motion.

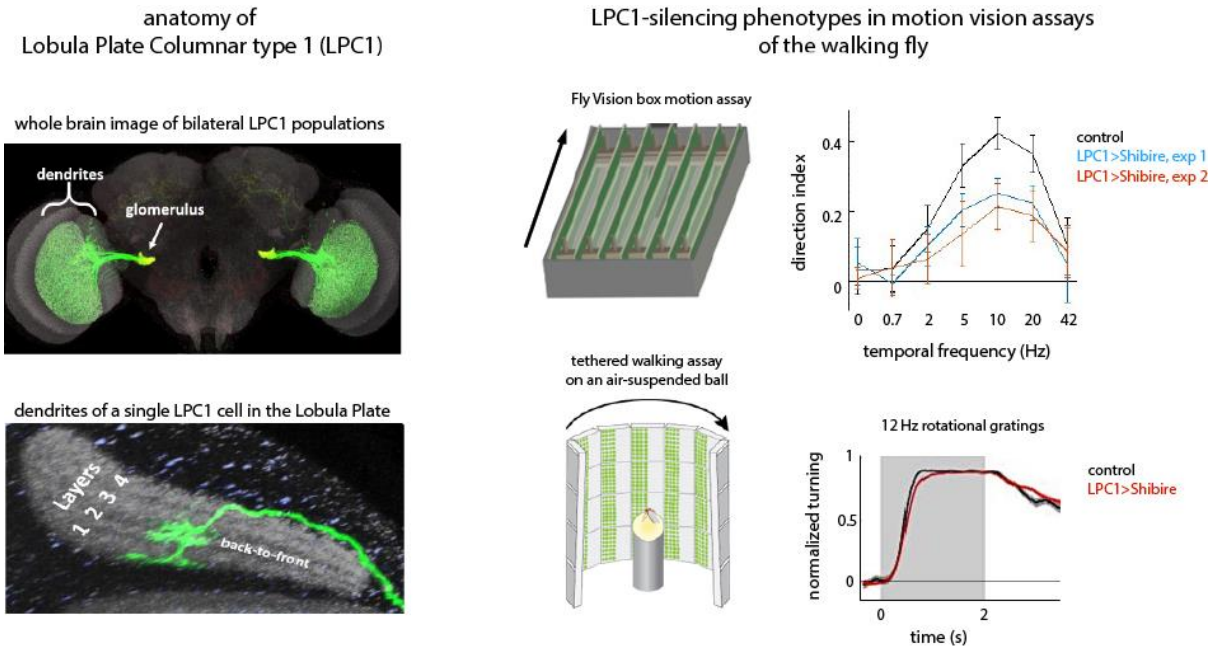

Figure 4.2: Anatomy of LPC1 and observed behavioral deficits from LPC1 silencing.

(left) Anatomy of LPC1 population, composed of ~100 small-field columnar cells, primarily branching in Lobula Plate layer 2 – images and identification by Aljoscha Nern. (right) Behavioral effects of LPC1 silencing through genetically targeted expression of Shibire. (top) LPC1 silencing caused a reduction in the directional response in the Fly Vision Box motion assay; figures and data from Jessica Eliason. (bottom) LPC1 silencing produced no large turning phenotypes in tethered rotational optomotor walking assay; figures and data from Shiuan-Tze Wu.

4.2.4 Aims of this chapter

The LPC1 cell-type was one of a relatively small number of uncharacterized optic lobe cells that produced a significant phenotype in the Fly Vision Box motion assay, but an early inability to observe a behavioral deficit from LPC1-silencing in a tethered walking assay was a source of mystery. The difference in display configurations between the Fly Vision Box and the cylindrical arena hinted to me that this cell-type may be selective to translational optic flow over rotational optic flow. Using the tools for generating and displaying visual stimuli developed in chapter 3, and the ability to target small-field VPNs (such as LPC1) with genetic tools for *Drosophila*, I was well prepared to evaluate this

possibility. I aimed to investigate the types of motion stimuli that LPC1 is selective for, and what behavioral function it may be serving in the visual control of locomotion.

4.3 Methods

4.3.1 Flies

Flies were reared under standard conditions (60% humidity, 16h light / 8h dark, cornmeal agar diet) at 25° C. Flies expressing the Chrimson channelrhodopsin (a red-light-gated ion channel which can depolarize neurons upon photoactivation) were reared on a cornmeal agar diet with a 1:250 concentration of retinol. Behavioral experiments were performed on female flies 3-5 days post-eclosion, while imaging experiments were performed on female flies 1-4 days post-eclosion. Cell type specific expression of indicators, silencers, and activators was achieved using the GAL4/UAS, LexA/LexAop, and Split-GAL4/UAS expression control systems (Luan, Peabody, Vinson, White, & yes, 2006; Pfeiffer, et al., 2010). Expression of the Chrimson channelrhodopsin in bilateral or unilateral (or empty) LPC1 populations was achieved using the FLP/FRT expression control system (Duffy, 2002). All genotypes used in this dissertation are listed in Table 4.1.

stock genotype	targeted cell-type	relevant indicator/effector	used in figures:
w^{+}(DL)/w^{1118}; 81A05-p65ADZp (attP40)/+(DL); VT031495-ZpGdbd(attP2)/ pJFRC7-20XUAS-IVS-GCaMP6m(VK00005)	LPC1 (SS02575)	GCaMP6m	3.13, 3.14, 4.3, 4.4, 4.7, 4.8, 4.9, 4.10
w^{+}(DL)/w^{1118}; VT057342-p65ADZp (attP40)/+(DL); VT044492-ZpGdbd(attP2)/ pJFRC7-20XUAS-IVS-GCaMP6m(VK00005)	LLPC1 (SS02407)	GCaMP6m	4.11, 4.12, 4.14, 4.15
w; VT002033-p65ADZp (attP40)/+(DL); 78A06-ZpGdbd(attP2)/ 20XUAS-Syn-OpGCamp6s(su(Hw)attpP1)	LPC1-interneuron (SS34952)	OpGCaMP6s	4.13, 4.14, 4.15
w+,pJFRC300-20XUAS-FRT>-dSTOP-FRT>-CsChrimson-mVenus(attP18),pBPhsFlp2::PEST(attP3); 81A05-p65ADZp (attP40)/+; VT031495-ZpGdbd(attP2)/ +	LPC1 (SS02575) (unilateral, bilateral, and none)	Chrimson	4.6
LexAop2-Syn21-opGCaMP6s; 395-AD/CyO; 395-DBD/Tm6b 81A05-LexA/CyO; UAS-Kir2.1/Tm6b	LPC1 (SS02575); TmY3 (SS00395)	GCaMP6s (LPC1); Kir2.1 (TmY3)	4.1
w^{+}(DL)/w^{1118}; 81A05-p65ADZp (attP40)/+(DL); UAS-ShibireTS1/Tm6b	LPC1 (SS02575)	Shibire	4.5

Table 4.1: List of fly genotypes used in this work.

4.3.2 *In vivo* preparation for tethered walking

Flies were prepared for walking behavior experiments as previously detailed (Strother et al., 2017) and summarized here. Wings of cold-anesthetized flies were immobilized with UV-curing glue (KOA 300-1; KEMXERT) at least 12 h prior to the experiments. On the day of experiments, each fly was glued to a tungsten rod (catalog #71600; A-M Systems) by the thorax and placed into an incubator (model PH09-DM, Thermoelectric Series; Darwin Chambers Company) set to 32 °C and 60% humidity for at least 25 min before the start of behavioral experiments.

4.3.3 Optogenetics

For optogenetic activation of Chrimson, a 660 nm fiber-coupled LED (Thorlabs Deep Red M660F1) controlled by an LED driver (Thorlabs LEDD1B) set to ~0.7 , was directed approximately 1 inch from the tethered fly with a light guide (400 µm, 0.39 NA SMA to ceramic ferrule patch cable, Thorlabs FT400EMT). Timing of the optogenetic stimulation was controlled using a timed analog output of the G3 display system. After each optogenetic experiment, the fly brain was dissected and imaged with an epifluorescence microscope to record the location of Chrimson expression (i.e. left optic lobe, right optic lobe, both, or neither). Data from flies expressing Chrimson in only the left or right optic lobes were combined to form the “unilateral” group (Figure 4.6), with the turning behaviors of the flies expressing Chrimson in the right optic lobe were flipped and averaged with those expressing in the left optic lobe to prevent directional responses from being averaged out.

4.3.4 Visual stimuli

For behavioral experiments, visual stimuli were presented to tethered flies using a G3 cylindrical LED arena (manufactured by IO Rodeo, http://www.iorodeo.com/; further details at https://bitbucket.org/mreiser/panels) constructed from 36 8x8 pixel LED modules containing green LEDs (UltraPure Green LED, IO Rodeo). The cylindrical arena covered 270° across the azimuth of the visual field and ~120° in elevation. The angular distance between pixels along the horizontal plane is 3.75^{o}. An earlier version of this system has been previously described (Reiser & Dickinson, 2008).

For calcium imaging experiments, visual stimuli were presented to tethered flies using the 240° G4 arena display system described in chapter 3. To further separate the LED emission spectra from GCaMP6m fluorescence, a low-pass gel filter (Deep Golden Amber gel filter, LEE Filters #L135S) was laid on top of the LEDs along with a diffusing filter (Full White Diffusion filter, LEE filters #216R) to prevent reflections from the gel filter.

All patterns that were displayed on the cylindrical LED arenas were generated using a set of MATLAB scripts for parameterizing and visualizing moving grating patterns for this display system,

described in Chapter 3. All experimental stimuli consisted of 100% contrast square-wave gratings set to 30° spatial wavelength. For tethered walking experiments, a single trial of visual stimuli started with 2 seconds of the display set to a uniform brightness (LEDs set to a level halfway between that of the bright and dark bars of the grating so the overall brightness does not change when the moving gratings appear), followed by 2 seconds of the moving grating stimuli, followed by another 2 seconds of the uniform frame. For optogenetic activation behavioral experiments, no grating pattern was displayed, only the uniform frame was displayed for 6 seconds with the 660nm red LED turning on for 1 second starting at the beginning of the 3rd second of the uniform frame. For calcium imaging experiments, a single trial consisted of 2 seconds of a uniform frame, followed by 1 second of moving gratings, followed by 6 seconds of the uniform frame; the increased time in between experimental visual stimuli allowed more time for the GCaMP6m fluorescence signal to return to baseline fluorescence levels. Experiments were organized using a randomized block trial structure – within a block, the complete set of visual stimuli were presented in a randomized order, and 3 blocks were presented such that each stimulus was shown at least 3 times. For imaging experiments, every trial was repeated 3 times; for most behavioral experiments, trials were repeated 4 times; for optogenetic activation experiments (660 nm LED off/LED on with the uniform visual stimulus), trials were repeated 15 times.

4.3.5 Tethered walking equipment and analysis

The methods used for these behavioral experiments have been detailed elsewhere (Strother et al., 2017) but are summarized here. Tethered flies were positioned onto an air-supported Styrofoam ball using 3-axis micromanipulators and two cameras (Firefly MV FFMV-03M2M and Basler 602f) that imaged the fly and ball from above and behind. The Styrofoam ball, measured at 9 mm diameter and 129-mg, was supported by 340 SCCM airflow regulated by a digital mass flow controller (Smart-Trak, Sierra Instruments). The complete setup, which included the visual LED arena (Reiser & Dickinson, 2008) and the treadmill system (Seelig et al., 2010) was housed within the incubator. Behavioral experiments were conducted at 34 °C and 60% humidity. The ball movement was tracked by two optical flow cameras (ADNS-6090; Avago Technologies) that measure image displacements. The camera measurements were acquired by a custom MATLAB (MathWorks, Natick, MA) program which runs the experiment, and these signals were transformed into 100 Hz measurements of forward, sideslip, and turning measurements (ball pitch, roll, and yaw), in arbitrary units. These measurements of displacement are scaled by 100/s to generate velocity signals (arbitrary units per second).

Only turning and forward measurements were analyzed and described in this work. The time-series of turning and forward measurements in response to multiple repetitions of each visual stimulus were averaged together to produce a mean turning and forward response for each fly, and this was computed for all visual stimuli. For the mean time-series of turning, all flies of a single genotype were then normalized to the 98th percentile turning measurement of all flies from that genotype (a more robust procedure than normalizing to peak), which scaled the values to range from approximately -1 to +1, where -1 represents an approximately maximum yaw left (counter-clockwise) turn and +1 indicates an approximately maximum yaw right (clockwise) turn. For the mean time-series of forward walking, all flies of a single genotype were normalized to the mean forward measurement during the 2 seconds prior to all visual stimuli (2 seconds of uniform frame preceding the experimental stimuli), scaling the values from approximately 0 to 1, where 1 represents the baseline forward walking prior to the start of experimental visual stimuli and 0 represents no forward walking. For summary plots, a single value of the turning and forward responses was calculated from the time-series by averaging the mean time-series values during the 2 seconds of open-loop visual stimulus presentation. Both time-series and summary data are plotted as mean of all flies of a single genotype +/- SEM.

4.3.6 2-photon imaging and analysis

Calcium imaging in the central brain region was conducted and analyzed using the same methods described in section 3.3.7. Additionally, to create fluorescence change maps (Figure 4.12), instead of calculating a time-series of fluorescence change using the mean value within an ROI, this calculation was performed on every pixel in the image independently and the fluorescence change value calculated for each pixel was then color-coded by the amount of fluorescence change.

4.3.7 Statistics

P-values were calculated using the Mann-Whitney U-test (“ranksum” function in MATLAB). The Benjamini-Hochberg Procedure was used to correct for the false discovery rate (FDR) associated with multiple comparisons; unless otherwise noted, 3 comparisons were made (1 for each temporal frequency of the same visual stimulus – 1, 3, and 9 Hz). Statistically significant differences were noted with 1 star for $p<0.05$ and FDR=0.05, and with 2 stars for $p<0.01$ and FDR=0.01.

4.4 Results

4.4.1 Calcium imaging of LPC1 shows selectivity for back-to-front translation

From preliminary studies of LPC1 by colleagues at Janelia, I became interested in the discrepancy between the strong LPC1 silencing phenotype in the Fly Vision Box motion assay and the tethered walking rotational assay (Figure 4.2). The differences in visual stimuli presented in these 2 assays, with stimuli in the Fly Vision Box appearing translational while stimuli in the tethered assay is explicitly rotational, I hypothesized that LPC1 may be selective to translation optic flow over rotation. Presenting the stimuli I previously generated for all optic flow types (described in section 3.4.2) to a tethered fly for calcium imaging in the LPC1 population, I directly tested this hypothesis (Figure 4.3). I observed that the unilateral (left-eye) LPC1 population was most selective back-to-front (regressive) translation even though the stimuli delivered with the 240° arena only stimulates a relatively small extent of the fly's visual field, thus containing less motion information than the same stimuli displayed on the 270° arena as shown in Figure 3.4. Furthermore, upon generating a linear prediction of the combined responses between both eye LPC1 populations by inferring how the opposite eye would respond (responses to bilaterally asymmetric stimuli are assumed to be flipped in direction), the selectivity to back-to-front translation appears even greater. These results are shown in Figure 4.3 for a 9 Hz temporal frequency of grating motion, which was found to maximally excite LPC1 out of a number of temporal frequencies tested (0.5, 1, 3, 6, 9, 12, 15, and 18 Hz).

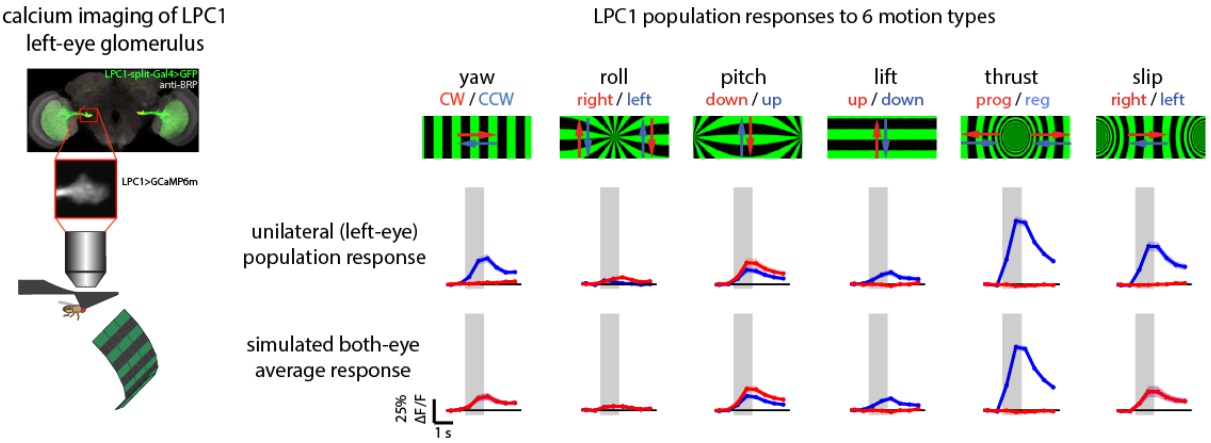

Figure 4.3: LPC1 population activity in response to optic flow types.

(left) 2-photon calcium imaging of the unilateral (left-eye) LPC1 population with stimuli delivered using the 240° arena; anatomy imaging from Aljoscha Nern. 6 motion types were presented, where the extent of the stimuli ranged from -90° to +90° in azimuth to prevent any portion of the stimuli from being occluded by the 20° mount (see Figure 3.11). (top-right) Unilateral LPC1 responses to the 6 motion types in both directions. (bottom-right) Predicted linear combined response of both left and right-eye LPC1 populations to the same stimuli: right-eye LPC1 responses are assumed to be the same as the left-eye for bilaterally symmetric stimuli (pitch, lift, thrust) and opposite for bilaterally asymmetric stimuli (yaw, roll, slip). Average +/- SEM of all flies (N=8) are plotted.

LPC1 was most selective to the back-to-front translation stimulus, though it was not immediately clear what components of this stimulus is responsible for this selectivity. As it is displayed on an upright cylindrical display, a thrust stimulus appears relatively complex when compared to simple motion in one of the 4 cardinal directions. The stimulus features a focus of contraction where the orientation of the gratings are always perpendicular to their direction of motion. Both the apparent speed and the apparent size of the bright and dark bars of the grating continually decrease (maintaining constant temporal frequency) until they can no longer be resolved by the resolution of the display near the pole of contraction. To understand what features of this complex visual stimulus LPC1 is selective toward, I created stimuli which removed the orientation change as well as the change in spatial wavelength/apparent speed of the thrust stimulus (Figure 4.4). I found that LPC1 selectivity was not affected by removing these components of the thrust stimulus, thus LPC1 appeared to primarily depend only on the horizontal component of thrust motion. A significant benefit to identifying that the horizontal component is sufficient to target LPC1's specificity is that this simple stimulus can also be displayed at reasonably high-speeds on the older G3 display system (due to its vertical uniformity), which has been used and validated for use in tethered walking experiments.

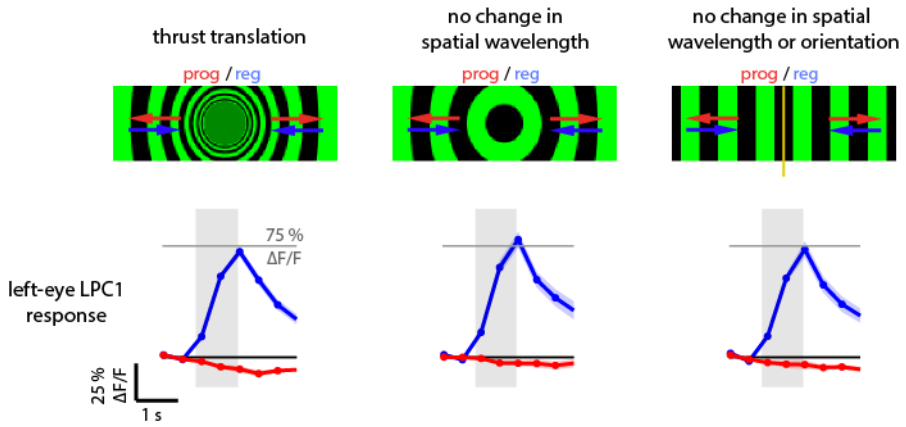

Figure 4.4: LPC1 excitation by type of back-to-front stimuli.

LPC1 activity during the presentation of different types of back-to-front and front-to-back stimuli. (left) Thrust grating stimuli on the 240° display. (middle) Stimuli which presents motion in the same directions as thrust stimuli but with constant spatial wavelength. (right) Stimuli which only reproduces the horizontal motion component of back-to-front and front-to-back thrust stimuli, at a constant spatial wavelength. Average +/- SEM of all flies (N=8) are plotted.

4.4.2 LPC1 modulates forward walking by back-to-front translation

Armed with the knowledge of the type of motion LPC1 is most selective to (back-to-front translation), I revisited tethered walking experiments in collaboration with fellow graduate student Jessica Eliason to see if any behavioral role can be attributed to LPC1 during walking. We used genetic tools to create genotypes of flies where LPC1 neurons could be silenced with heat using the Shibire effector or activated with red light using the Chrimson effector. Both the forward-walking and turning behaviors were measured in tethered flies while walking on an air-suspended ball during the presentation of visual stimuli using a G3 arena display. We found that simple front-to-back and back-to-front motion did not produce a turning response as expected (since they have equal amount of CW and CCW rotational motion), but both caused flies to reduce their forward walking. However, the significant reduction in forward walking caused by back-to-front motion was abolished in LPC1-silenced flies, further linking LPC1 to the detection of back-to-front translation (Figure 4.5). Turning responses to CW and CCW rotational stimuli was not affected by LPC1-silencing, again demonstrating the specificity of LPC1 to back-to-front motion.

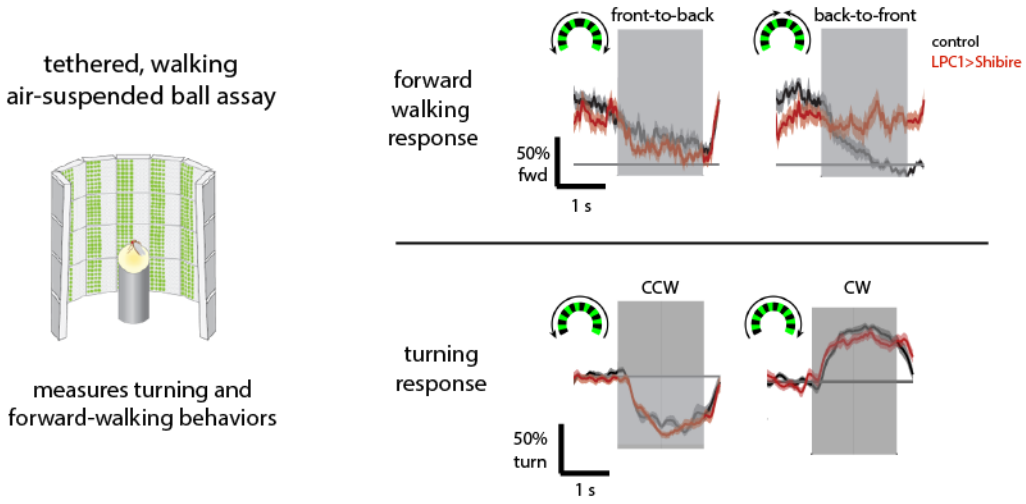

Figure 4.5: Effects of LPC1 silencing on walking behaviors.

(left) Cartoon of the tethered walking assay. A tethered fly mimics walking by spinning an air-suspended ball while visual stimuli is presented on a G3 LED arena. (top-right) Changes in forward-walking measurements during back-to-front and front-to-back translation stimuli (9 Hz temporal frequency) – the LPC1-silencing phenotype was observed in response to back-to-front motion only. (bottom-right) Turning responses caused by CCW and CW yaw rotational stimuli, no LPC1-silencing phenotype observed. Cartoons of each stimuli are displayed next to the response in radial view – simulated view from above the arena, but where the increasing arena height (arena rows) is displayed as an increasing radius. Average responses +/- SEM of all flies of each genotype (control N=20; LPC1-Shibire N=20) are plotted.

The behavioral consequence of silencing LPC1 was that the presentation of back-to-front translation no longer caused walking flies to stop forward walking. To further investigate this behavioral link to LPC1, we activated both bilateral and unilateral populations of LPC1 using genetically targeted expression of the Chrimson channelrhodopsin (Figure 4.6). In the absence of visual stimuli, the optogenetic activation of bilateral LPC1 caused a significant reduction in forward walking and had no effect on turning, as expected, since bilateral LPC1 excitation is associated with stimuli that is back-to-front on both eyes (i.e. not a rotational stimulus). Furthermore, activating only a unilateral LPC1 population also caused a reduction in forward walking without a simultaneous turning response, even though back-to-front motion on only one eye is partially consistent with rotational motion (the back-to-front half of rotational motion.) This provides further evidence that LPC1 is both highly selective to the detection of back-to-front translational (and not rotational) motion and is tightly coupled to forward walking (and not turning) behaviors.

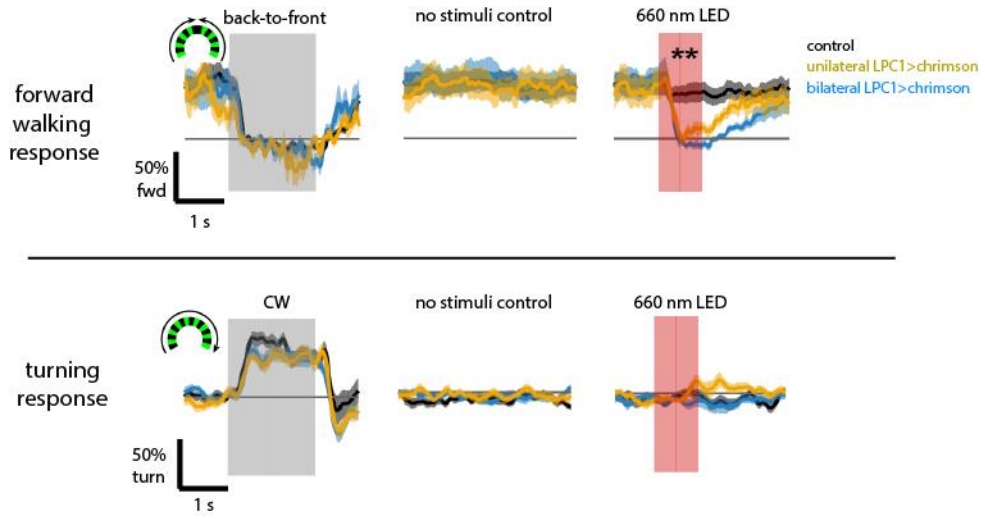

Figure 4.6: Effects of LPC1 activation on walking behaviors.

(top) Measurement of forward walking in response to a back-to-front visual stimulus (left), no stimulus (middle), or during optogenetic activation (right) of bilateral and unilateral populations of LPC1. All genotypes of flies tested come from the same genotype stock, but either express the Chrimson channelrhodopsin in LPC1 bilaterally, unilaterally, and do not express Chrimson at all, using the FLP/FRT expression control system (section 4.3.1). (bottom) Measurement of turning in response to a CW rotational visual stimulus, no stimulus, or during optogenetic activation of LPC1. Average response +/- SEM of all flies of each genotype (control N=14, unilateral N=17, bilateral N=19) are plotted.

4.4.3 Selectivity to back-to-front translation depends on contralateral motion

Multiple lines of evidence pointed to LPC1 being highly selective to a back-to-front translation stimulus (primarily, the horizontal component of back-to-front translation), but it was not yet clear how a unilateral LPC1 population gains this selectivity. To further explore how the unilateral (left-eye) LPC1 population gains selectivity to back-to-front translation over rotation, I presented motion in the 4 cardinal directions to the left (ipsilateral) and right (contralateral) eyes independently. I observed a complete selectivity to back-to-front motion on the ipsilateral eye over all other directions. A more comprehensive version of this experiment was described in Figure 3.13 which came to the same conclusion – the unilateral LPC1 population is selectively excited by ipsilateral back-to-front motion. This was also predicted by the LPC1 anatomy in the Lobula Plate (LP layer 2 inputs encode back-to-front motion) but does not explain selectivity to back-to-front translation over CW rotation as both stimuli produce significant back-to-front motion on the ipsilateral eye.

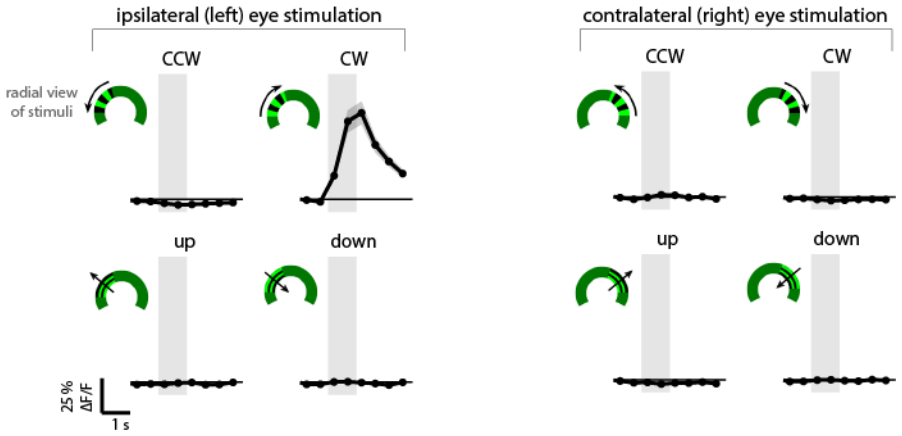

Figure 4.7: LPC1 selectivity to 4 cardinal motion directions on the ipsilateral and contralateral eye.

Back-to-front, front-to-back, up and down motions presented to left and right eyes individually. Extent of left-eye stimuli ranged from -20° to -90° in azimuth to avoid occlusion due to the mount and to avoid the binocular overlap region (see Figure 3.11). Extent of right-eye stimuli ranged from +20° to +90°. Average +/ SEM of all flies (N=10) are plotted.

Responses to translational motion were further explored by presenting translational motion with the focus of expansion (FOE) located every 30 degrees around the azimuth of the fly; this set of stimuli represents a gradual shift in translational motion direction from pure front-to-back translation to pure back-to-front. The unilateral LPC1 population again showed to be highly selective to back-to-front translation (Figure 4.8, top), with the amount of ipsilateral back-to-front motion being a fair predictor of LPC1 responses. A linear combination of left and right-eye LPC1 population responses predicts even greater selectivity to back-to-front translation, where a gradient in response is seen based on the degree of back-to-front motion (Figure 4.8, bottom). However, in the unilateral LPC1 responses to the varying FOE stimuli, a strong asymmetry in the responses was observed that could not be explained simply by the amount of ipsilateral back-to-front motion present in the stimuli. Much of the extra variance appeared to be explained by the amount of contralateral front-to-back motion that was present in the stimuli; for stimuli containing the same amount of ipsilateral back-to-front motion, more contralateral front-to-back motion seemed to cause a significant reduction in LPC1's response.

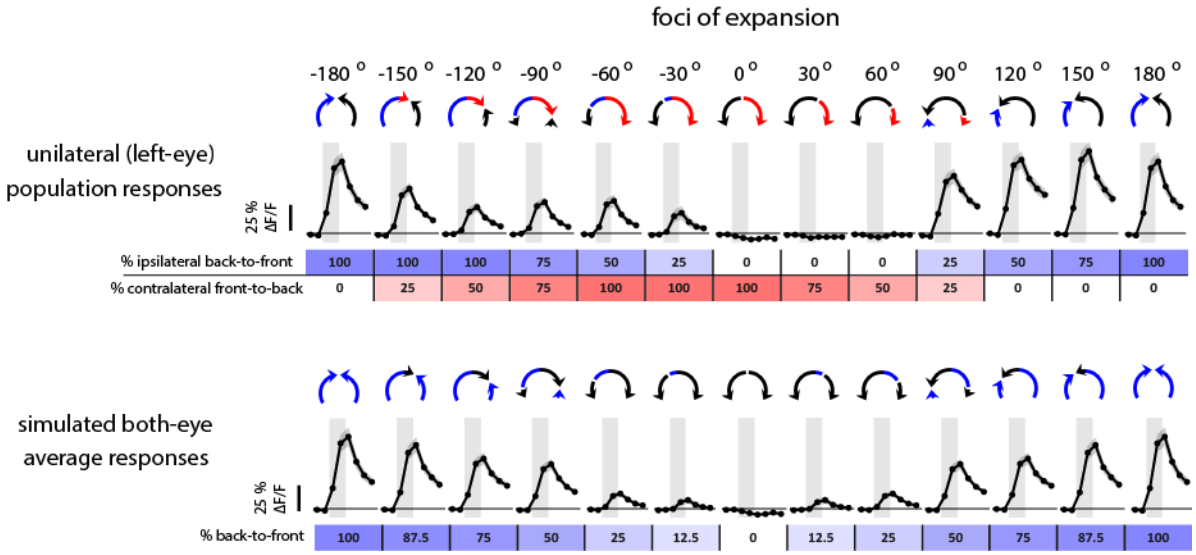

Figure 4.8: LPC1 responses to translational motion from different foci of expansion.

(top) LPC1 responses to translation stimuli along foci of expansion (FOE) located every 30° along the azimuth of the visual field; a FOE located at 0° represents pure front-to-back translation and an FOE located at +/- 180° represents pure back-to-front translation. The amount of ipsilateral back-to-front motion is calculated for each stimulus and shown below, color coded in blue, and the location of this back-to-front component of the stimulus is shown above. Similarly, the amount of contralateral front-to-back motion is calculated and shown in red. (bottom) Linear combination of responses of left and right-eye LPC1 populations to foci of expansion stimuli. The amount of combined back-to-front motion on both eyes is color coded in blue. Average +/- SEM of all flies (N=10) are plotted.

The suppression/inhibition of LPC1 responses by contralateral front-to-back motion could explain LPC1's selectivity to back-to-front translation over rotation. To directly test this hypothesis, I measured LPC1 responses to ipsilateral back-to-front motion and observed how this excitation is modulated by the simultaneous presentation of motion on the contralateral eye (Figure 4.9). I found a very significant modulation by motion presented to the contralateral eye at multiple temporal frequencies; LPC1 excitation is enhanced by back-to-front motion and greatly reduced by front-to-back motion on the contralateral eye. This modulation was observed even when presenting stimuli which covers a smaller extent of the visual field (in azimuth) to avoid the binocular overlap region and occlusion by the mount, which could have been confounding factors. Since a contralateral back-to-front stimulus did not excite LPC1 on its own (Figure 4.7), the enhancement by contralateral back-to-front motion may be caused by the removal contralateral inhibition. These observations – excitation by ipsilateral back-to-front motion and inhibition by contralateral front-to-back motion – provide evidence for a very simple mechanism to distinguish between translation and self-rotation.

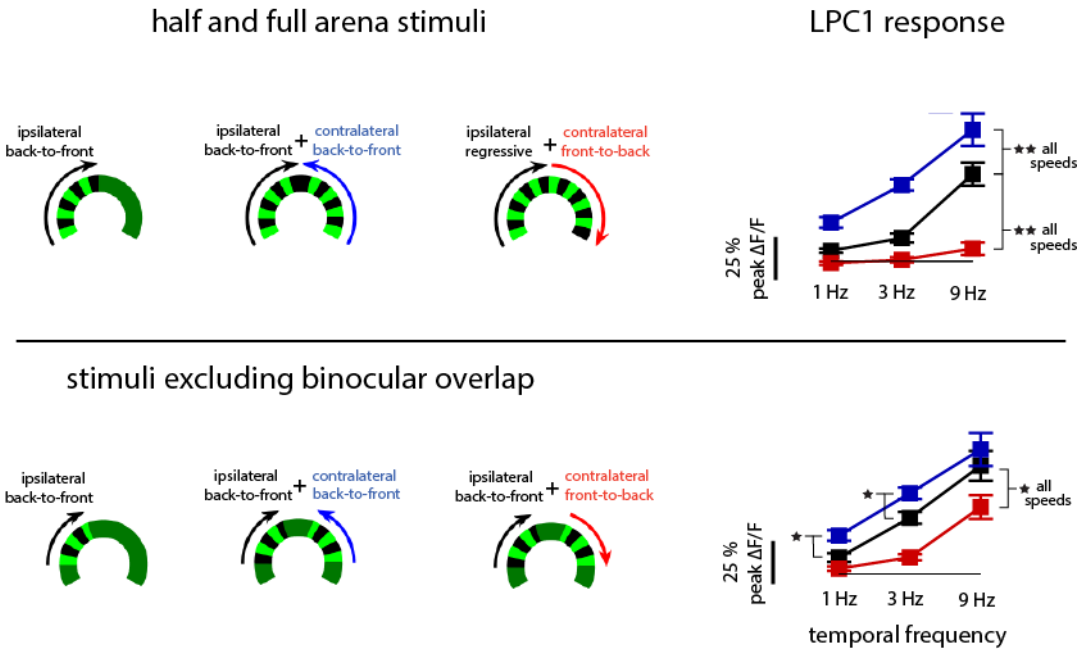

Figure 4.9: Modulation of LPC1 activity by contralateral motion.

(top) Unilateral (left-eye) LPC1 population responses to ipsilateral back-to-front motion and the change in responses caused by the simultaneous presentation of contralateral front-to-back or back-to-front motion. Peak fluorescence change is plotted for motion stimuli at 3 temporal frequencies (1, 3, and 9 Hz). Data in black represents LPC1 responses to ipsilateral back-to-front motion alone; data in red represent LPC1 responses to ipsilateral back-to-front and contralateral front-to-back motion presented simultaneously; data in blue represent LPC1 responses to ipsilateral back-to-front and contralateral back-to-front motion presented simultaneously. Statistically significant differences between responses were noted with stars (1 star for $p<0.05$ and FDR=5%; 2 stars for $p<0.01$, FDR=1%). (bottom) Stimuli which exclude the region of binocular overlap and region of occlusion by the imaging mount: left eye stimulus ranges from -90° to -20° in longitude of the fly visual field; right eye stimulus ranges from 20° to 90°. Average +/- SEM of all flies (N=10) are plotted.

4.4.4 High-speed tuning dependent on non-T4/T5 input

LPC1 being downstream of Lobula Plate layer 2 T4 and T5 cells predicted its excitation by ipsilateral back-to-front motion, but there were multiple observations that it did not predict. One such observation is that LPC1 activity is modulated by contralateral-eye motion, which was described in the previous section. Another curious observation is that LPC1 is tuned for unexpectedly high temporal frequencies (TFs); functional imaging in T4 and T5 cells have previously found that they are most strongly excited by 1-3 Hz TF motion, with responses being much smaller at 9 Hz (Strother et al., 2017). In contrast, I observed LPC1 to be much more strongly excited by 9 Hz TF motion over 3 or 1 Hz.

To attempt to identify other sources for these unique properties of LPC1, tracing and synapse tagging was conducted by the Janelia Connectome Annotation Team (CAT) on the full-adult fly brain (FAFB) EM volume (Zheng et al., 2018) to identify strong synaptic partners to LPC1. Based on their findings, TmY3 cells are also a major input to LPC1 cells in the Lobula Plate. To understand what role this cell type may be playing in the context of LPC1's stimulus encoding properties, a *Drosophila* stock genotype expressing GCaMP6s in LPC1 and Kir2.1 (a strong neuronal silencer) in TmY3 cells was generated by Jessica Eliason. With TmY3 silenced, I found that the modulation of LPC1 responses by contralateral motion appeared unaffected, but the temporal frequency tuning shifted significantly toward lower frequencies, potentially implicating TmY3 in high-speed motion detection (Figure 4.10).

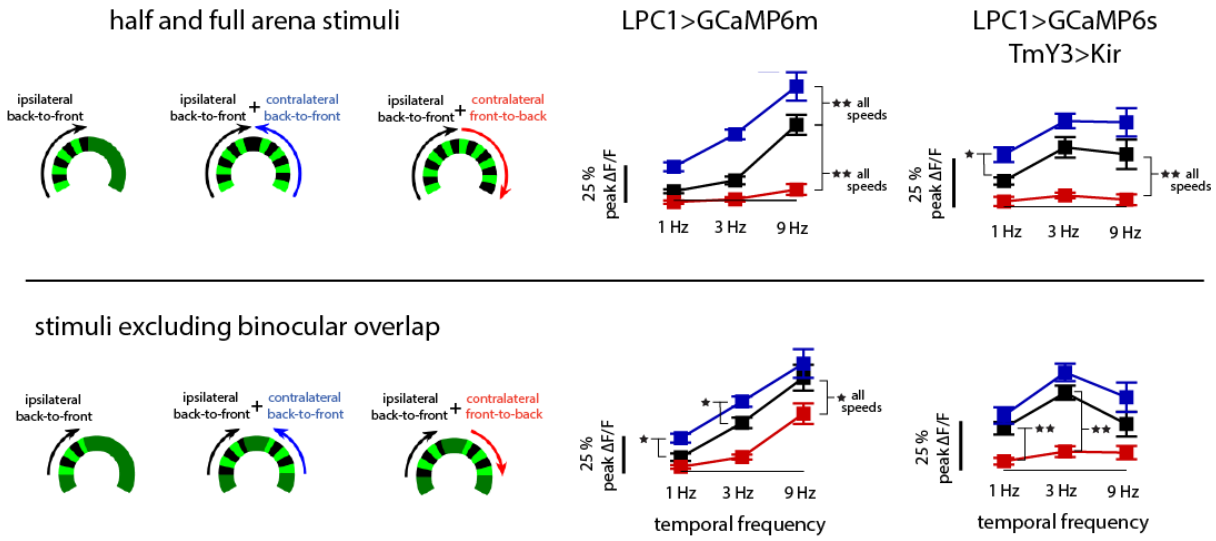

Figure 4.10: TmY3 silencing effects on LPC1 TF tuning.

(top) Left-eye LPC1 population responses to ipsilateral back-to-front motion and the change in responses caused by simultaneous contralateral front-to-back/back-to-front motion. Peak fluorescence change is plotted for motion stimuli at 3 temporal frequencies (1, 3, and 9 Hz). Statistically significant differences between responses were noted with stars (1 star for $p<0.05$ and FDR=5%; 2 stars for $p<0.01$ and FDR=1%). (bottom) Stimuli which exclude the region of binocular overlap and region of occlusion by the imaging mount: left eye stimulus ranges from -90° to -20° in longitude of the fly visual field; right eye stimulus ranges from 20° to 90°. (right) Effects of silencing TmY3 cells on LPC1 responses, which shifted LPC1 tuning toward lower temporal frequencies. Average +/- SEM of all flies (N=10 for LPC1>GCaMP6m; N=6 for LPC1>GCaMP6s/TmY3>Kir2.1) are plotted.

4.4.5 LLPC1 and the detection of front-to-back motion

After the discovery of LPC1's role in translational motion detection, similar small-field cell populations were identified to expand our understanding of the wider network of small-field VPNs. One such cell-type, named Lobula-Lobula Plate Columnar type 1 (LLPC1), receives input from layer 1 of the Lobula Plate, the layer encoding front-to-back motion. Similar to LPC1, LLPC1 dendrites are columnar and small-field in the Lobula Plate, and their axons project to a central glomerulus close in proximity to that of the LPC1 glomerulus. Calcium imaging of LLPC1 in this glomerulus produced similar results to that of LPC1 but for the opposite direction of motion – unilateral LLPC1 is highly selective to front-to-back motion on the ipsilateral eye, as predicted by Lobula Plate layer 1 inputs (Figure 4.11).

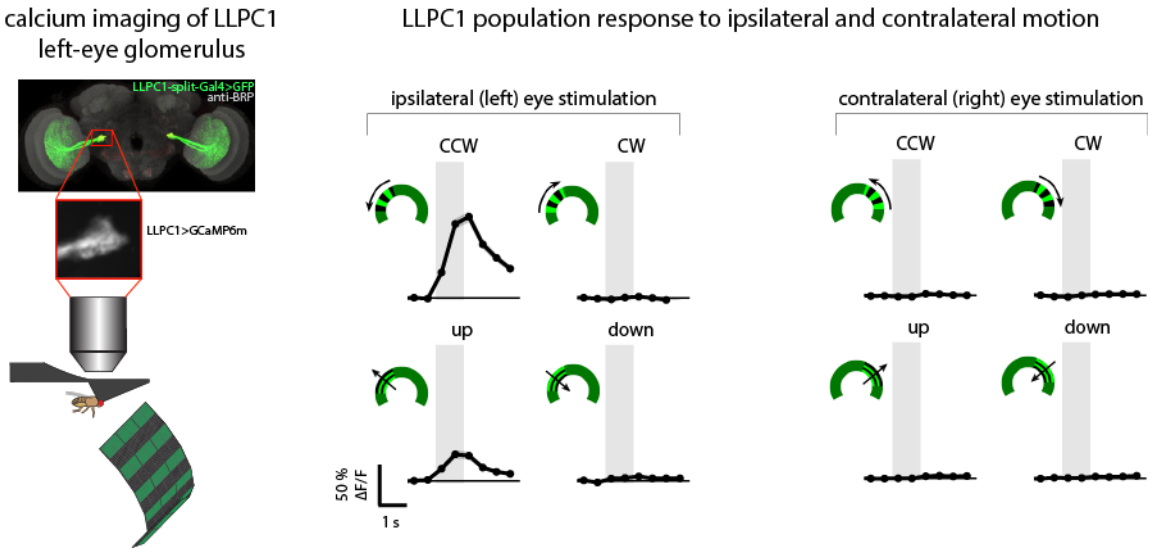

Figure 4.11: LLPC1 selectivity to 4 cardinal motion directions on the ipsilateral and contralateral eye.

(left) 2-photon calcium imaging of the unilateral (left-eye) LLPC1 population; anatomy imaging from Aljoscha Nern. Back-to-front, front-to-back, up and down motions were presented to left and right eyes individually. Extent of left-eye stimuli ranged from -20° to -90° in azimuth to avoid occlusion due to the mount and to avoid the binocular overlap region (see Figure 3.11). Extent of right-eye stimuli ranged from +20° to +90°. Average +/ SEM of all flies (N=10) are plotted.

In addition to front-to-back motion, I observed that LLPC1 was slightly excited by upward motion on the ipsilateral eye; however, a closer analysis of the LLPC1 split-GAL4 line and its motion responses indicate a possible contamination by some cells which receive input from Lobula Plate layer 3 (the layer encoding up motion). A potential subpopulation on the inferior side of the LLPC1 glomerulus is identifiable as separate from the main glomerulus; the ROI I used for generating

population average responses (in Figure 4.11) includes both the main glomeruli and the potential contaminants. By mapping the fluorescence change of each pixel within the ROI in response to different motion directions, I found that the main glomerulus region is excited by front-to-back motion while the inferior end is selectively excited by upward motion, suggesting that this split-GAL4 line may include a small number of LP layer 3 cells.

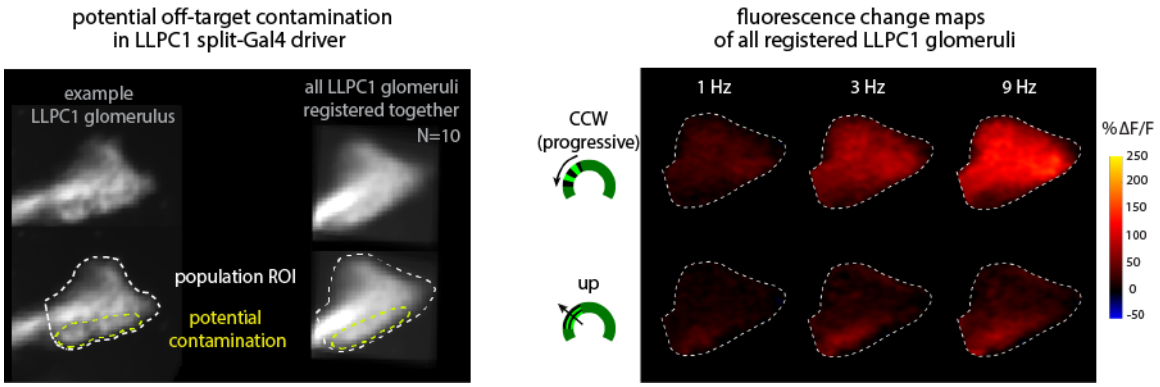

Figure 4.12: LLPC1 driver line potential contamination by LP layer 3 cells.

(left) Mean fluorescence images of the LLPC1 split-GAL4 line glomerulus; both a single example glomerulus and an average image of all 10 tested LLPC1 glomeruli (registered together) are shown. The ROIs used for measuring the LLPC1 population average responses (resulting in data in Figure 4.11) are shown in white, and the potential contaminating cells/region of cells are circled in yellow. (right) Peak fluorescence change maps of the LLPC1 glomerulus (N=10 LLPC1 glomeruli average) in response to front-to-back and up stimuli at 1, 3, and 9 Hz temporal frequency.

I collected one more piece of evidence that LLPC1 primarily detects front-to-back motion and little-to-no upward motion. EM tracing and synapse tagging by the Janelia Connectome Annotation Team (CAT) identified a single large cell (named LPC1-interneuron) in the PLP which receives input from many LLPC1 cells and is presynaptic to many LPC1 cells. Measuring the responses of the LPC1-interneuron to single-eye motion showed that it is highly selected to front-to-back motion with only a very slight upward response at the preferred temporal frequency (9 Hz) (Figure 4.13). Since this neuron was tagged as being downstream of LLPC1 cells, if LLPC1 was actually excited by upward motion to a substantial degree, I would have expected a larger response to upward motion in the LPC1-interneuron.

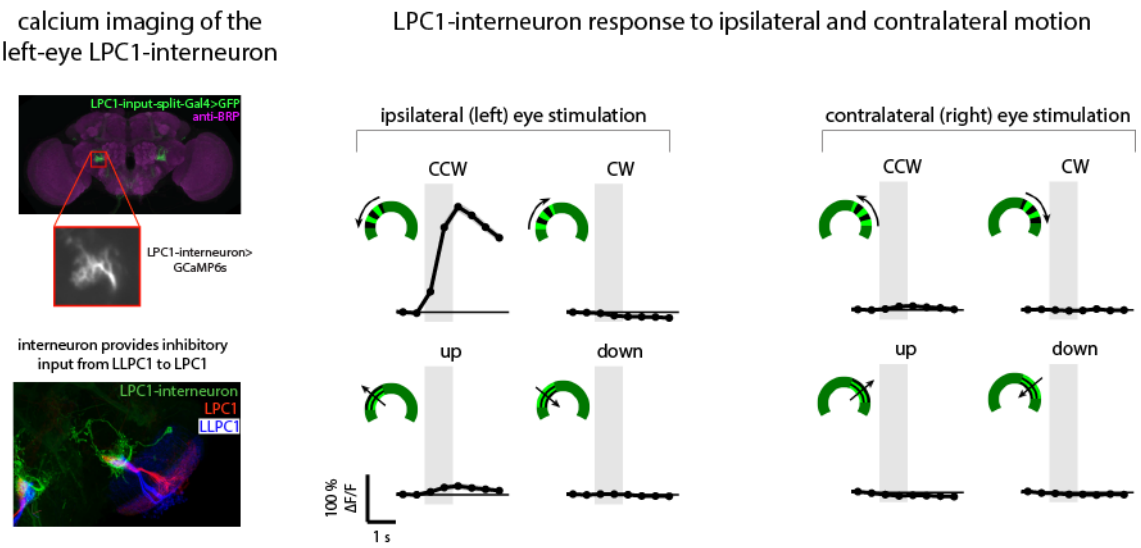

Figure 4.13: LPC1-interneuron selectivity to 4 motion directions on the ipsilateral and contralateral eye.

(top-left) 2-photon calcium imaging of the unilateral (left-eye) LPC1-interneuron; anatomy imaging from Aljoscha Nern. (bottom-left) Back-to-front, front-to-back, up and down motions were presented to left and right eyes individually. Extent of left-eye stimuli ranged from -20° to -90° in azimuth to avoid occlusion due to the mount and to avoid the binocular overlap region (see Figure 3.11). Extent of right-eye stimuli ranged from +20° to +90°. Average +/ SEM of all flies (N=4) are plotted.

Presenting translation gratings with a shifting focus of expansion again showed that both front-to-back cell-types (the LLPC1 population and the LPC1-interneuron) are highly selective to front-to-back motion in each unilateral population and are even more selective when estimating a linear combined response between both eyes, with a clear gradient in response that tracks the degree of front-to-back motion. Furthermore, it seems that contralateral suppression, this time by back-to-front motion, may be taking place.

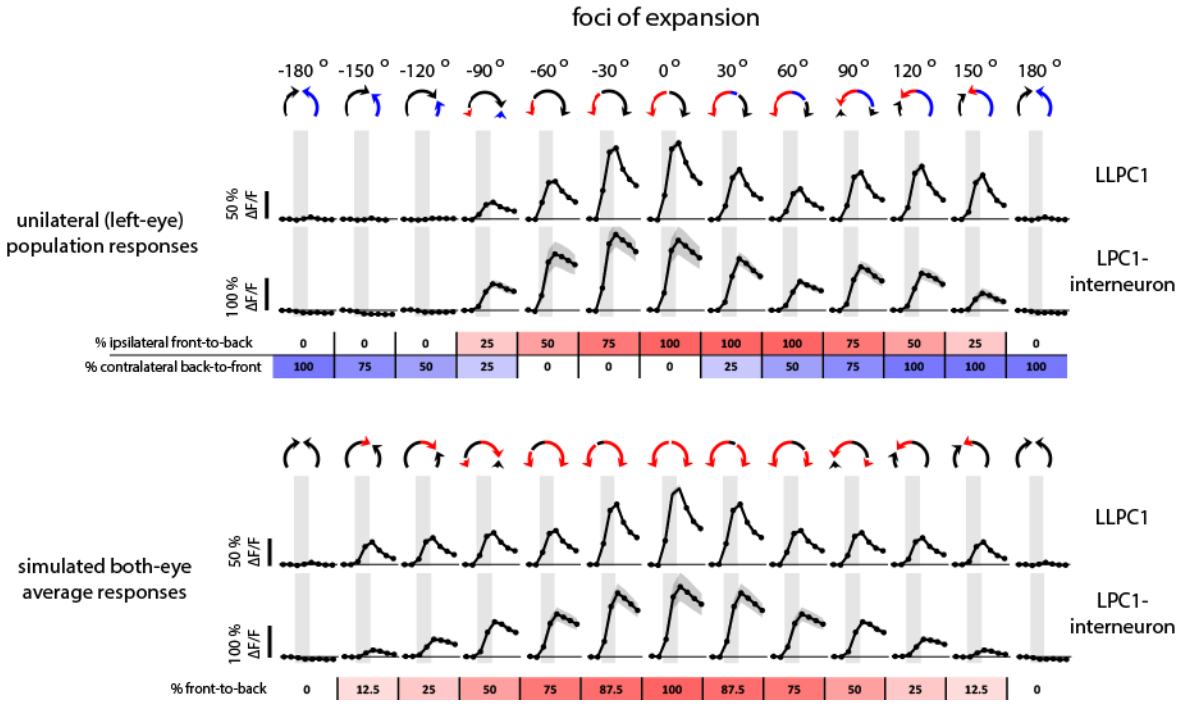

Figure 4.14: LLPC1 and LPC1-interneuron responses to translational motion from different foci of expansion.

(top) LLPC1 and LPC1-interneuron responses to translation stimuli along foci of expansion (FOE) located every 30° along the azimuth of the visual field; a FOE located at 0° represents pure front-to-back translation and an FOE located at +/- 180° represents pure back-to-front translation. The amount of ipsilateral front-to-back motion and contralateral back-to-front motion is calculated for each stimulus, color coded in red and blue, respectively. (bottom) Linear combination of responses of left and right-eye LLPC1 and LPC1-interneuron cells to foci of expansion stimuli. The amount of combined front-to-back motion on both eyes is color coded in red. Average +/- SEM of all flies (LLPC1 N=10; LPC1-interneuron N=4) are plotted.

A direct test of the effects of contralateral motion on LLPC1 and the LPC1-interneuron also showed significant modulation. This simple mechanism for gaining selectivity to translation over rotation appears to be identical for both front-to-back motion in LLPC1 (and the LPC1-interneuron) and back-to-front motion in LPC1.

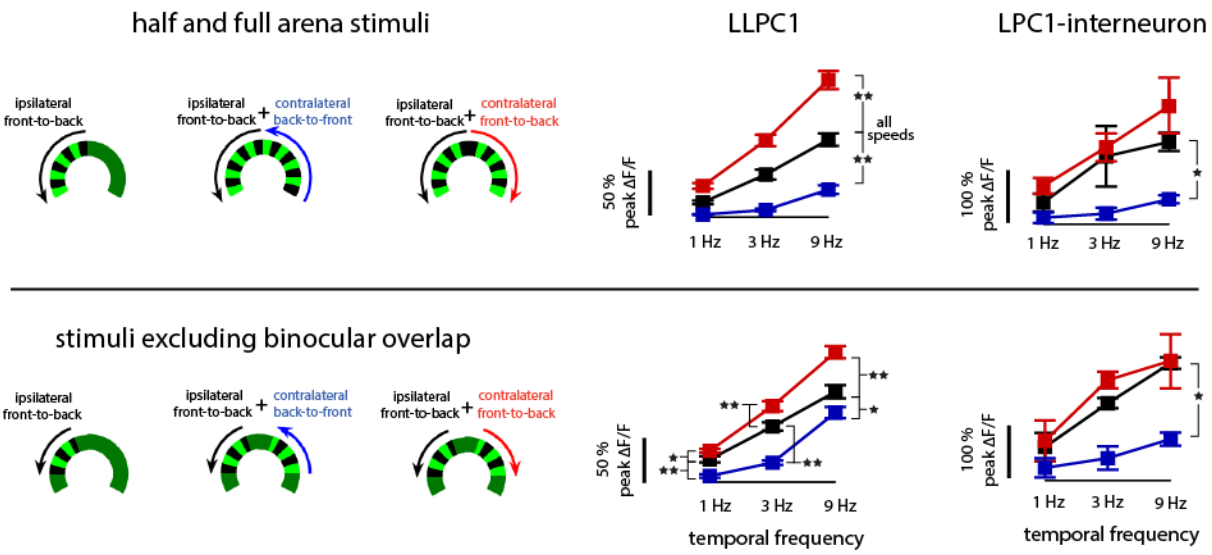

Figure 4.15: Modulation of LLPC1 and LPC1-input activity by contralateral motion.

(top) Unilateral (left-eye) LLPC1 population and LPC1-interneuron responses to ipsilateral front-to-back motion and the change in responses caused by the simultaneous presentation of contralateral front-to-back or back-to-front motion. Peak fluorescence change is plotted for motion stimuli at 3 temporal frequencies (1, 3, and 9 Hz). Data in black represents responses to ipsilateral front-to-back motion alone; data in red represent responses to ipsilateral front-to-back and contralateral front-to-back motion presented simultaneously; data in blue represent responses to ipsilateral front-to-back and contralateral back-to-front motion presented simultaneously. Statistically significant differences between responses were noted with stars (1 star for $p<0.05$ and FDR=5%; 2 stars for $p<0.01$, FDR=1%). (bottom) Stimuli which exclude the region of binocular overlap and region of occlusion by the imaging mount: left eye stimulus ranges from -90° to -20° in longitude of the fly visual field; right eye stimulus ranges from 20° to 90°. Average +/- SEM of all flies (LLPC1 N=10; LPC1-interneuron N=4) are plotted.

4.5 Discussion

Our early interest in the LPC1 cell-type can be attributed in large part due to the significant silencing phenotype observed in the Fly Vision Box motion assay. The behavioral measurement recorded in this assay is not simply a measurement of turning or forward walking, but the net direction of movement inside this corridor relative to the direction of drifting gratings; this is a complex measurement that aggregates the effects of many aspects of walking behavior and vision. Consequently, understanding the effects of silencing neurons has required follow-up experiments in more controlled conditions such as the tethered walking assay. The visual stimuli presented in the Fly Vision Box is also relatively complex: the configuration of LEDs along a wall of the corridor and numerous reflections of these LEDs on the other surfaces of the corridor causes a drifting grating

along the LEDs to appear much like a horizontally-translating starfield. This property of the assay may have inadvertently benefited our investigation of visual motion circuits by exposing translational-motion deficits of forward-walking flies when LPC1 neurons are silenced. A more conventional rotation/turning assay would almost certainly not have uncovered a role for these neurons.

Single-fly silencing and activation assays gave us the ability to infer what role LPC1 is likely playing in the systems of visual perception and behavioral control of walking, though the data acquired using these methods must be considered in the context of the limitations of the methods. LPC1 was targeted for silencing and activation using the genetic toolkit for cell-type specific control in *Drosophila*, namely using split-GAL4 expression control systems. Our ability to isolate the function of LPC1 cells is thus dependent on the quality of the split-GAL4 line, i.e. how well it is targeting every LPC1 cell and if it is successfully excluding cells from other cell-types or other parts of the network. Anatomical imaging of the LPC1 split-GAL4 line expressing GFP (Figure 4.2) and connectomics from Janelia's Connectome Annotation Team (CAT) provided good evidence that this was an exceptionally good line for cell-type-specificity. Even so, the act of inserting exogenous genes or sequences into the fly's genome along with strong promoters to increase the expression of the effector might have unintended effects. The insertion points (or "landing sites") of the new sequences into the genome has been shown to profoundly affect the expression of the transgene due to position effects (Spradling & Rubin, 1983), but they may also cause disruption of endogenous expression; large amount of expression of the effector genes could take resources from natural expression patterns, potentially changing the functional properties of the targeted cell-type.

Because of these considerations, we tried to compare all experimental transgenic fly lines to as genetically similar control flies as possible. For silencing experiments, this meant using control fly lines with the same inserted effector gene (Shibire or Chrimson) but only one half of the split-GAL4 insertions, making the transgenics between test and control groups as similar as possible. Further care was taken with activation experiments using the FLP/FRT expression control system (Duffy, 2002) which allowed for control flies to be from the same transgenic line but with expression controlled by a heat shock delivered early in development. The choice of effector was also made deliberately to prevent unintended effects common with other methods. Shibire, a neuronal silencer, is only activated by higher temperatures (Kitamoto, 2001), and by rearing both experimental and matched control flies on low temperature until just before the experiment, we aimed to prevent this neuronal deactivation from affecting normal patterns of development. Chrimson was chosen for neuronal activation due to it being significantly red-shifted (Klapoetke et al., 2014) to allow a separation between LED color which optogenetically activates the targeted cell

type and LED color used to present visual motion stimuli, though the separation was not entirely complete. Earlier versions of the activation experiments shown in Figure 4.6 suggested that both bright green light from the visual display slightly activated Chrimson, and bright red light for optogenetic activation caused a slight startle response in control flies not expressing Chrimson. By reducing the brightness of both light sources, we appeared to minimize these unintended effects, though optogenetic activation has other inherent limitations such as potentially unnatural temporal dynamics and synchronicity of activation. Despite these numerous limitations in methods that I used to study the LPC1 cell type, the observation that silencing, activating, and functional imaging of this cell type all produced consistent results that pointed to LPC1's role in translation motion selectivity and control of forward walking gives greater confidence than can be achieved with any single method.

Through calcium imaging experiments (Figure 4.9), I observed that unilateral LPC1 and LLPC1 populations gain selectivity for translation over rotation by inhibition from the contralateral eye to specific motion directions. This is a simple yet reliable method to gain this selectivity, as yaw rotations produce motion in the same horizontal direction on both eyes whereas thrust translation will produce horizontal motion in opposite directions (Figure 4.16). We have been highly interested in mapping the source(s) of this potential contralateral suppression/inhibition of LPC1. This search has been carried out through Janelia's Connectome Annotation Team (CAT) in the FAFB data set. As we could not find a suitable Layer 2 input in the Lobula Plate, the team has instead focused on potential direct connections between the LPC1 glomerulus and the contralateral optic lobe or posterior lateral protocerebrum. To date, no simple circuit has been identified with all the desired anatomical requirements. This search did uncover the LPC1-interneuron, which first appeared to be the best candidate for providing inhibition to LPC1 by contralateral front-to-back motion. This neuron is the only neuron that provides a large number of input synapses (annotated and counted by Henrique Ludwig in CAT) onto every LPC1 cell in the central glomerulus. Furthermore, the LPC1-interneuron is putatively GABAergic based on GAD1-antibody staining by collaborator Aljoscha Nern. However, through calcium imaging of the LPC1-interneuron, I found that this cell type is not excited by contralateral motion of any direction, so it is unlikely to be the source of contralateral inhibition (Figure 4.13). The LPC1-interneuron does respond strongly to ipsilateral front-to-back motion—suggesting that it inhibits LPC1 in response to this motion direction. This input, which could mediate 'motion opponency', may serve to increase LPC1's selectivity to back-to-front motion. Ipsilateral inhibition by front-to-back motion may be visible as slight hyperpolarization in Figure 4.7, as well as inhibition in Figure 3.14 in the S1 (south-ipsilateral) spatial location.

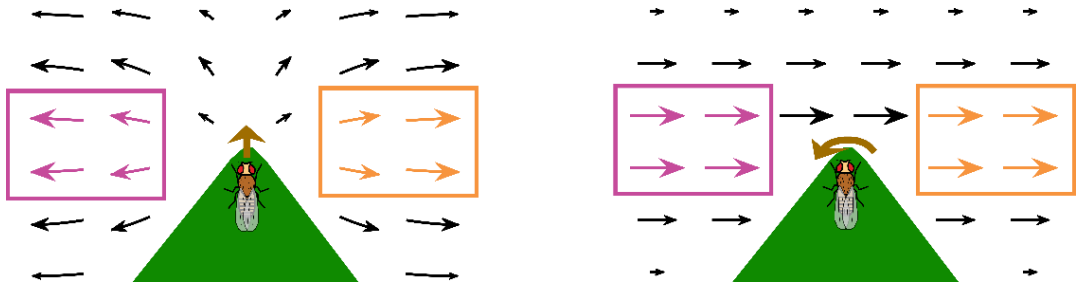

Figure 4.16: Flow-fields associated with forward-walking and turning.

(left) Flow-field associated with forward-walking (Mercator projection of arrows, cosine corrected for length) from a walking fly's point of view. Regions of left and right-eye visual fields (left eye region in magenta, right eye in orange) are presented with local motion vectors in opposite directions. (right) Flow-field associated with a CCW turn from a walking fly's perspective, where the left and right eye regions are presented with local motion vectors in the same direction. The difference in combinations of front-to-back/back-to-front motion between these two motion types appears to be the main driver in LPC1 and LLPC1's selectivity to translation over rotation.

Apart from identifying LPC1 and LLPC1 as important components of translational motion vision pathways, characterizing these neurons revealed another interesting feature. Both LPC1 and LLPC1 neurons were found to have a greater response at a 9 Hz temporal frequency (TF) than 1 or 3 Hz (Figures 4.9 and 4.15). This closely matches the TF tuning of behavioral responses to visual stimuli such as turning or forward-walking (e.g. Figure 4.2). This is quite surprising since the TF tuning of LPTCs (Chiappe, Seelig, Reiser, & Jayaraman, 2010; Suver, Mamiya, & Dickinson, 2012) and T4/T5 cells (Strother et al., 2018) in non-behaving flies is quite a bit slower (~1 Hz) than the behavioral TF optimum. It is interesting that for responses to motion stimuli simulating thrust translation, there is no discrepancy in TF tuning between neuronal excitation and behavior just one step downstream of T4/T5 cells. Silencing TmY3 neurons (another cell type investigated because of a phenotype in the Fly Vision Box) produced a significant downward shift in the TF tuning of LPC1 cells (Figure 4.10), suggesting the possibility that TmY3 somehow contributes to high-speed motion vision. One potentially confounding variable in the dataset where I observed this shift in TF tuning is that I used GCaMP6m (medium speed GCaMP6) to image LPC1 cells in their normal condition but GCaMP6s (slow speed GCaMP6) to image LPC1 when TmY3 was silenced. This choice was made due to the convenient availability of a genetic construct that drives expression of GCaMP6s in LPC1 (using the

LexA/LexAop system) that was compatible with a construct that drives Kir expression in TmY3 (using the GAL4/UAS system). While the difference in temporal dynamics between these two indicators is not expected to cause the kind of change in TF tuning I observed, it remains a confounding variable that deserves follow-up. If the speed tuning of LPC1s is indeed enhanced by non-T4/T5 inputs, this finding is significant for two reasons. First, it may establish the first example of speed tuning that is distinct from the mechanism of directional selectivity: in the standard framework for motion detection, speed tuning emerges from the very same mechanism of directional selectivity, whereas here, a neuron that may or may not itself also measure the direction of motion (TmY3) does contribute to the speed tuning of motion sensitive LPC1 cells. The second reason is that broader speed tuning is, from simple theoretical considerations, expected to be a feature of translational, but not rotational optic flow since objects at different distances produce widely differing amounts of relative motion. This further supports our proposal that LPC1 and LLPC1 neurons regulate translational optic flow-guided locomotion.

While our observation that LPC1 and LLPC1 are most strongly excited by translation optic flow suggests that these neurons may be involved in detecting the fly's self-translation, a different potential function of the motion selectivity of these cells should be considered. Rather than being (solely) matched filters for self-translation, they may be conceptualized as detecting some specific motion that is *not* associated with self-*rotation*. For example, the detection of fast back-to-front motion (but not in the context of self-rotation) can serve as a reliable detector for moving objects (Zabala et al., 2012), where it has been observed that detection of a back-to-front moving object caused flies to cease forward walking, possibly to avoid collisions. In agreement with this prior research, we too observed that the detection of back-to-front motion caused flies to cease or reduce forward walking (Figures 4.5 and 4.6). It has also been proposed that the detection of generalized regressive (back-to-front) motion – rightward motion on the left eye and leftward motion on the right eye – is a reliable method for collision avoidance (Chalupka, Dickinson, & Perona, 2016). Since our behavioral experiments also determined that LPC1 is tightly linked to the cessation or reduction of forward walking, the mechanism by which LPC1 gains selectivity to back-to-front motion may also represent a neural mechanism for moving-object detection and collision avoidance.

In contrast to the well-studied large-field Lobula Plate Tangential Cells, our investigation has uncovered several new cell types that encode small-field visual motion and participate in regulating locomotion. In addition to LPC1 and LLPC1, other small-field Lobula Plate visual projection cell types have recently been identified by our collaborator Aljoscha Nern (with help from Janelia's Fly Light project). While the neurons are still being characterized, these cell types are believed to include small-field neurons that receive input from the Lobula Plate layers 3 and 4; if these cell types

modulated by contralateral motion in a similar way as LPC1 and LLPC1, they may be able to differentiate between motion induced by roll rotations and lift translations, which each produce different combinations of upward and downward motion. With the tools developed and described in chapter 3 and the experiment types described in chapters 3 and 4 which take advantage of genetic tools that allow us to target these small-field cell populations, we are in an ideal position to continue exploring the larger network surrounding small-field visual projection neurons and the detection of translation optic flow. The exploration of central brain circuits will reveal if, where, and how the large-field and small-field motion encoding neurons interact, and ultimately how these cells contribute to visual control of locomotion.

Chapter 5: Final discussion and future directions

In this thesis, I described and discussed results from three projects undertaken over the course of my PhD program at the University of Cambridge and the HHMI Janelia Research Campus. The first involved developing and validating a new method for delivering dyes for anatomical and functional imaging, which I then used to study auditory processing in locusts and crickets. The second involved the development of a visual stimulation and experimental control system and its use in studying the visual control of behavior in fruit flies. In the third and final project, I characterized two newly described classes of visual projection cells in flies and implicated their function in the visual detection of translational motion and control of walking.

In the upcoming sections, I will highlight what I think are particularly significant results from each of the three projects and will provide context for why these represent significant advances in their respective fields. I will also discuss some future directions which appear most promising, both for further developing these new methods and for advancing our understanding of the neural mechanisms of sensation.

5.1 Electrophoretic dye delivery and cricket calling-song selectivity

In chapter 2, I described the progress made in developing a simple, cheap, and relatively non-invasive/non-destructive method for delivering anatomical dyes, tracers, and functional indicators into populations of neurons for insect research. I focused this method primarily in locusts and crickets for their experimental convenience and because they are attractive model systems to understand the neural basis of insect acoustic communication, but there are no obvious constraints to applying this method to other species. This method was developed to aid neuroscience research in animal models which lack a well-developed library of tools for genetically targeting neuron subpopulations, which applies to many animal species beyond just most insects. The optimal electrophoretic parameters for dye delivery may not be the same for different model systems but finding the ideal parameters could be as simple as comparing whole-nerve field potentials taken before and after the procedure and relating the results to those gathered from the locust (Figure 2.5); adjusting the parameters until a modest reduction in whole-nerve field potential amplitude is observed may be the easiest way to adapt this method to other systems.

The most noteworthy strength of this dye delivery method is that the target nerve tissue is not physically penetrated and that the function of the labelled neurons is not destroyed by the procedure, which affords many new potential applications. One such example would be for the delivery of plasmids for genetic modification of the target cells, which has been accomplished with

single cell electroporation (Haas et al., 2001) but may be an even more powerful technique if it could be applied to large populations of cells. In this way, the toolkit for genetic manipulation that has been developed and used primarily in the most popular model systems (Sjulson et al., 2016) can be taken advantage of for other species, even the very obscure. If this method could be demonstrated to apply to a variety of systems, then choosing the ideal species for any particular experimental question or sensory/behavioral modality could depend primarily on whichever system most closely suits the experimental question without worrying whether a lack of experimental tools available for that system will hinder the research.

Another new application of the method which I began to take advantage of is in searching for new, uncharacterized cells in a network of interest, such as the network for calling song detection in crickets. Due to the large size of the dye delivery pipette, large regions of nerve tissue can be measured for field-potentials and stained with an anatomical/functional indicator. Using a species-specific calling song as a probe stimulus, I could apply the pipette tip to different regions of the cricket brain in search for field potentials evoked by the stimulus (Figure 2.9). It was this feature that led to a potential new area of investigation in the cricket auditory system.

There have been a small number of characterized sound frequency selective cell types in the cricket brain, namely the ascending neurons AN-1 and AN-2 and brain interneurons BNC-1 and BNC-2 (Huber & Thorson, 1985). These cells show a selectivity toward the sound frequency of the species-specific calling song, but the parameters of a calling song which mediate phonotaxis is not only the sound frequency but also rate of sound pulses (which defines the chirps and trills of the species-specific calling song.) To my knowledge, no cells have yet been identified in the cricket brain which are selective to the species-specific pulse rate. However, in one electrophoretic dye staining in the cricket brain which was guided by calling-song-evoked local field potentials, a region of labelled neurons did appear more strongly activated by an auditory stimulus that was presented at the species-specific pulse rate as compared to slower or faster rates, even though the stimuli all had the same sound frequency and duty cycle (Figure 2.10). How the cells in this region might be connected to known auditory system cells is unknown, as the epifluorescence microscopy procedures used in this project could not resolve individual cells in this staining. To identify individual pulse-rate-selective cells within this identified region, this dye delivery method may need to be paired with higher resolution confocal or multiphoton microscopy techniques, of which there has been much progress in recent years (Igarashi et al., 2018). Identifying pulse-rate-selective circuits and exploring how this selectivity is generated appears to be a highly exciting area for follow-up investigation, and which is very feasible to pursue in the immediate future using this new electrophoretic dye delivery method.

5.2 Visual stimuli for tethered animal research

In the field of vision research in animal models, different labs tend to build their own display systems to suit their specific experimental needs. No single solution for delivering visual stimuli has dominated the field as the different categories of display types each have their own sets of technical strengths and limitations. At the HHMI Janelia Research Campus, I joined an effort to design a new generation of a modular visual stimulus system (dubbed "G4") which aimed to address most or all technical requirements of vision research experiments. In addition to this engineering/design project, my primary research focus in the lab of Michael Reiser was in studying neural circuits for motion vision in the fly, and my experience with the previous ("G3") modular LED display left much to be desired in the speed and complexity of stimuli that could be delivered. This further motivated me to see the G4 system fully operational so that I could improve the experimental design of my other projects.

For example, when I became interested in the possibility of a cell type that was selective to stimuli encoding forward/backward translation (LPC1, the subject of chapter 4), I realized that displaying a well-designed translation optic flow stimulus with the G3 display system would have been limited to slow speed (as low as 1 Hz temporal frequency) and/or choppy motion. The G4 display system, however, is designed to operate at a much faster refresh rate (allowing up to 62.5 Hz temporal frequency) and smoother motion regardless of the complexity of the stimulus. This feature allowed me to think about generating stimuli that would most accurately represent the type of motion I wanted to present to a tethered fly without having to worry about the technical limitations of the display. The stimulus design strategy I decided to pursue was to take the cylindrical grating stimulus that's been used for many decades in vision research and extrapolate from it to represent rotation around (or translation along) any axis, rather than just the vertical axis (Figure 3.4). These stimuli led to my initial discovery of the LPC1 cell type as being translation selective (Figure 4.3). Furthermore, I found that this selectivity was maximal at temporal frequencies around 9 Hz, meaning if I had attempted this experiment using a G3 display (which could not display these stimuli as fast as 9 Hz), I may have missed this translation selectivity entirely.

The high-speed operation of the G4 system underlies several important and useful applications of the system, such as characterizing flight behaviors to high-speed motion (Figures 3.6-3.10) or receptive-field mapping of cells tuned to high temporal frequencies (Figures 3.12-3.14). Though the application that I find most exciting and which is currently being followed up on is to accommodate more sophisticated closed-loop virtual reality experiments. A typical closed-loop experiment such as the stripe-fixation assay operates by acquiring a single channel of behavioral measurement (in this

case, a measurement of turning) and updating which pattern in a set of pre-rendered patterns is displayed on the LED arena (Figure 3.16). The G4 system, however, can acquire up to 4 separate channels of behavioral measurements and use them to render frames on-line, widely expanding the potential experimental options. For instance, a closed-loop environment could be generated which incorporates yaw, roll, pitch, and forward translation behaviors of a flying fly, simulating a highly complex assay of flight stabilization, navigation, and/or object tracking.

The impediment to conducting this type of sophisticated virtual reality experiment is now no longer the display technology but the method of behavioral measurement. Optical sensing of wingbeat amplitudes (the method used in this thesis to quantify flying fly behaviors) is well-suited for detecting turning behaviors but much less so for other rotational or translational behaviors. A camera-based tracking system using modern advances in machine vision technology may be the best solution to detect and quantify these more complex flight behaviors. The ability to put tethered animals (such as those in a functional imaging or electrophysiology setup) into highly naturalistic and interactive virtual environments could give us vastly improved access to understanding the neural mechanisms behind complex visual processing and behavioral strategies.

5.3 Neural circuits for translation selectivity in flies

In the Drosophila motion vision system, it is well understood that direction-selective T4 and T5 cells converge in the Lobula Plate in a highly organized manner, with cells selective to each of the 4 cardinal directions separated into 4 distinct layers of the Lobula Plate and with retinotopy preserved across each layer (Borst, Haag, & Reiff, 2010b). These cells are commonly referred to as elementary motion detectors (EMDs) since each cell is only selective to motion in a single direction at a single position in the fly's visual field. EMDs are not by themselves capable of differentiating between different types of motion such as those caused by a looming predator or a self-rotation, though these different motion types will elicit very different behavioral reactions. Wide-field visual projection neurons whose dendrites span large regions of the Lobula Plate are capable of integrating motion information in a meaningful way so as to encode patterns of optic flow induced by self-motion, such as HS cells for yaw rotation and VS cells for pitch rotation (Krapp & Hengstenberg, 1996). The project I described in chapter 4 involves investigating a similar type of motion information integration in visual projection neurons, but for optic flow induced by forward/backward translation and by populations of small-field cells rather than individual wide-field cells.

The translation selectivity of these small-field VPN populations (LPC1 and LLPC1) was observed in population average calcium activity (Figures 4.8 and 4.14). However, if these cell types are only

translation selective in their population average response, then the question arises: why are these cell-types composed of many small-field cells instead of being single wide-field visual projection neurons like HS or VS cells? Multiple hypotheses can be considered as to why small-field cells might confer a benefit over wide-field cells in this context. One possibility is that small-field cells could have different spatial tuning properties than wide-field cells, making them more strongly tuned for detecting small moving (translating) objects than global patterns of self-motion. Some evidence already suggests that LPC1 is important for moving object detection and collision avoidance, as its activation causes an abrupt reduction/stop in forward walking (Figure 4.5) and matches previous research on back-to-front motion detection implicated in collision avoidance (Zabala et al., 2012). LLPC1 could plausibly have a similar collision avoidance function, as a fly's forward-motion is expected to produce optic flow that matches LLPC1's selectivity and that will be greater when objects become closer due to motion parallax. In addition to small-field cells potentially being more strongly tuned to small-field motion, having a population of small-field cells rather than a single wide-field cell can preserve the spatial location of motion for downstream circuits of motion detection; in this way, small-field object detectors could not only serve as a warning signal to the central brain about a potential collision, but also transmit the location of the approaching object to the central brain.

One more potential (and possibly most interesting) function of LLPC1 could be to act as a critical component in the fly's ability to navigate its environment. In the past few years, an exciting new discovery in the field of visual control of navigation in *Drosophila* is orientation stabilization in the central complex (Green & Maimon, 2018; Seelig & Jayaraman, 2015). This system essentially acts as an internal compass for the fly, using visual information to maintain an accurate internal representation of heading. However, to successfully navigate an environment an animal is required to not only maintain an internal representation of heading but also an internal representation of distance travelled, or "path integration". One mechanism which has been recently proposed to model these two components in the bee puts forth that the central complex acts as the compass and optic-flow-sensitive circuits act as the path integrator (Stone et al., 2017). After identifying the role of LPCs for translation detection, I can think of no better candidate for a path integrator in *Drosophila* than LLPC1, as it is highly selective to the optic flow associated with forward translation (Figures 4.14 and 4.15). This suggests an exciting direction for new research in fly navigation where the role of LLPC1 in navigation assays could be directly tested. Does LLPC1 silencing disrupt path integration in the fly? Would LLPC1 activation trick the fly into thinking it has travelled farther than it has? I am eager to investigate these possibilities in the very near future.

5.4 Concluding remarks

The three projects described in this thesis, while not entirely connected, are all united under the theme of studying the neural mechanisms of sensation and of developing new and improved methods to enable such research.

Powerful methods for neuroscience research have existed for decades (e.g. voltage clamp, neuronal backfills) and much more can still be learned (and are still being learned) from continuing to use these older techniques, but there are many benefits to developing new methods. Every experimental technique has its own set of limitations and caveats, some of which have been discussed in this dissertation. For example, electrophysiology can be destructive/invasive and may require putting the target animal in an unnatural or undesired behavioral state, and calcium imaging may interfere with natural cellular properties and can mask or average out fast electrical activity. But each method also has its own set of strengths and experimental questions it is best suited for, with some methods being so powerful as to have had a profound impact on the history of neuroscience research. The development of the Golgi stain played a critical role in establishing the neuron doctrine and revolutionizing the field of neuroscience (Pannese, 1999), and the development of the patch clamp technique allowed for a new way to understand fundamental cellular processes through observation of individual ion channel function (Liem, Simard, Song, & Tewari, 1995). But not every new method has to be hailed as groundbreaking or revolutionary to be important. Often a new method will only be an incremental improvement over previous techniques, but any improvement which makes a method simpler, faster, cheaper, or more widely applicable reduces the opportunity cost of implementing or utilizing inferior techniques, which can speed up scientific progress on a wide scale. There is also a benefit to using multiple different methods to address a single experimental question; if experiments utilizing multiple techniques – each with their own set of assumptions or limitations – all point in the same direction, that can provide stronger evidence for or against a hypothesis than any individual method could.

While developing new methods has many potential benefits, method-building must not be done for its own sake but always in service of answering a scientific question that would be more difficult (or impossible) to answer with existing methods. I see this collaboration between method-building and experimentalism as being key to continue advancing the neurosciences. In this thesis, I took advantage of the effectiveness of using state-of-the-art methods and developing new/improved techniques when the need arose, to better understand the neural mechanisms underlying animal sensation and behavior.

References

Abràmoff, M. D., Magalhães, P. J., & Ram, S. J. (2004). Image processing with ImageJ. *Biophotonics*, *11*(7), 36–42. Retrieved from https://dspace.library.uu.nl/handle/1874/204900

Alexander, R. D. (1957). Sound production and associated behavior in insects. Retrieved from https://kb.osu.edu/dspace/bitstream/handle/1811/4430/1/V57N02_101.pdf

Banghart, M., Borges, K., Isacoff, E., Trauner, D., & Kramer, R. H. (2004). Light-activated ion channels for remote control of neuronal firing. *Nature Neuroscience*, *7*(12), 1381–1386. https://doi.org/10.1038/nn1356

Barnes, C. A. (1979). Memory deficits associated with senescence: a neurophysiological and behavioral study in the rat. *Journal of Comparative and Physiological Psychology*, *93*(1), 74–104. Retrieved from http://www.ncbi.nlm.nih.gov/pubmed/221551

Bianco, I. H., & Engert, F. (2015). Visuomotor transformations underlying hunting behavior in zebrafish. *Current Biology : CB*, *25*(7), 831–846. https://doi.org/10.1016/j.cub.2015.01.042

Boeddeker, N., Kern, R., & Egelhaaf, M. (2003). Chasing a dummy target: smooth pursuit and velocity control in male blowflies. *Proceedings. Biological Sciences*, *270*(1513), 393–399. https://doi.org/10.1098/rspb.2002.2240

Borst, A. (2014). Fly visual course control: behaviour, algorithms and circuits. *Nature Reviews Neuroscience*, *15*(9), 590–599. https://doi.org/10.1038/nrn3799

Borst, A., Haag, J., & Reiff, D. F. (2010a). Fly Motion Vision. *Annual Review of Neuroscience*, *33*(1), 49–70. https://doi.org/10.1146/annurev-neuro-060909-153155

Borst, A., Haag, J., & Reiff, D. F. (2010b). Fly Motion Vision. *Annual Review of Neuroscience*, *33*(1), 49–70. https://doi.org/10.1146/annurev-neuro-060909-153155

Braitenberg, V. (1967). Patterns of projection in the visual system of the fly. I. Retina-lamina projections. *Experimental Brain Research*, *3*(3), 271–298. https://doi.org/10.1007/BF00235589

Brand, A. H., & Perrimon, N. (1993). Targeted gene expression as a means of altering cell fates and generating dominant phenotypes. *Development (Cambridge, England)*, *118*(2), 401–415. Retrieved from http://www.ncbi.nlm.nih.gov/pubmed/8223268

Brandt, H. M., & Apkarian, A. V. (1992). Biotin-dextran: a sensitive anterograde tracer for neuroanatomic studies in rat and monkey. *Journal of Neuroscience Methods*, *45*(1–2), 35–40. https://doi.org/10.1016/0165-0270(92)90041-B

Brembs, B., & Heisenberg, M. (2000). The operant and the classical in conditioned orientation of Drosophila melanogaster at the flight simulator. *Learning & Memory (Cold Spring Harbor, N.Y.)*, *7*(2), 104–115. Retrieved from http://www.ncbi.nlm.nih.gov/pubmed/10753977

Buchanan, J. T. (1993). Electrophysiological properties of identified classes of lamprey spinal neurons. *Journal of Neurophysiology*, *70*(6), 2313–2325. https://doi.org/10.1152/jn.1993.70.6.2313

Buchner, E. (1971). *Dunkelanregung des stationaeren Flugs der Fruchtfliege Drosophila*. University of Tuebingen.

Carlson, S. D., Juang, J.-L., Hilgers, S. L., & Garment, M. B. (2000). Blood Barriers of the Insect. *Annual Review of Entomology*, *45*(1), 151–174. https://doi.org/10.1146/annurev.ento.45.1.151

Chalfie, M., Tu, Y., Euskirchen, G., Ward, W. W., & Prasher, D. C. (1994). Green fluorescent protein as a marker for gene expression. *Science (New York, N.Y.)*, *263*(5148), 802–805. https://doi.org/10.1126/SCIENCE.8303295

Chalupka, K., Dickinson, M., & Perona, P. (2016). Generalized regressive motion: a visual cue to collision. *Bioinspiration & Biomimetics*, *11*(4), 046008. https://doi.org/10.1088/1748-3190/11/4/046008

Chen, T., Wardill, T. J., Sun, Y., Pulver, S. R., Renninger, S. L., Baohan, A., … Kim, D. S. (2013). Ultrasensitive fluorescent proteins for imaging neuronal activity. *Nature*, *499*(7458), 295–300. https://doi.org/10.1038/nature12354

Chiappe, M. E., Seelig, J. D., Reiser, M. B., & Jayaraman, V. (2010). Walking Modulates Speed Sensitivity in Drosophila Motion Vision. *Current Biology*, *20*(16), 1470–1475. https://doi.org/10.1016/j.cub.2010.06.072

Chow, D. M., Theobald, J. C., & Frye, M. A. (2011). An Olfactory Circuit Increases the Fidelity of Visual Behavior. *Journal of Neuroscience*, *31*(42), 15035–15047. https://doi.org/10.1523/JNEUROSCI.1736-11.2011

Davis, F. P., Nern, A., Picard, S., Reiser, M. B., Rubin, G. M., Eddy, S. R., & Henry, G. L. (2018). A genetic, genomic, and computational resource for exploring neural circuit function. *BioRxiv*, 385476. https://doi.org/10.1101/385476

Demerec, M. (1965). *Biology of Drosophila*. New York: Hafner Press.

Dickinson, M. H., & Muijres, F. T. (2016). The aerodynamics and control of free flight manoeuvres in Drosophila. *Philosophical Transactions of the Royal Society of London. Series B, Biological*

Sciences, *371*(1704), 20150388. https://doi.org/10.1098/rstb.2015.0388

Dombeck, D. A., Khabbaz, A. N., Collman, F., Adelman, T. L., & Tank, D. W. (2007). Imaging Large-Scale Neural Activity with Cellular Resolution in Awake, Mobile Mice. *Neuron*, *56*(1), 43–57. https://doi.org/10.1016/j.neuron.2007.08.003

Dombeck, D. A., & Reiser, M. B. (2012). Real neuroscience in virtual worlds. *Current Opinion in Neurobiology*, *22*(1), 3–10. https://doi.org/10.1016/J.CONB.2011.10.015

Duffy, J. B. (2002). GAL4 system in Drosophila: A fly geneticist's swiss army knife. *Genesis*, *34*(1–2), 1–15. https://doi.org/10.1002/gene.10150

Dukhin, S. S., & Derjaguin, B. V. (1974). *Electrokinetic Phenomena, J. Willey and Sons.o Title*. J. Willey and Sons.

Eilers, J., Augustine, G. J., & Konnerth, A. (1995). Subthreshold synaptic Ca2+ signalling in fine dendrites and spines of cerebellar Purkinje neurons. *Nature*, *373*(6510), 155–158. https://doi.org/10.1038/373155a0

Eliason, J. (2017). *Single Neuron Contributions to Sensory Behaviors in Drosophila melanogaster*. Emory University. Retrieved from https://etd.library.emory.edu/concern/etds/8g84mm241?locale=en

Elliott, C., Vijayakumar, V., Zink, W., & Hansen, R. (2007). National Instruments LabVIEW: A Programming Environment for Laboratory Automation and Measurement. *Journal of the Association for Laboratory Automation*, *12*(1), 17–24. https://doi.org/10.1016/j.jala.2006.07.012

Ewert, C. J. (1980). *Neuroethology: An Introduction to the Neurophysiological Fundamentals of Behavior*. Berlin/Heidelberg/New York: Springer-Verlag.

Fischbach, K.-F., & Dittrich, A. P. M. (1989). The optic lobe of Drosophila melanogaster. I. A Golgi analysis of wild-type structure. *Cell and Tissue Research*, *258*(3). https://doi.org/10.1007/BF00218858

Fisher, Y. E., Silies, M., & Clandinin, T. R. (2015). Orientation Selectivity Sharpens Motion Detection in Drosophila. *Neuron*, *88*(2), 390–402. https://doi.org/10.1016/j.neuron.2015.09.033

Gilbert, C., Penisten, D. K., & DeVoe, R. D. (1991). Discrimination of visual motion from flicker by identified neurons in the medulla of the fleshfly Sarcophaga bullata. *Journal of Comparative Physiology. A, Sensory, Neural, and Behavioral Physiology*, *168*(6), 653–673. Retrieved from http://www.ncbi.nlm.nih.gov/pubmed/1920163

Gotz, K. G. (1964). Optomotorische Untersuchung des visuellen systems einiger Augenmutanten der Fruchtfliege Drosophila. *Kybernetik*, *2*(2), 77–92. https://doi.org/10.1007/BF00288561

Gotz, K. G. (1968). Flight control in Drosophila by visual perception of motion. *Kybernetik*, *4*(6), 199–208. https://doi.org/10.1007/BF00272517

Green, J., & Maimon, G. (2018). Building a heading signal from anatomically defined neuron types in the Drosophila central complex. *Current Opinion in Neurobiology*, *52*, 156–164. https://doi.org/10.1016/j.conb.2018.06.010

Gruntman, E., Romani, S., & Reiser, M. B. (2018). Simple integration of fast excitation and offset, delayed inhibition computes directional selectivity in Drosophila. *Nature Neuroscience*, *21*(2), 250–257. https://doi.org/10.1038/s41593-017-0046-4

Haas, K., Sin, W. C., Javaherian, A., Li, Z., & Cline, H. T. (2001). Single-cell electroporation for gene transfer in vivo. *Neuron*, *29*(3), 583–591. Retrieved from http://www.ncbi.nlm.nih.gov/pubmed/11301019

Hammer, M., & Menzel, R. (1995). Learning and memory in the honeybee. *The Journal of Neuroscience : The Official Journal of the Society for Neuroscience*, *15*(3 Pt 1), 1617–1630. Retrieved from http://www.ncbi.nlm.nih.gov/pubmed/7891123

Harvey-Clark, C. (2011). IACUC Challenges in Invertebrate Research. *ILAR Journal*, *52*(2), 213–220. https://doi.org/10.1093/ilar.52.2.213

Hassenstein, B., & Reichardt, W. (1956). Systemtheoretische Analyse der Zeit-, Reihenfolgen- und Vorzeichenauswertung bei der Bewegungsperzeption des Rüsselkäfers Chlorophanus. *Zeitschrift Für Naturforschung B*, *11*(9–10), 513–524. https://doi.org/10.1515/znb-1956-9-1004

Hausen, K. (1982). Motion sensitive interneurons in the optomotor system of the fly. *Biological Cybernetics*, *45*(2), 143–156. https://doi.org/10.1007/BF00335241

Hausen, K. (1984). The Lobula-Complex of the Fly: Structure, Function and Significance in Visual Behaviour. In *Photoreception and Vision in Invertebrates* (pp. 523–559). Boston, MA: Springer US. https://doi.org/10.1007/978-1-4613-2743-1_15

Hedwig, B. (2006). Pulses, patterns and paths: neurobiology of acoustic behaviour in crickets. *Journal of Comparative Physiology A*, *192*(7), 677–689. https://doi.org/10.1007/s00359-006-0115-8

Hodgkin, A. L., Huxley, A. F., & Katz, B. (1952). Measurement of current-voltage relations in the membrane of the giant axon of Loligo. *The Journal of Physiology*, *116*(4), 424–448. Retrieved from http://www.ncbi.nlm.nih.gov/pubmed/14946712

Horch, H. W., Sheldon, E., Cutting, C. C., Williams, C. R., Riker, D. M., Peckler, H. R., & Sangal, R. B. (2011). Bilateral Consequences of Chronic Unilateral Deafferentation in the Auditory System of the Cricket Gryllus bimaculatus. *Developmental Neuroscience*, *33*(1), 21–37. https://doi.org/10.1159/000322887

Hoyle, G. (1984). The scope of neuroethology. *Behavioral and Brain Sciences*, *7*(03), 367. https://doi.org/10.1017/S0140525X0001863X

Huang, Q., Zhou, D., & DiFiglia, M. (1992). Neurobiotin™, a useful neuroanatomical tracer for in vivo anterograde, retrograde and transneuronal tract-tracing and for in vitro labeling of neurons. *J. of Neuroscience Methods*, *41*(1), 31–43. https://doi.org/10.1016/0165-0270(92)90121-S

Hubel, D. H., & Wiesel, T. N. (1962). Receptive fields, binocular interaction and functional architecture in the cat's visual cortex. *The Journal of Physiology*, *160*(1), 106–154. Retrieved from http://www.ncbi.nlm.nih.gov/pubmed/14449617

Huber, F. (1990). Cricket Neuroethology: Neuronal Basis of Intraspecific Acoustic Communication. *Advances in the Study of Behavior*, *19*, 299–356. https://doi.org/10.1016/S0065-3454(08)60206-5

Huber, F., & Thorson, J. (1985). Cricket Auditory Communication. *Scientific American*. Scientific American, a division of Nature America, Inc. https://doi.org/10.2307/24967872

Igarashi, M., Nozumi, M., Wu, L.-G., Zanacchi, F. C., Katona, I., Barna, L., … Boyden, E. (2018). New observations in neuroscience using superresolution microscopy. *Journal of Neuroscience*, *38*(44), 9459–9467. https://doi.org/10.1523/JNEUROSCI.1678-18.2018

Isaacson, M. D., & Hedwig, B. (2017). Electrophoresis of polar fluorescent tracers through the nerve sheath labels neuronal populations for anatomical and functional imaging. *Scientific Reports*, *7*. https://doi.org/10.1038/srep40433

Jacobs, K., Otte, B., & Lakes-Harlan, R. (1999). Tympanal receptor cells of Schistocerca gregaria: Correlation of soma positions and dendrite attachment sites, central projections and physiologies. *Journal of Experimental Zoology*, *283*(3), 270–285. https://doi.org/10.1002/(SICI)1097-010X(19990215)283:3<270::AID-JEZ5>3.0.CO;2-C

Jenett, A., Rubin, G. M., Ngo, T.-T. B., Shepherd, D., Murphy, C., Dionne, H., … Zugates, C. T. (2012). A GAL4-Driver Line Resource for Drosophila Neurobiology. *Cell Reports*, *2*(4), 991–1001. https://doi.org/10.1016/j.celrep.2012.09.011

Joesch, M., Schnell, B., Raghu, S. V., Reiff, D. F., & Borst, A. (2010). ON and OFF pathways in Drosophila motion vision. *Nature*, *468*(7321), 300–304. https://doi.org/10.1038/nature09545

Johnson, I. (1998). Review: Fluorescent probes for living cells. *The Histochemical Journal*, *30*(3), 123–140. https://doi.org/10.1023/A:1003287101868

Keifer, J., & Summers, C. H. (2016). Putting the “Biology” Back into “Neurobiology”: The Strength of Diversity in Animal Model Systems for Neuroscience Research. *Frontiers in Systems Neuroscience*, *10*, 69. https://doi.org/10.3389/fnsys.2016.00069

Kitamoto, T. (2001). Conditional modification of behavior in Drosophila by targeted expression of a temperature-sensitive shibire allele in defined neurons. *Journal of Neurobiology*, *47*(2), 81–92. Retrieved from http://www.ncbi.nlm.nih.gov/pubmed/11291099

Klapoetke, N. C., Murata, Y., Kim, S. S., Pulver, S. R., Birdsey-Benson, A., Cho, Y. K., … Boyden, E. S. (2014). Independent optical excitation of distinct neural populations. *Nature Methods*, *11*(3), 338–346. https://doi.org/10.1038/nmeth.2836

Krapp, H. G., Hengstenberg, B., & Hengstenberg, R. (1998). Dendritic Structure and Receptive-Field Organization of Optic Flow Processing Interneurons in the Fly. *Journal of Neurophysiology*, *79*(4), 1902–1917. https://doi.org/10.1152/jn.1998.79.4.1902

Krapp, H. G., & Hengstenberg, R. (1996). Estimation of self-motion by optic flow processing in single visual interneurons. *Nature*, *384*(6608), 463–466. https://doi.org/10.1038/384463a0

Krapp, H. G., & Hengstenberg, R. (1997). A fast stimulus procedure to determine local receptive field properties of motion-sensitive visual interneurons. *Vision Research*, *37*(2), 225–234. Retrieved from http://www.ncbi.nlm.nih.gov/pubmed/9068822

Kristensson, K., & Olsson, Y. (1976). Retrograde transport of horseradish peroxidase in transected axons. 3. Entry into injured axons and subsequent localization in perikaryon. *Brain Research*, *115*(2), 201–213. Retrieved from http://www.ncbi.nlm.nih.gov/pubmed/61782

Lehmann, F. O., & Dickinson, M. H. (1997). The changes in power requirements and muscle efficiency during elevated force production in the fruit fly Drosophila melanogaster. *Journal of Experimental Biology*, *200*(7).

Leong, J. C. S., Esch, J. J., Poole, B., Ganguli, S., & Clandinin, T. R. (2016). Direction Selectivity in Drosophila Emerges from Preferred-Direction Enhancement and Null-Direction Suppression. *Journal of Neuroscience*, *36*(31), 8078–8092. https://doi.org/10.1523/JNEUROSCI.1272-16.2016

Liem, L. K., Simard, J. M., Song, Y., & Tewari, K. (1995). The patch clamp technique. *Neurosurgery*, *36*(2), 382–392. Retrieved from http://www.ncbi.nlm.nih.gov/pubmed/7537356

Lindemann, J. P., Kern, R., Michaelis, C., Meyer, P., van Hateren, J. H., & Egelhaaf, M. (2003). FliMax,

a novel stimulus device for panoramic and highspeed presentation of behaviourally generated optic flow. *Vision Research*, *43*(7), 779–791. Retrieved from http://www.ncbi.nlm.nih.gov/pubmed/12639604

Lister, R. G. (1987). The use of a plus-maze to measure anxiety in the mouse. *Psychopharmacology*, *92*(2), 180–185. https://doi.org/10.1007/BF00177912

Liu, G., Seiler, H., Wen, A., Zars, T., Ito, K., Wolf, R., … Liu, L. (2006). Distinct memory traces for two visual features in the Drosophila brain. *Nature*, *439*(7076), 551–556. https://doi.org/10.1038/nature04381

Longden, K. D., Wicklein, M., Hardcastle, B. J., Huston, S. J., & Krapp, H. G. (2017). Spike Burst Coding of Translatory Optic Flow and Depth from Motion in the Fly Visual System. *Current Biology : CB*, *27*(21), 3225–3236.e3. https://doi.org/10.1016/j.cub.2017.09.044

Luo, L., Callaway, E. M., & Svoboda, K. (2008). Genetic dissection of neural circuits. *Neuron*, *57*(5), 634–660. https://doi.org/10.1016/j.neuron.2008.01.002

Maimon, G., Straw, A. D., & Dickinson, M. H. (2010). Active flight increases the gain of visual motion processing in Drosophila. *Nature Neuroscience*, *13*(3), 393–399. https://doi.org/10.1038/nn.2492

Maisak, M. S., Haag, J., Ammer, G., Serbe, E., Meier, M., Leonhardt, A., … Borst, A. (2013). A directional tuning map of Drosophila elementary motion detectors. *Nature*, *500*(7461), 212–216. https://doi.org/10.1038/nature12320

Malkin, R., McDonagh, T. R., Mhatre, N., Scott, T. S., & Robert, D. (2014). Energy localization and frequency analysis in the locust ear. *Journal of the Royal Society, Interface*, *11*(90), 20130857. https://doi.org/10.1098/rsif.2013.0857

Miall, R. C. (1978). The flicker fusion frequencies of six laboratory insects, and the response of the compound eye to mains fluorescent 'ripple.' *Physiological Entomology*, *3*(2), 99–106. https://doi.org/10.1111/j.1365-3032.1978.tb00139.x

Miyawaki, A., Llopis, J., Heim, R., McCaffery, J. M., Adams, J. A., Ikura, M., & Tsien, R. Y. (1997). Fluorescent indicators for Ca2+based on green fluorescent proteins and calmodulin. *Nature*, *388*(6645), 882–887. https://doi.org/10.1038/42264

Morgan, T. H. (1915). *The Mechanism of Mendelian Heredity*. New York: H. Holt and Company.

Nuffield. (2005). *The ethics of research involving animals*. Retrieved from http://nuffieldbioethics.org/wp-content/uploads/The-ethics-of-research-involving-animals-full-

report.pdf

Ofstad, T. A., Zuker, C. S., & Reiser, M. B. (2011). Visual place learning in Drosophila melanogaster. *Nature*, *474*(7350), 204–207. https://doi.org/10.1038/nature10131

Ogawa, H., & Kajita, Y. (2015). Ca2+ imaging of cricket protocerebrum responses to air current stimulation. *Neuroscience Letters*, *584*, 282–286. https://doi.org/10.1016/j.neulet.2014.10.042

Okada, J., & Toh, Y. (2004). Antennal system in cockroaches: a biological model of active tactile sensing. *International Congress Series*, *1269*, 57–60. https://doi.org/10.1016/J.ICS.2004.05.014

Osorio, D., & Vorobyev, M. (2005). Photoreceptor spectral sensitivities in terrestrial animals: adaptations for luminance and colour vision. *Proceedings. Biological Sciences*, *272*(1574), 1745–1752. https://doi.org/10.1098/rspb.2005.3156

Pannese, E. (1999). The Golgi Stain: Invention, Diffusion and Impact on Neurosciences. *Journal of the History of the Neurosciences*, *8*(2), 132–140. https://doi.org/10.1076/jhin.8.2.132.1847

Panser, K., Tirian, L., Schulze, F., Villalba, S., Jefferis, G. S. X. E., Bühler, K., & Straw, A. D. (2016). Automatic Segmentation of Drosophila Neural Compartments Using GAL4 Expression Data Reveals Novel Visual Pathways. *Current Biology*, *26*(15), 1943–1954. https://doi.org/10.1016/j.cub.2016.05.052

Pikal, M. J. (2001). The role of electroosmotic flow in transdermal iontophoresis. *Advanced Drug Delivery Reviews*, *46*(1–3), 281–305. Retrieved from http://www.ncbi.nlm.nih.gov/pubmed/11259844

Pitman, R. M., Tweedle, C. D., & Cohen, M. J. (1972). Branching of central neurons: intracellular cobalt injection for light and electron microscopy. *Science (New York, N.Y.)*, *176*(4033), 412–414. https://doi.org/10.1126/SCIENCE.176.4033.412

Rawat, S., Vengurlekar, S., Rakesh, B., Jain, S., & Srikarti, G. (2008). Transdermal delivery by iontophoresis. *Indian Journal of Pharmaceutical Sciences*, *70*(1), 5–10. https://doi.org/10.4103/0250-474X.40324

Rehbein, H. (1976). Auditory neurons in the ventral cord of the locust: Morphological and functional properties. *Journal of Comparative Physiology*, *110*(3), 233–250. https://doi.org/10.1007/BF00659142

Rehbein, H., Kalmring, K., & Römer, H. (1974). Structure and function of acoustic neurons in the thoracic ventral nerve cord of Locusta migratoria (Acrididae). *Journal of Comparative Physiology*, *95*(3), 263–280. https://doi.org/10.1007/BF00625448

Reiser, M. B., & Dickinson, M. H. (2008). A modular display system for insect behavioral neuroscience. *Journal of Neuroscience Methods*, *167*(2), 127–139. https://doi.org/10.1016/j.jneumeth.2007.07.019

Ringach, D. L., Shapley, R. M., & Hawken, M. J. (2002). Orientation selectivity in macaque V1: diversity and laminar dependence. *The Journal of Neuroscience : The Official Journal of the Society for Neuroscience*, *22*(13), 5639–5651. https://doi.org/20026567

Robie, A. A., Hirokawa, J., Edwards, A. W., Simpson, J. H., Reiser, M. B., & Branson, K. (2017). Mapping the Neural Substrates of Behavior. *Cell*, *170*, 393–406. https://doi.org/10.1016/j.cell.2017.06.032

Rodríguez, A., Didiano, D., & Desplan, C. (2012). Power tools for gene expression and clonal analysis in Drosophila. *Nature Methods*, *9*(1), 47–55. https://doi.org/10.1038/nmeth.1800

Roesel von Rosenhof, A. J. (1749). *Insectenbelustigung zweyter Theil, welcher acht Klassen verschiedener sowohl inlaendischer als auch einiger auslaendischer Insecten enthaelt*. Nuernberg: Fleischmann JJ.

Scholl, B., Tan, A. Y. Y., Corey, J., & Priebe, N. J. (2013). Emergence of Orientation Selectivity in the Mammalian Visual Pathway. *Journal of Neuroscience*, *33*(26), 10616–10624. https://doi.org/10.1523/JNEUROSCI.0404-13.2013

Schöneich, S., & Hedwig, B. (2015). Corollary discharge inhibition of wind-sensitive cercal giant interneurons in the singing field cricket. *Journal of Neurophysiology*, *113*(1), 390–399. https://doi.org/10.1152/jn.00520.2014

Schöneich, S., Schildberger, K., & Stevenson, P. A. (2011). Neuronal organization of a fast-mediating cephalothoracic pathway for antennal-tactile information in the cricket (Gryllus bimaculatus DeGeer). *The Journal of Comparative Neurology*, *519*(9), 1677–1690. https://doi.org/10.1002/cne.22594

Schulze-Hagen, K., & Birkhead, T. R. (2015). The ethology and life history of birds: the forgotten contributions of Oskar, Magdalena and Katharina Heinroth. *Journal of Ornithology*, *156*(1), 9–18. https://doi.org/10.1007/s10336-014-1091-3

Scully, L. R., & Bidochka, M. J. (2006). Developing insect models for the study of current and emerging human pathogens. *FEMS Microbiology Letters*, *263*(1), 1–9. https://doi.org/10.1111/j.1574-6968.2006.00388.x

Seelig, J. D., Chiappe, E. M., Lott, G. K., Dutta, A., Osborne, J. E., Reiser, M. B., & Jayaraman, V. (2010). Two-photon calcium imaging from head-fixed Drosophila during optomotor walking

behavior. *Nature Methods*, *7*(7), 535–540. https://doi.org/10.1038/nmeth.1468

Seelig, J. D., & Jayaraman, V. (2015). Neural dynamics for landmark orientation and angular path integration. *Nature*, *521*(7551), 186–191. https://doi.org/10.1038/nature14446

Silies, M., Gohl, D. M., & Clandinin, T. R. (2014). Motion-Detecting Circuits in Flies: Coming into View. *Annual Review of Neuroscience*, *37*(1), 307–327. https://doi.org/10.1146/annurev-neuro-071013-013931

Sjulson, L., Cassataro, D., DasGupta, S., & Miesenböck, G. (2016). Cell-Specific Targeting of Genetically Encoded Tools for Neuroscience. *Annual Review of Genetics*, *50*, 571–594. https://doi.org/10.1146/annurev-genet-120215-035011

Sobel, E. C., & Tank, D. W. (1994). In Vivo Ca2+ Dynamics in a Cricket Auditory Neuron: An Example of Chemical Computation. *Science*, *263*(5148), 823–826. https://doi.org/10.1126/science.263.5148.823

Spalthoff, C., Gerdes, R., & Kurtz, R. (2012). Neuronal representation of visual motion and orientation in the fly medulla. *Frontiers in Neural Circuits*, *6*, 72. https://doi.org/10.3389/fncir.2012.00072

Spradling, A. C., & Rubin, G. M. (1983). The effect of chromosomal position on the expression of the Drosophila xanthine dehydrogenase gene. *Cell*, *34*(1), 47–57. https://doi.org/10.1016/0092-8674(83)90135-6

Stone, T., Webb, B., Adden, A., Weddig, N. Ben, Honkanen, A., Templin, R., … Heinze, S. (2017). An Anatomically Constrained Model for Path Integration in the Bee Brain. *Current Biology*, *27*(20), 3069–3085.e11. https://doi.org/10.1016/j.cub.2017.08.052

Stosiek, C., Garaschuk, O., Holthoff, K., & Konnerth, A. (2003). In vivo two-photon calcium imaging of neuronal networks. *Proceedings of the National Academy of Sciences of the United States of America*, *100*(12), 7319–7324. https://doi.org/10.1073/pnas.1232232100

Strausfield, N. J., & Blest, A. D. (1970). Golgi studies on insects Part I. The optic lobes of Lepidoptera. *Philosophical Transactions of the Royal Society B: Biological Sciences*, *258*(820).

Straw, A. D., Lee, S., & Dickinson, M. H. (2010). Visual Control of Altitude in Flying Drosophila. *Current Biology*, *20*(17), 1550–1556. https://doi.org/10.1016/J.CUB.2010.07.025

Stretton, A. O., & Kravitz, E. A. (1968). Neuronal geometry: determination with a technique of intracellular dye injection. *Science (New York, N.Y.)*, *162*(3849), 132–134. Retrieved from http://www.ncbi.nlm.nih.gov/pubmed/4175300

Strother, J. A., Nern, A., & Reiser, M. B. (2014). Direct observation of ON and OFF pathways in the Drosophila visual system. *Current Biology : CB*, *24*(9), 976–983. https://doi.org/10.1016/j.cub.2014.03.017

Strother, J. A., Wu, S.-T., Rogers, E. M., Eliason, J. L. M., Wong, A. M., Nern, A., & Reiser, M. B. (2018). Behavioral state modulates the ON visual motion pathway of Drosophila. *Proceedings of the National Academy of Sciences of the United States of America*, *115*(1), E102–E111. https://doi.org/10.1073/pnas.1703090115

Strother, J. A., Wu, S.-T., Wong, A. M., Nern, A., Rogers, E. M., Le, J. Q., … Reiser, M. B. (2017). The Emergence of Directional Selectivity in the Visual Motion Pathway of Drosophila. *Neuron*, *94*(1), 168–182.e10. https://doi.org/10.1016/j.neuron.2017.03.010

Suver, M. P., Mamiya, A., & Dickinson, M. H. (2012). Octopamine Neurons Mediate Flight-Induced Modulation of Visual Processing in Drosophila. *Current Biology*, *22*(24), 2294–2302. https://doi.org/10.1016/j.cub.2012.10.034

Takalo, J., Piironen, A., Honkanen, A., Lempeä, M., Aikio, M., Tuukkanen, T., & Vähäsöyrinki, M. (2012). A fast and flexible panoramic virtual reality system for behavioural and electrophysiological experiments. *Scientific Reports*, *2*(1), 324. https://doi.org/10.1038/srep00324

Takemura, S., Nern, A., Chklovskii, D. B., Scheffer, L. K., Rubin, G. M., & Meinertzhagen, I. A. (2017). The comprehensive connectome of a neural substrate for 'ON' motion detection in Drosophila. *ELife*, *6*. https://doi.org/10.7554/eLife.24394

Theobald, J. C., Ringach, D. L., & Frye, M. A. (2010). Dynamics of optomotor responses in Drosophila to perturbations in optic flow. *The Journal of Experimental Biology*, *213*(Pt 8), 1366–1375. https://doi.org/10.1242/jeb.037945

Thorson, J., Weber, T., & Huber, F. (1982). Auditory behavior of the cricket. *Journal of Comparative Physiology ? A*, *146*(3), 361–378. https://doi.org/10.1007/BF00612706

Tinbergen, N. (1963). On aims and methods of Ethology. *Zeitschrift Für Tierpsychologie*, *20*(4), 410–433. https://doi.org/10.1111/j.1439-0310.1963.tb01161.x

Von Holst, E., & Mittelstaedt, H. (2011). The Principle of Reafference : Interactions Between the Central Nervous System and the Peripheral Organs. Retrieved from https://www.semanticscholar.org/paper/The-Principle-of-Reafference-%3A-Interactions-Between-E.VONHOLSTAN-H./96d8482fc6f7fd77ef6700ad60279d419f5eba55

Von Holst, E., & Mittlestaedt, H. (1950). Das reafferenzprinzip. *Naturwissenschaften*, *37*(20), 464–

476.

Wagner, W. E., & Reiser, M. G. (2000). The importance of calling song and courtship song in female mate choice in the variable field cricket. *Animal Behaviour*, *59*(6), 1219–1226. https://doi.org/10.1006/ANBE.1999.1428

Wald, G. (1964). The Receptors of Human Color Vision. *Science*, *145*(3636), 1007–1016. https://doi.org/10.1126/SCIENCE.145.3636.1007

Weaver, J. C., & Chizmadzhev, Y. A. (1996). Theory of electroporation: A review. *Bioelectrochemistry and Bioenergetics*, *41*(2), 135–160. https://doi.org/10.1016/S0302-4598(96)05062-3

Wehner, R. (2003). Desert ant navigation: how miniature brains solve complex tasks. *Journal of Comparative Physiology A: Sensory, Neural, and Behavioral Physiology*, *189*(8), 579–588. https://doi.org/10.1007/s00359-003-0431-1

Yager, D. D. (1999). Structure, development, and evolution of insect auditory systems. *Microscopy Research and Technique*, *47*(6), 380–400. https://doi.org/10.1002/(SICI)1097-0029(19991215)47:6<380::AID-JEMT3>3.0.CO;2-P

Yartsev, M. M. (2017). The emperor's new wardrobe: Rebalancing diversity of animal models in neuroscience research. *Science (New York, N.Y.)*, *358*(6362), 466–469. https://doi.org/10.1126/science.aan8865

Zabala, F., Polidoro, P., Robie, A., Branson, K., Perona, P., & Dickinson, M. H. (2012). A simple strategy for detecting moving objects during locomotion revealed by animal-robot interactions. *Current Biology : CB*, *22*(14), 1344–1350. https://doi.org/10.1016/j.cub.2012.05.024

Zheng, Z., Lauritzen, J. S., Perlman, E., Robinson, C. G., Nichols, M., Milkie, D., … Bock, D. D. (2018). A Complete Electron Microscopy Volume of the Brain of Adult Drosophila melanogaster. *Cell*, *174*(3), 730–743.e22. https://doi.org/10.1016/j.cell.2018.06.019